UNIVERSITÉ DE STRASBOURG

EDSC Ecole Doctorale des Sciences Chimiques

ÉCOLE DOCTORALE DES SCIENCES CHIMIQUES

CNRS 7199 Conception et Application de Molécules Bioactives

THÈSE

présentée par

Xiang LI

soutenue le : **07 Novembre 2012**

pour obtenir le grade de

Docteur de l'université de Strasbourg

Discipline / Spécialité : Chimie

Nano-émulsions radio-opaques iodées pour applications précliniques en imagerie par rayons X

THÈSE dirigée par :

M. VANDAMME Thierry	Professeur, Université de Strasbourg

RAPPORTEURS :

Mme. BERQUE-BESTEL Isabelle	Professeur, Université de Bordeaux Segalen
M. FESSI Hatem	Professeur, Université de Lyon 1

MEMBRES DU JURY :

Mme. BARRATT Gillian	Directeur de recherche, Université Paris-Sud
M. SOLER Luc	Professeur, Université de Strasbourg
M. ANTON Nicolas	Maître de conférences, Université de Strasbourg

Remerciements

Le travail présenté dans cette thèse a été réalisé au sein de l'unité CNRS 7199 conception et application de molécules bioactives, équipe pharmacie biogalénique, Université de Strasbourg. Je tiens donc à remercier très chaleureusement toutes les personnes qui m'ont accompagnée, de près ou de loin pour parcourir ce chemin.

J'adresse tout d'abord mes très sincères remerciements à mon directeur de thèse, le Professeur Thierry Vandamme qui m'a donné l'opportunité de développer ce sujet de thèse très intéressant et a assuré la direction de mes travaux. Je vous remercie pour m'avoir acceptée dans votre master «Ingénierie pharmaceutique» afin d'approfondir mes connaissances en galénique et pour m'avoir accueillie dans votre laboratoire pour mon stage de Master 2 ainsi que pour ces trois années de thèse. J'ai énormément apprécié la confiance que vous m'avez accordée et les libertés que vous m'avez laissées en ce qui concernait mon travail. Vous m'avez ouvert la porte du domaine de la recherche et m'avez permis de partager et communiquer mon expérience avec des chercheurs internationaux. Vous m'avez toujours soutenue et encouragée.

Je tiens tout particulièrement à remercier les Professeurs Gillian Barratt, Isabelle Berque-Bestel, Hatem Fessi et Luc Soler pour m'avoir fait l'honneur d'accepter de juger ce travail.

Je remercie chaleureusement le Docteur Nicolas Anton pour m'avoir encadrée depuis le stage de Master 2. Merci à toi Nicolas d'avoir travaillé avec moi pendant ces quatre années. Tu m'as toujours aidée à trouver des solutions aux difficultés techniques que j'ai rencontrées au laboratoire. Je te remercie aussi pour tous les échanges que nous avons eus pour faire progresser le sujet. J'ai apprécié ta grande disponibilité et l'intérêt que tu as porté à ce projet.

Je tiens à remercier le Docteur Guy Zuber. Durant ces trois ans, votre patience, votre passion et tous vos conseils toujours très pratiques ont été l'un des moteurs de cette thèse. Vous m'avez beaucoup aidée à surmonter les difficultés techniques rencontrées au cours de ces trois ans en matière de chimie mais aussi de biologie. J'ai été très heureuse de travailler avec vous !

Je tiens à remercier la Docteur Minjie Zhao. Merci à toi de répondre à toutes mes questions scientifiques et aussi pour ton aide précieuse dans la vie quotidienne. Grâce à toi, j'ai appris à travailler sur la CLHP et à tirer profit de toute expérience.

Un grand merci aussi aux thésards du labo, Carole Schanté et Pierre Sae Houer. Merci de m'avoir accompagnée au début quand je suis arrivée au labo. J'ai été très contente de vous rencontrer. Je me souviendrais longtemps de la soirée de flamingo de Carole et de tous les repas de labo organisés par Pierre. Merci pour toutes vos invitations… Grâce à vous, je ne me suis jamais sentie seule !

Mes remerciements s'adressent aussi aux stagiaires du laboratoire. Tout d'abord les filles souriantes et passionnantes, Anh Thu Hoang, Elsa Burgard et Marion Chappaz et le seul garçon, toujours très sympathique, Julien Sirman! J'ai été très contente de passer six mois avec vous au labo ! Ensuite, Emmanuel Aman, un garçon très sérieux et dynamique au travail. C'était super sympa d'observer les cellules, de faire les tests cellulaires et de partager le ménage de la salle de culture avec toi. Puis Kubra Pelit, qui nous a aidés à développer les paires appropriées d'huile et de surfactant pour former des nano-émulsions par la méthode d'émulsification spontanée. Et aussi merci pour tous les repas turcs auxquels tu nous as invités ! Merci à Claire Loos et Charlotte Rousseau, avec qui j'ai eu le plaisir de développer d'autres huiles iodées à partir de l'α-tocophérol. C'était très sympa de partager six mois de travail avec vous.

Je tiens aussi à remercier toute l'équipe du Professeur Eric Marchioni avec qui j'ai passé des bons moments durant ces trois ans…

Un immense merci à tous mes amis chinois et français. Michèle et Kent, Emilienne et Thomas, Sun Xiaohua et Wang Lianxing, Zhang Huimin, Xue Xiaoxi, Wang Zidan, avec qui j'ai partagé tant de moments inoubliables… J'étais très contente de vous rencontrer en France ! Et aussi merci à tous mes meilleurs amis à Pékin, Xu Shan, Yan Wei, Zheng Hao, Peng Jingbo, que je connais depuis très longtemps. Cela fait 5 ans que nous sommes très éloignés, mais vous ne m'avez jamais oubliée ! Lire et répondre à vos messages est toujours un moment que j'apprécie beaucoup. Vous comptez énormément pour moi !

Enfin, je remercie de tout cœur ma famille, qui me soutient depuis si longtemps. Mes grands-parents, qui m'ont toujours accompagnée. Vous êtes mes trésors ! Ma tante, Ya Ling, qui partage toutes ses expériences et ses sentiments avec moi et me donne de très bons conseils depuis si longtemps. J'apprends beaucoup avec toi. Papa, qui m'a toujours encouragée et qui m'a toujours faite passer en priorité. Sans toi je n'en serai simplement pas là ! Maman, la personne la plus importante pour moi ! La conversation avec toi chaque jour est le moteur pour commencer une bonne journée. Je sais bien qu'il n'y a que toi, maman, qui peut faire preuve tant de patience et de compréhension. Je voulais simplement te remercier pour tous les sacrifices que tu as faits pour moi et de m'avoir choisie comme ta fille.

Merci à tous !

Table of content

Introduction générale

Nano-émulsions radio-opaques iodées pour applications précliniques en imagerie par rayons X

La micro-tomodensitométrie à rayons X (dite micro-CT, CT = Computed Tomography), est une technique d'imagerie de haute résolution qui consiste d'une part à mesurer l'absorption des rayons X par les tissus, et d'autre part de reconstruire les images et les structures anatomiques en 3 dimensions par traitement informatique. Le préfixe micro vient du fait que les scanners, en comparaison avec ceux utilisés pour l'être humain, sont de dimensions réduites et adaptés au petit animal, réduisant aussi la définition (d'où la haute résolution), pour arriver à des voxels (« pixels » 3D) de 93µm × 93µm × 93µm. La micro-densitométrie à rayons X est beaucoup utilisée pour tester des petits échantillons sur des petits animaux lors d'études précliniques et sert depuis quelques années comme outil pour étudier l'origine, la progression et le traitement des maladies mortelles humaines.

L'agent de contraste est une substance capable d'améliorer la visibilité des structures d'un organe ou d'un liquide organique *in vivo*. Dans le cas de la micro-CT, les tissus mous sont contrastés par des éléments lourds. Les produits de contraste iodés commercialisés sont des molécules iodées hydrophiles de faibles poids moléculaires qui présentent certaines limites aux applications de la micro-CT, telles que l'élimination rapide par la voie rénale, le faible contraste vasculaire, une distribution non spécifique, et occasionnellement une toxicité rénale. Le temps de réalisation d'une mesure en micro-CT est de l'ordre d'une dizaine de minutes, temps durant lequel les produits hydrophiles décrits ci-dessus sont éliminés, ce qui rend impossible les mesures. Pour pallier à ces problèmes, différents produits de contraste décrits dans la littérature ont été synthétisés afin d'avoir une longue rémanence vasculaire. Ces produits de contraste sont sous forme galénique de nanoparticules lipidiques ou des polymères contenant ou encapsulant des atomes de haut poids moléculaires, *e.g*. de l'iode, de l'or ou du bismuth. Ces objets nanoparticulaires sont par exemple des liposomes, des nano-émulsions, des micelles ou des nanoparticules polymères.

Nous nous sommes proposés dans le cadre de ce travail de thèse d'étudier d'une part des nano-émulsions iodées afin d'avoir une longue rémanence vasculaire *in vivo*, une meilleure biocompatibilité et d'autre part de mettre au point une synthèse et une formulation plus simples que celles des agents de contraste nanoparticulaires commercialisés (*e.g*. Fenestra®LC, Fenestra®VC). L'iode a été choisi dans cette étude en raison de son fort pouvoir contrastant, sa bonne sécurité et son coût relativement bas par rapport aux autres substances contrastantes. Les nano-émulsions sont généralement définies comme des gouttelettes d'huile-dans-eau en présentant un diamètre entre 20 et 300 nm. Elles sont maintenant largement utilisées dans les domaines industriel et pharmaceutique, grâce à leur bonne stabilité pendant plusieurs mois. De plus, la dispersion des nano-gouttes est très homogène dans la phase

continue et leur structure biphasique est appropriée pour être un nano-vecteur de principes actifs hydrophobes et d'agents de contraste afin d'avoir une libération prolongée, ciblée ou contrôlée. Les procédés de préparation des nano-émulsions comprennent deux grandes méthodes : haute-énergie et basse-énergie. Nous nous somme intéressés dans le cadre de ce travail à la formulation de nano-émulsions par la méthode de basse-énergie, encore appelée méthode d'émulsification spontanée. Les mécanismes d'émulsification utilisent les propriétés intrinsèques des surfactants et sont basés sur les affinités particulières entre les molécules amphiphiles et les phases aqueuse et lipidique. Cette méthode permet de générer des gouttes de tailles nanométriques de façon spontanée sans apport d'énergie (autre que celle pour homogénéiser le mélange), simplement en mélangeant deux liquides. Les molécules amphiphiles (surfactants non-ioniques) hydrophiles sont solubilisées dans la phase huileuse à température ambiante. Ces molécules amphiphiles, bien qu'étant hydrophiles (balance hydrophile-lipophile ~ 14, pour celles que l'on a utilisé) sont aussi solubles dans la phase huileuse. Cependant, le contact de la phase aqueuse induit un déplacement brutal des surfactants de la phase huileuse *vers* la phase aqueuse. Ce phénomène de transfert est supposé être à l'origine de la formation des nano-gouttes d'huile dispersées dans l'eau.

L'objectif de l'étude était donc de synthétiser des huiles iodées constituant la phase huileuse de nano-émulsions et ensuite de les utiliser pour réaliser des nano-émulsions formées par la méthode d'émulsification spontanée. Les nano-émulsions iodées ainsi formulées ainsi que leurs stabilités ont fait l'objet d'études particulières et de caractérisations par diverses méthodes. Leur toxicité a été évaluée *in vitro*. Leurs propriétés contrastantes ainsi que leurs pharmacocinétiques ont été évaluées *in vivo* sur des souris. Trois nouveaux agents de contrastes iodés ont ainsi pu être synthétisés au laboratoire. Ceux-ci permettent la préparation aisée de nano-émulsions injectables dotées de propriétés contrastes.

La première partie de la thèse comprend un chapitre bibliographie (**Chapitre 1**) qui introduit tous les concepts et le contexte de cette thèse (les agents de contraste nanoparticulaires pour l'imagerie à rayons X, et la génération et caractérisation des nano-émulsions). Dans le chapitre 1 sont présentés différents agents de contrastes nanoparticulaires existants dans la littérature et leurs utilisations pour les applications précliniques par micro-CT ainsi que la génération des nano-émulsions et les différentes méthodes de préparation des nano-émulsions. Les résultats expérimentaux sont ensuite présentés dans les deux chapitres suivants.

La première huile iodée (**Chapitre2.1**) a été dévelopée à partir d'une huile commercialisée de Labrafil® M 1944 CS par la réaction de Wijs. Les nano-émulsions de type huile-dans-eau ont été préparées à partir de molécules hydrophobes iodées par la méthode d'émulsification spontanée. Brièvement, le Labrafil® M 1944 CS iodé a d'abord été mélangée avec le surfactant (Cremophor®

ELP) à un SOR (Surfactant Oil Ratio) choisi (SOR = poids de surfactant/ (poids de surfactant+poids de l'huile) × 100). Une proportion définie de phase aqueuse (un tampon phosphate) a ensuite été ajoutée dans le mélange d'huile-surfactant sous agitation mécanique. Les nano-émulsions ont été formées spontanément au moment du mélange des deux phases. Les nano-émulsions stables de Labrafil® M 1944 CS iodé ont été obtenues à partir d'un SOR = 15% et la teneur en iode était environ de 85 mg I / mL. Un contraste prolongé pendant 4 h a été observé après avoir injecté ces nano-émulsions de Labrafil® M 1944 CS iodées chez la souris.

La deuxième huile iodée (**Chapitre 2.2**) a été synthétisée sur la base de la structure de Labrafil® M 1944 CS (Macrogoglyceridorum oleates), afin d'augmenter la teneur en iode dans l'huile comparée à celle obtenue de Labrafil® M 1944 CS. Cette huile reconstituée a été synthétisée en greffant deux chaînes d'acide gras sur une chaîne de polyéthylène glycol 300 (PEG 300) par estérification en utilisant du chlorure de thionyle. Le monochlorure d'iode était ensuite additionné sur les doubles liaisons des chaînes d'acides gras insaturés de l'huile reconstituée par la réaction de Wijs. La structure de l'huile reconstituée était similaire à celle du Labrafil® M 1944 CS. Afin d'être plus chargée en iode, les acides gras de l'huile reconstituée avaient un nombre de doubles liaisons plus élevé que celui du Labrafil® M 1944 CS. La teneur en iode de cette huile reconstituée peut en effet atteindre 33,87%, soit être 1,3 fois plus élevé que celle de Labrafil® M 1944 CS iodé.

Les nano-émulsions de l'huile reconstituée iodée ont été formées à partir d'un SOR = 30%. Les nano-émulsions ayant une stabilité plus élevée ont été obtenues avec un SOR = 60%. Le pourcentage élevé de ce SOR conduit malheureusement à une teneur de 5,4% en iode qui était de ce fait plus faible que celle obtenue avec du Labrafil® M 1944 CS iodé puisque dans ce cas le taux d'iode était de 8,3%. Dans ce dernier cas, la quantité de surfactant a dû être augmentée pour former des nano-émulsions stables lorsque l'huile était plus chargée en iode. Ceci peut expliquer la diminution de la teneur en iode dans la formulation finale des nano-émulsions de l'huile reconstituée iodée par rapport à celle des nano-émulsions de Labrafil® M 1944 CS iodé. Après la mise en contact de ces nano-émulsions iodées avec des érythrocytes pendant 1 h, une coagulation du sang a été observée. Suite à l'injection de ces nano-émulsions iodées chez des souris Suisse, on a enregistré la mort de ces animaux après deux minutes. De ce fait, les nano-émulsions constituées de cette huile iodée ont été considérées comme un agent de contraste non approprié pour des applications précliniques.

Pour pouvoir disposer d'une huile iodée non-toxique ayant une élimination par la voie hépatique afin d'obtenir un pouvoir contrastant spécifique au niveau du foie, une troisième huile iodée a été synthétisée. (**Chapitre 3.1**). Cette troisième huile iodée a été synthétisée par le greffage d'une molécule iodée (acide 2,3,5-triiodobenzoïque) sur un lipide naturel (α-tocophérol). L'α-tocophérol a été choisi en raison de sa bonne biocompatibilité, de sa structure appropriée pour former des nano-

émulsions par la méthode d'émulsification spontanée et de sa voie d'élimination par le foie. La partie iodée était différente de celle de l'huile reconstituée iodée mentionnée ci-dessus. L'acide 2,3,5-triiodobenzoïque a été choisi pour donner un pouvoir contrastant à la molécule hydrophobe synthétisée. Cet acide iodé est la substance de base des agents de contraste iodés commercialisés. L'acide 2,3,5-triiodobenzoïque a été greffé sur le groupement phénol de l'α-tocophérol par une réaction d'estérification. La synthèse ne contient qu'une étape et le rendement de l'α-tocophérol iodé est satisfaisant (plus de 80% après l'étape de purification). Les nano-émulsions de type huile-dans-eau ont été préparées à partir de cette nouvelle molécule hydrophobe iodée de la même façon que celle qui avait été utilisée pour la première huile iodée décrite ci-dessus. Le surfactant utilisé était du Cremphor® ELP et la phase aqueuse était constituée d'un tampon phosphate afin d'avoir la même osmolalité que celle enregistrée *in vivo*. Les nano-émulsions de l'α-tocophérol iodée ont été formées à partir d'un SOR = 30% et les nano-émulsions ayant une stabilité plus élevée ont été obtenues à partir d'un SOR = 40%. La taille des nano-émulsions qui ont un SOR = 40% était environ de 85 nm et la teneur en iode a été déterminée à environ 106 mg I / mL soit presque 2 fois plus élevée que celle du Fenestra® qui est d'environ 55 mg I / mL.

Avant de réaliser les tests *in vivo*, chez des petits animaux de laboratoire, la biocompatibilité des nano-émulsions contenant de l'α-tocophérol iodé a d'abord été évaluée à l'aide de l'étude de stabilité des nano-émulsions en présence de sérum, du test d'hémolyse, et du test de cytotoxicité (test MTT). Les nano-émulsions iodées ont été mises en contact pendant 5 h avec des érythrocytes de mouton (dans un rapport de 10% en volume) pour mimer les conditions d'injection *in vivo*. Le résultat a montré que les nano-émulsions n'avaient induit ni hémolyse supérieure à 5% jusqu'à 5 h ni une tendance croissante d'hémolyse au cours du temps. Ces nano-émulsions iodées ont montré aussi une très bonne stabilité en présence de sérum pendant 20 h. La cytotoxicité du nouvel agent de contraste a été évaluée par le test MTT. Les nano-émulsions de l'α-tocophérol iodé ont été mises en contact avec des cellules hépatiques de souris (BNL_CL2) pendant 24 h. Les résultats ont indiqué une bonne biocompatibilité jusqu'à une concentration de 0,27 mg I /10^4 cellules, ce qui représente une concentration beaucoup plus élevée que celle retrouvée *in vivo*. Une autre étude sur l'aorte thoracique de rat a montré que les nano-émulsions de l'α-tocophérol iodé n'entrainent pas d'altération vasculaire, notamment pas d'altération de la fonction d'endothéliale suite à une exposition prolongée (**Chapitre 3.2**). L'ensemble des résultats obtenus a montré que les nano-émulsions à base de l'α-tocophérol iodé avaient une très bonne biocompatibilité.

Suite aux essais de biocompatibilité, nous avons réalisé des essais *in vivo* sur des souris afin d'évaluer les propriétés contrastantes des nano-émulsions contenant de l'α-tocophérol iodé ainsi que leur pharmacocinétique. 0,18 ml des nano-émulsions de l'α-tocophérol iodé ont été injectées par voie intraveineuse chez des souris Suisse. Des contrastes significatifs ont été observés pendant plus de 9 h

au niveau des ventricules cardiaques, des grandes artères et des veines. Le contraste observé au niveau du cœur 9 h après injection signifie que les gouttelettes de nano-émulsions restent dans la circulation sanguine. Un contraste significatif a été observé au niveau du foie tout de suite après injection ainsi qu'une forte accumulation de ces nano-émulsions iodées dans le foie 48 h après injection. La forte accumulation de l'agent de contraste iodé au niveau du foie indiquerait que ces nano-émulsions pourraient être éliminées par voie hépatique. Le contraste significatif du foie demeurait plus de 134 jours après l'injection. Le contraste prolongé après une seule injection du produit de contraste est souhaitable de sorte à conduire à une diminution de la toxicité potentielle causée par l'injection répétée d'un même produit.

Ce nouvel agent de contraste basé sur des nano-émulsions contenant de l'α-tocophérol iodé présente d'excellentes propriétés contrastantes pour différents organes. Un contraste prolongé a été observé dans la circulation sanguine et une accumulation persistante s'en suit au niveau du foie. L'ensemble des résultats obtenus a montré que ce nouvel agent de contraste iodé combine à la fois les propriétés d'un agent de contraste à longue rémanence vasculaire et un agent de contraste spécifique du foie.

En conclusion, ce travail de thèse a eu pour objectif le développement d'agents de contraste iodés sous formes de nano-émulsions pour des applications précliniques en imagerie biomédicale. Trois différentes huiles iodées ont été synthétisées et utilisées comme partie contrastante dans les nano-émulsions. Enfin, les nano-émulsions de l'α-tocophérol iodé nous ont permis d'atteindre l'objectif de cette thèse. Ces nano-émulsions iodées ont montré une très bonne biocompatibilité et combinent à la fois les propriétés d'un agent de contraste à longue rémanence vasculaire et un agent de contraste spécifique du foie.

De nombreuses perspectives s'ouvrent suite à ce travail, notamment sur le système de nano-émulsions de l'α-tocophérol iodé. Dans un premier temps, il sera primordial d'évaluer la toxicité de nano-émulsions contenant de l'α-tocophérol iodé par des études anatomiques et des études biologiques. L'objectif est de compléter les études de toxicité à long terme, ce qui est un des points essentiels pour tous les agents de contraste nanoparticulaires. De plus, les nano-émulsions contenant de l'α-tocophérol iodé conduisent à une accumulation hépatique significative et prolongée. Par conséquent, l'évaluation du seuil de la toxicité du produit destiné à une imagerie hépatique par injection répétée devient très importante. Les études ultérieures seront axées sur l'utilisation de ce nouvel agent de contraste nano-émulsionné contenant de l'α-tocophérol iodé dans le cadre de la vectorisation passive du foie. Les nanoparticules s'accumulent dans les sites sains du foie en raison de la présence de cellules de Kupffer et des hépatocytes et donnent lieu à une hyper-atténuation du tissu sain et à une hypo-atténuation aux sites métastasiques du foie. Les nano-émulsions iodées développées dans le cadre de ce travail doctoral pourraient dans ce cas être un agent de contraste co-administré avec un agent anticancéreux

hépatique afin d'aider à évaluer l'efficacité thérapeutique au cours du temps sans devoir réinjecter le produit de contraste pendant plus de 4 mois chez un même sujet. Les nano-émulsions de l'α-tocophérol iodé développées dans ce travail peuvent aussi être considérées comme un outil pour des études de la vectorisation active. Des molécules spécifiques aux différents organes peuvent être greffées à la surface de ces nano-émulsions en fonction des cibles.

Chapter1.

(1). Nanoparticulate contrast agents for Preclinical Targeted X-rays imaging

(2). Nano-emulsions: Overview and Applications

Ce premier chapitre reprend les différents concepts et le contexte de cette thèse. Il est consisté en deux grandes parties : 1) la présentation globale des agents de contraste nanoparticulaires et 2) la formulation générale des nano-émulsions. Nous présenterons dans un premier temps les différents agents de contrastes nanoparticulaires mentionnés dans la littérature et leurs utilisations pour les applications précliniques par rayons X. Dans un second temps, nous nous intéresserons à la formulation générale et aux différents procédés de préparation des nano-émulsions.

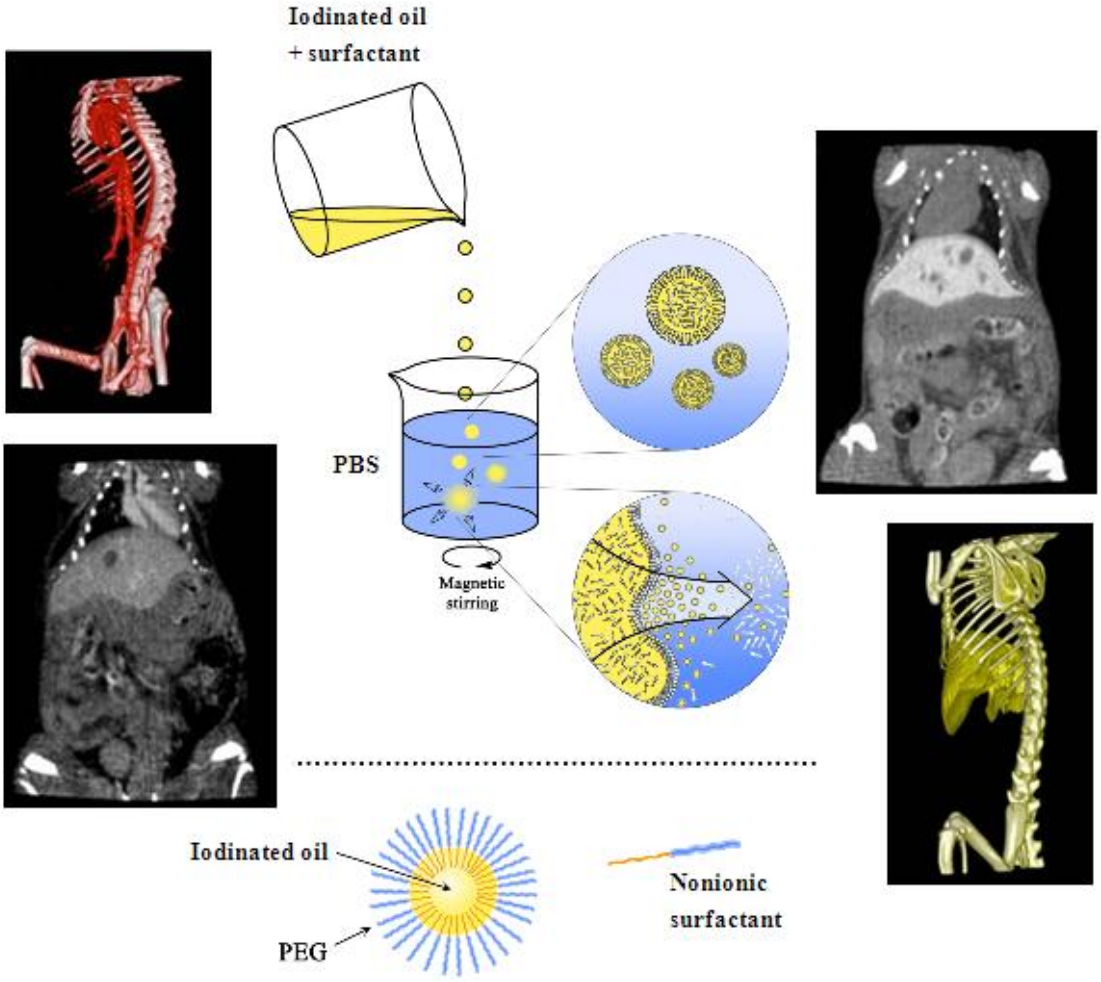

Contrast Agents for Preclinical Targeted X-ray Imaging

Xiang Li[a], Nicolas Anton[a], Guy Zuber[a], Thierry Vandamme[a,*]

[a] *Université de Strasbourg, Faculté de Pharmacie, 74 route du Rhin, 67401 Illkirch Cedex, France; CNRS 7199 Laboratoire de Conception et Application de Molécules Bioactives, équipe de Pharmacie Biogalénique, 67401 Illkirch Cedex, France.*

Abstract

Micro-computed tomography (micro-CT) is a widely used three-dimensional radiographic imaging technology for small animal models. This imaging modality is cost-effective, fast, and accurate (allows detecting metastases as small as 300 μm), appears as an interesting compromise for preclinical research on tumor imaging. However, the main limitation of micro-CT lies in the poor efficacy or toxicity of the contrast agents. Moreover, contrast agents for micro-CT have to be stealth nanoparticulate systems, *i.e.* preventing their rapid renal clearance. The chemical composition and physicochemical properties will condition their uptake and elimination pathways, and therefore all the biological fluids, organs, and tissues trough this elimination route of the nanoparticles will be contrasted. Furthermore, several technologies playing on the nanoparticles properties, aim to influencing these biological pathways in order to induce their accumulation onto given targeted sites, organs of tumors. In function of the methodologies carried out, taking benefit or not of the action of immune system, of the natural response of the organism like hepatocyte uptake or enhanced permeation and retention effect, or even accumulation due to ligand / receptor interactions, the technologies are called passive or active targeted imaging. Through the present review, we present the state-of-the-art of targeted X-ray imaging technologies, discussing the recent advanced of *in vivo* targeting of nanoparticulate contrast agents, and the influence of the formulations, nature of the nanocarrier, nature and concentration of the X-ray contrasting materials, effect of the surface properties, functionalization and bioconjugation.

Key words: Computed tomography, micro-CT, X-ray imaging, targeting, nano-emulsion

1. Introduction

Over the last century, the main progress of medicine lies in the development of medical imaging. Whatever, the imaging technology (X-ray or *computed tomography* (CT), echography, magnetic resonance imaging (MRI), positron emission tomography (PET), single-photon emission computed tomography (SPECT) and optical imaging), the principle still remains the same: to build a two-dimensional (2D) or three-dimensional (3D) image containing useful information thanks to a contrast within the image, highlighting the physiology or metabolism of the patient. In the

*Corresponding author
Email addresses: vandamme@unistra.fr (Thierry Vandamme)

case the contrast is naturally present, it is generally improved through contrast agents administrated. Then, the dynamic behavior of contrast agents in the body allows observing anatomic or pathologic structure, invisible without contrast agent. If medical imaging has seen an extensive development over the last decades, the contrast agents remain very limited, and the main limit for human is their toxicity. In addition, for the last years, imagers were specifically developed for small laboratory animals, for preclinical research, and notably in the field of oncology. This technology allows reducing the number of animal for experimental protocols, in accordance to the ethical guidelines on animal experimentation. Some other limitations of preclinical imaging lies in the cost of imagers and specific contrast agents, but also their toxicity. Moreover, functional imaging based on the radioactive labeling of tissues (PET, SPECT) involves additional drawbacks regarding supply, storage, managing of radioactive animals and wastes. This explains the great emergence of preclinical optical imaging, which concerns 19% of the images performed. However, optical imaging (like fluorescence) has a very low signal penetration in the body, which is the main limitation of this technology for small laboratory animal, even more true for human. Moreover, the low spatial resolution and the absence of signal for non-labeled tissues do not allow obtaining anatomic images only with the optical modality. This is precisely why the solution for providing a complete solution passes through its association with another modality. In this respect, 43% of the images are multimodal. The second most cost-effective and efficient modality is the computed tomography (X-ray scanner), but constitutes today only 7% of the medical images done, which is likely linked to the costs and limits of the X-ray contrast agents. Hence, the most recent apparatuses combine theses two modalities.

In this context the development of non-toxic, cost-effective, and multimodal contrast agent appears as a fundamental issue in the today's medical research. Biological targeting of contrast agents definitively enters in these objectives since it contributes to the efficiency the imaging properties of the product, along with reducing the amount administrated, and thus the toxicity and price. In addition and more generally, targeting of tissues, organs, or pathologies, provides another dimension of the applications of contrast agents. These new contrast agents have to answer the needs of researchers, that is to say a better detection of tumors and a better follow-up of the response of treatments (49% and 68% of the images, respectively). Likewise, these technologies allow the visualization of the tumor growth in time, and therefore allow evaluating the *in vivo* efficient of a therapy. Actually, 70% of the medical imaging concern cancer research. One of the final objectives can be found in medical advances like the image guided mini-invasive or non-invasive surgery, consisting in operating a patient with using a 3D medical image to guide the surgeon or an automated robotic system.

To summarize, the design and development of efficient, cost-effective, and multimodal contrast agent constitutes major research and economic issues, and especially for cancer research. Moreover, contrast agents for X-ray imaging modality emerges as a very hot challenge today, since the commercially available solutions are not really satisfactory. In the present paper, we propose to review in detail contrast agents for CT imaging, and more particularly the CT targeted imaging technology, which only emerged in the last five years, and potentially offers huge potentials in terms of advanced diagnosis of tumors and personalized therapies.

CT contrast agents currently used for human are iodinated hydrosoluble molecules. These molecules have some

well-known limitations, like a fast renal clearance and acute renal toxicity, giving them incompatible some applications, and notably the image guided surgery (CT for human) or their use in micro-CT (for small laboratory animal). As a result, using human CT contrast agent for preclinical imaging is simply impossible insofar as they are rapidly eliminated from the small laboratory animal (in less than 20 seconds) while the best preclinical imagers need at least one minute for completing the acquisition (and the standards ones need 12 minutes). This is precisely the reason why many research efforts were led form the last decade to develop specific products in order to increase the residence time in bloodstream of CT contrast agents. Their optimized properties can be easily summarized in four points as follows. ***(i)*** Contrast agent should present a dimension sufficiently high to reduce or avoid the renal clearance: the X-ray contrasting atoms have to be encapsulated in a nanocarrier with an ideal size around 100 nm. ***(ii)*** These nanoparticles (NPs) must have a functionalized surface conferring stealth properties, which is generally done with grafting hydrophilic like polyethylene glycol (PEG). ***(iii)*** Loading of contrasting atoms should be sufficiently high to allow their using as CT contrast agent (ideally for iodine, around 100 mg of iodine per mL). ***(iv)*** NPs contrast agent should be non-toxic on the one hand, and should not modify the biological metabolisms after their administration (which is the case today with the currently available preclinical CT contrast agents, like Fenestra® or ExiTron®). However, the formulation of nanoparticle, in contrast to single contrasting molecules, involves controlling the *in vivo* stability of the nanocarriers themselves, their toxicity, as well as other aspect like their elimination from the body.

Specific commercially available contrast agent for micro-CT were developed and exhibit a circulation time in blood pool of around 4 hours before being progressively eliminated by the liver through the biliary system in 7 days. Such a product applied to the human would present a considerable advantage for all the image-guided mini-invasive surgery procedures, since all the images necessary for the operation can be performed with only one administration of contrast agents, and without associating potential renal toxicity. However, the toxicity of all the available products is not negligible and prohibits any transposition to human, and the current high price limits their usage for preclinical research.

Several new strategies of formulation of such nanoparticulate contrast agents for CT preclinical imaging were undertaken from a few decades, giving rise to realistic solutions fulfilling the specifications above-described. However, any "ideal" solution is proposed, that is to say that each one presents a limiting drawback, like a multi-step chemistry, multi-step formulation process, a low contrasting atoms concentration, a significant toxicity, or a poor biocompatibility. The emerging solutions will be found in the optimization of these recent advanced, and this passes through the simplification of the formulations and increase of the contrast agent encapsulation ratio, meaning that the amount to be injected is also reduced, which directly consequences in a reduction of the toxicity and side effects. In this context, targeting the nanocarriers to specific organs, tissues or disease like tumor, not only contribute to the optimization above-described reducing the amount of contrast agent necessary to obtain an exploitable signal, but also opens a new dimension allowing emphasizing biological areas not specifically distinguishable with the classical contrast agent, even in a same organ like hepatic tumors [1]. In the case of tumor or lymph node detections targeted imaging showed significant preliminary results, giving this technology as very promising for advanced diagnosis and image-guided

surgery.

In the present article, we propose to review of the state-of-the-art of the *targeted X-ray imaging technology* and their preclinical applications. Even if targeted imaging is an important challenge in numerous medical domains, it is only from the last years that effective research works on targeted imaging for computed tomography were reported. This likely due to the very complexity of the challenged, including fulfilling the four points described above from ***(i)*** to ***(iv)***, along with the control of the NPs targeting either through a passive targeting of tumors known as "enhanced permeability and retention effect" (EPR effect), or through the active targeting with ligand / receptor technology. In a first part, we will focus on the types and formulation of contrast agent nanocarriers, and then, in a second part, we will review their adaptability to the targeting technologies in function of the biological target, to the choice of the ligand / receptor couple, and to the resulting *in vivo* results, *e.g.* pharmacokinetics. In this second part, the critical points involved in the formulation of targeted X-ray contrast agent will be exposed, illustrated with the solutions detailed in literature, detailing the technologies involved and the experimental limits. The idea is to allow the researcher to find experimental solutions easily reproducible in function of the biological target, the type of nanocarrier, and the imaging technology. In a third, we propose a discussion on the most recent advances of targeted imaging and the interest and potential of combining targeted imaging with drug delivery.

2. Micro-computed tomography

X-ray based imaging, as discussed above, is considered as a good cost-effective compromise, able to provide high throughput and adequate 3D resolution [2]. Micro-CT is a three-dimensional radiographic imaging technology having numerous advantages like noninvasive high spatial resolution, allowing to work on small laboratory animal [3, 4]. Based on clinical CT principle, which is the acquisition of the X-ray attenuation through the specimen, micro-CT apparatuses present a design adapted to the preclinical research on mice or rats [5]. The basic setup consists of coupling the X-ray source with a high resolution X-ray detector [6–8] following two possible configurations: ***(i)*** Either both source and detectors rotate around the animal or ***(ii)*** the specimen is rotated within the fixed source and detector [9]. The most common commercial apparatuses are designed following the former configuration, which allows imaging of the animal without tight fixations [2, 8, 10]. The different projections acquired through different angles are analyzed with specific software and give a three-dimensional matrix of voxels, each one containing the average X-ray attenuation of the area. One significant advantage of micro-CT is the voxel resolution between 1 and 100 μm, decisively adapted to the preclinical applications and much higher than that the one of clinical CT [4, 5, 11, 12].

In this respect, micro-CT scanners provide either anatomic or functional information of specimen with the appropriate contrast agent [13]. In addition, CT imaging is the only structural imaging modality allowing the high resolution volumetric study of vascular structures. This even permits visualizing of neo-vasculature or angiogenesis involved in some pathology [4]. Micro-CT is also an important tool for longitudinal imaging of tumor develop-

ment, by providing a more accurate assessment of metastatic progression and as well emphasizing the efficacy of therapeutic treatments [14]. However, a limit of this technology lies in the fact that the classical contrast agent, even long-circulating or tissue specific contrast agents, do not allow the direct detection of lesions or tumors, and especially the detection of early metastasis and small lesions. It is due to the generally poor natural contrast between tumor and healthy tissue. For this reason, many efforts are focused on the development of targeted contrast media [15–17]. As a result the detection volume of early metastasis by targeted contrast agent-loaded NPs can be decreased as small as $\sim 300\ \mu$m [18–20].

To conclude on the limits of the micro-CT technology itself, we have to consider the ionizing effect. Indeed, to maintain the images quality as the voxel size is decreased, the X-ray exposure must be increased. The dose of a single anatomical image is around 0.1 Gy. Higher imaging doses of 1.5 Gy have been reported for cardiac gated imaging in mice but should never exceed 6 Gy, even in multiple sequential scans procedure, because this threshold is considered as lethal for a small rodent [8].

3. Blood pool contrast agents: A prerequisite for targeted imaging

As discussed in the Introduction section, the clinically water soluble contrast agents are not compatible with micro-CT applications, hence the necessity to develop surface-controlled NPs containing high Z-number atoms [21–25]. Once injected, these NPs have to enhance a contrast in the desired biological target, that is to say blood pool, organ, tissue, or specific site like tumor. In all cases, their rapid elimination from the body has to be avoided.

On the one hand, the control of particle size can reduce renal elimination through glomerular filtration (with pore diameter from 50 to 100 nm [26]). A diameter distribution centered on values higher than 100 nm generally prevents such renal elimination. On the other hand, in order to avoid the rapid recognition of these NPs by the immune system, their surface must be controlled and/or modified to develop stealth properties. This is simply a fundamental parameter conditioning the biological efficiency of the contrast agent.

Thus, NPs interface should present hydrophilic properties, resulting in, along with their nanoscale, to minimize uptake by the mononuclear phagocytes system (MPS) and/or the reticuloendothelial system (RES) [27]. The surface modification can be achieved using biocompatible hydrophilic polymers like polyethylene glycol (PEG) and its derivatives [28–31].

Besides, it appears that a decrease at minimum of the elimination time of the nanopartculate carriers is simply a *basic condition* for designing particles for targeted imaging. Indeed, targeting a carrier is based on the gradual accumulation at a given biological site, implying a long circulation in bloodstream of these carriers, letting the time to the specific affinities with the targeted sites to become visible. In other words, the first step of the formulation of a targeted contrast agent for micro-CT, is the optimization of the blood pool residence time.

As the nature of the nanocarrier itself has a crucial role in the expected *in vivo* result, let us first present below the different nanoparticles generally used as template for contrast agent encapsulation and surface modification, for the

fabrication of tools for targeted imaging.

3.1. nano-emulsions

Nano-emulsions consist of suspensions of nano-droplets sizing from 20 to 200 nm, generally oil-in-water emulsions [32–37]. Oil-in-water nano-emulsions were shown to be promising template for CT imaging, owing to their potential for encapsulating high proportion of lipophilic contrast agents, and their great stability in suspension [38–41]. In addition, with controlling the surface properties (*e.g.* with using PEGylated surfactants), the opsonization by RES system is reduced, and the nano-emulsions can exhibit stealth properties, thus prolonging the circulation time [31, 38].

To date, commercially available nano-emulsions based contrast agent for X-ray imaging were formulated from poly-iodinated triglyceride (ITG) [38, 42, 43]. Two types exists, either announced as blood pool or hepatocyte-selective contrast agents for preclinical imaging [44–48]. The former, Fenestra VC® (vascular contrast), and the latter, Fenestra LC® (liver contrast), both present an iodine concentration around 50 mg I/mL [38, 42, 43]. ITG are formulated in the form of synthetic lipid nano-emulsion, stabilized with phospholipids, cholesterol, and PEGylated lipids for the blood pool version, are optimized to resemble chylomicron remnants systems [44]. Using PEGylated nano-emulsions gives a contrast to major vessels, liver parenchyma from vasculature, spleen and even very thin tumor vessels [43, 49]. Iodinated nano-emulsion based contrast agents constituted an important advance for the users of micro-CT scanner, and mainly for structural imaging.

Besides the commercial iodinated nano-emulsions described above, some new example were recently reported in literature. The principle remains simple, and the results can be efficient: it consists of the synthesis of iodinated oil at high iodine content, and its formulation in the form nano-emulsions with surface controlled and low toxicity. An example is given by de Vries *et al.* [50], where the authors synthesized three iodinated oils through the condensation of 2,3,5-triiodobenzoic acid to either 2-octanol or 3,7-dimethyl-1-octanol or 2-methyl heptanoic acid. Surfactant used to stabilize the nano-droplets were: a lipid DSPC (1,2-distearoyl-sn-glycero-3-phosphocholine), a Pluronic F68 (PEG-b-poly(propylene oxide)-b-PEG, or a PBD-PEO (poly(butadiene)-b-PEG). Compared to the commercial iodinated nano-emulsions (Fenestra®), all these emulsions showed a significantly lower toxivity on MTT tests. The most promising candidate found by these authors were the system PBD-PEO / 3,7-dimethyloctyl 2,3,5-triiodobenzoate. As a result, they induced an excellent *in vivo* contrast enhancement of the vasculature with long circulation time (higher than 3 hours), without any signs of acute toxicity. The last advanced in that field lies in optimized systems combining simple iodination chemistry, simple nano-emulsification process (spontaneous emulsification), simple surface control and any toxicity. These novel systems are based on low-energy nano-emulsification processes applied to iodinated oils [39–41], and they allow reaching iodine concentration around 142 mg Iodine/mL, and half-life in bloodstream up to 10 h. The first example illustrated in Fig. 1 A is a stealth nano-emulsion formulated from a iodinated vitamin E by spontaneous emulsification [41]. Vitamin E is taken as non-toxic molecules naturally present in the organism for the reducing the potential toxicity of the contrast agent. Triiodobenzoic acid was covalently grafted on vitamin E,

conferring to the core of the nano-emulsion droplets a high iodine content, around 41.8 wt.%, and therefore a great attenuation properties of the nano-emulsions, as well as a very poor toxicity. Fig. 1 A shows the vasculature 30 min after i.v. administration, with half life being 10 h. The vascular system clearly appears contrasted over the mouse body (Fig. 1 A_1), the product allow emphasizing the blood compartment in heart (Fig. 1 A_2) or the irrigation of the liver (Fig. 1 A_2). In the same way, we have recently design nano-emulsions formulated from commercial iodinated oil (Lipiodol® from Guerbet, Paris) generated through spontaneous emulsification. The contrast in the blood compartment, showing the organ irrigation, is significantly enhanced as illustrated in Fig. 1 B acquired 30 minutes after i.v. injection. These two latter examples showed a really cost-effective formulation for potential industrial transposition, since the nano-emulsification generally involved strong energy supplying (*e.g.* with high pressure homogenizer), which can be get round spontaneous processes, for the same result.

Besides, others interesting reports show the potential of these lipid nano-emulsions, owing to their long blood pool circulation time, for imaging of lymph nodes [51–53]. In addition, since the transport of lipids from intestine to the blood circulation, by chylomicrons, primarily occurs through the lymphatic system, such nano-emulsions found application as percutaneous CT lymphographic agent [54]. They selectively and sustainably enhanced the contrast of lymph nodes after subcutaneous administration, as well as inducing a significant contrast of more distant node groups. Such targeted imaging persisted until 480 min after injection [54].

Another example of efficient nano-emulsions for micro-CT imaging lies in functionalized tantalum oxide (TaO_x) containing nano-droplets [55]. In that case, the surface modification consists in a pegylation and optical labeling with rhodamine-B-isothiocyanate. Nano-emulsions were intravenously administrated in rats showing a prolonged blood pool contrast enhancement followed by a gradual accumulation of iodine the liver and spleen. It follows therefrom that TaOx lipid nano-emulsions is efficient as contrast agent for have potentials for angiography, but also as RES-targeted imaging, improving the detection of metastases in liver and lymph nodes.

3.2. Liposomes

Liposomal based contrast agents for CT imaging have been developed for 20 years to increase the *in vivo* residence time in small animals [22, 56–58]. The first preparations were based on the encapsulation in stealth liposomes of the above-discussed hydrophilic iodinated contrast agents like iodixanol [59] or iomeprol [60]. The reported concentration of iodine of the suspension can vary from 30 mg/mL [22] to higher than 100 mg/mL [61], actually relies on the liposome preparation and formulations methods. This latter example from Ref. [61] showing the efficiency of liposomal-based as contrast agents for blood pool (heart) contrast enhancement is illustrated in Fig. 1 C. Different organs, such as aorta, pulmonary vasculature, heart, liver and spleen were well visualized with these iodinated liposomes [21, 61–63]. In the case of long circulating contrast agents, the stealth properties are insured by PEG grafting onto the liposomes surfaces [61, 62]. Such tools were used to detect and study the pulmonary emboli in rabbits [62]. They showed good and uniform opacification of blood pool, and thus of the pulmonary artery, with a detectable contrast enhancement stable until 4 h after injection. Liposome containing hydrophilic contrast agents attained efficacy

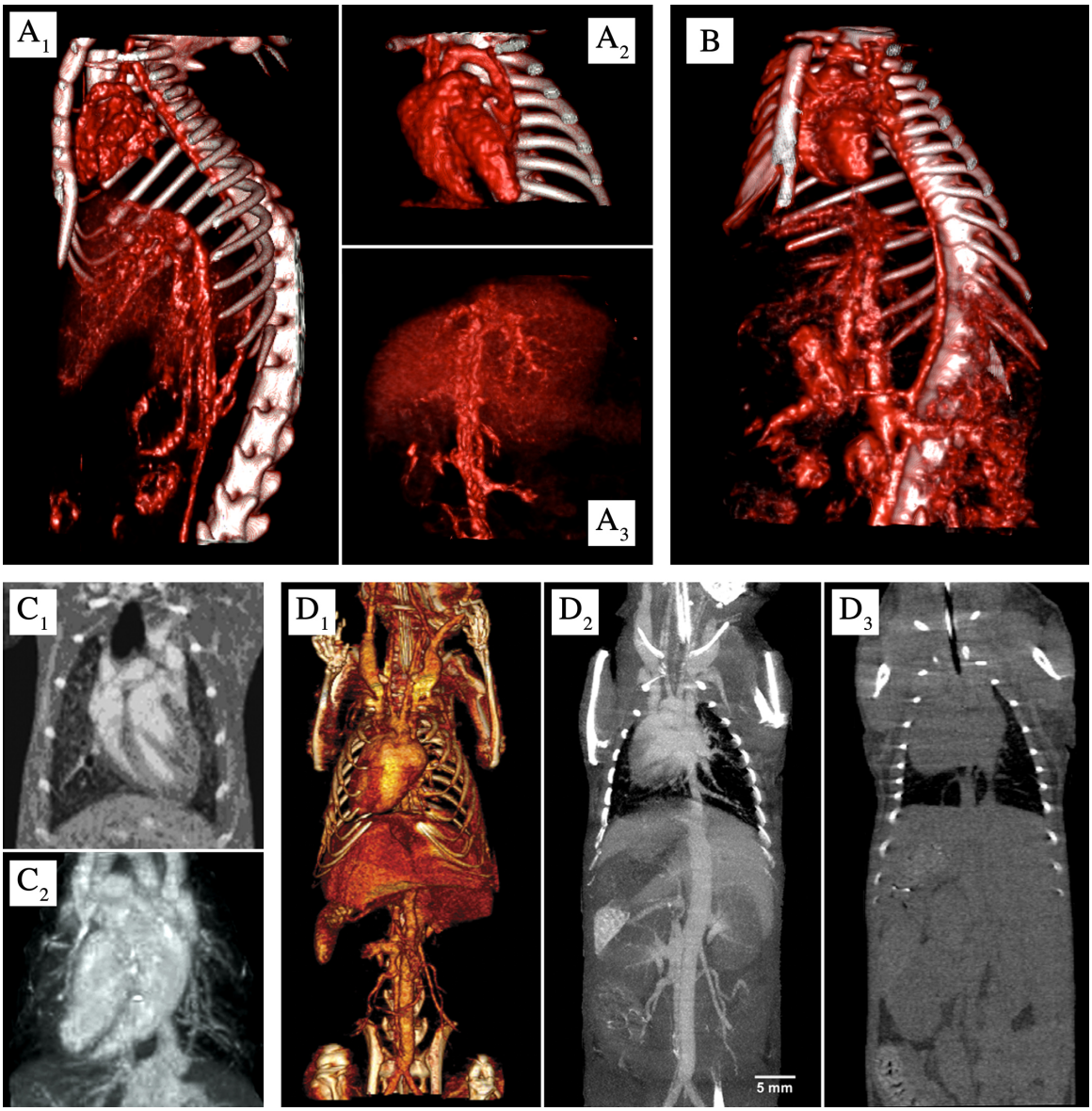

Figure 1: Micro-CT imaging of blood pool. (A) From Ref. [41]: 3D reconstruction of blood compartment after i.v. administration of long circulating nano-emulsion in mouse. Acquisition 30 min post-injection, oil: iodinated vitamine E nano-emulsions, process: spontaneous emulsification, surfactant: PEGylated nonionic Cremophor ELP®. (A_1) whole animal body showing the organ irrigation, (A_2) detail on heart, (A_3) detail on the liver vasculature. (B) From Ref. [40]: 3D reconstruction of blood compartment after i.v. administration of long circulating nano-emulsion in mouse. Acquisition 30 min post-injection, oil: Lipiodol®, process: spontaneous emulsification, surfactant: PEGylated nonionic Cremophor ELP®. (C) From Ref. [41]: Vascular constrast enhancement 60 min after i.v. injection of iodixanol-containing liposome in mouse. (C_1) Coronal section of heart, (C_2) maximal intensity projection of cardiac and pulmonary vascular trees. (D) From Ref. [81]: (D_1) and (D_2) CT angiography acquired 30 min after i.v. injection of ExiTron nano 12000® in mouse. (D_1) 3D image reconstruction and (D_2) maximum intensity projection in coronal orientation. (D_3) curved maximum intensity projection in coronal orientation before injection (control).

and safety assessment in human phase-I clinical trial. It is noteworthy that such a formulation involved significant experimental difficulties resulting in costly production, like the control of the stability of this complex structure, the control of the iodinated molecule leakage, the formulation and purification.

X-ray contrasting liposomes can also be obtained through the chemical grafting of the contrating atoms onto the lipids. Iodoliposomes were firstly prepared and used as imaging contrast agent by Elrod *et al.* [64]. Iodine was located exclusively within the bilayer, giving a concentration of the solutions around 40 mg I/mL.

3.3. Polymeric nanoparticles

Many different types of polymeric NPs have been developed as contrast agents in the literature. They may be sub-classified as dendrimers [65, 66], nanocapsules [67], nanotubes [68] or polymer-coated NPs [69–71].

Dendrimers are a class of highly branched, synthetic macromolecules with well-defined structures [72, 73]. Incorporation of high Z-number atoms is either done by their grafting onto the particle surface, or through their concentration and encapsulation in the dendrimer core. The literature reports examples for which the formulation is based on a clinical hydrosoluble iodinated molecule (*e.g.* iobitridol) grafted onto the outer layer of a dendritic polylysine, by a condensation reaction with the terminal free amino groups, while the dendrimer core is made with PEG [65]. Likewise, another example [66] presents the formulation of iododendrimers through the grafting of hydrophilic triiodo amino acid (DMAA-IPA) onto the surface of PAMAM dendrimers (G-4-(DMAA-IPA)$_{37}$). The entrapment of X-ray contrasting materials within the dendrimer core also appears as an interesting option in the formulation of X-ray nanoparticulate contrast agents, *e.g.* by a specific in situ reduction of $HAuCl_4$ forming gold nanocrystals in the dendrimer core [74–76]. In order to optimize the contrasting properties, combination a several approaches can also be considered, like the one described by Guo *et al.* [77] incorporated both gold NPs and iodinated contrast agent (complexation with diatrizoic acid, DTA) within one single PAMAM dendrimers. These sophisticated nanocomplexes showed high X-ray attenuation properties up to twice the one of the clinically available hydrophilic iodinated molecules like Omnipaque®. However, to date, the limitation of these dendrimer based X-ray contrast agents is their poor residence in blood pool, no longer than 30 minutes after injection [65, 75]. This problem found a natural solution with the surface functionalization with the PEGylation of NPs, *e.g.* with gold-entrapped dendrimers [78]. Once intraperitoneal administrated in mice, these latter gold containing PEG-dendrimers have been showed to be efficient blood pool contrast agents, but also interestingly efficient for tumor targeting imaging. The obvious enhancement of the entire tumor area has been seen until 6 h after injection, in the absence of surface bioconjugation, attributed in that case to the EPR effect presented above [79].

Let us regard now the other types of polymeric nanoparticles designed as X-ray contrast agents. Even if iodine is a good compromise between price, toxicity and X-ray attenuation properties, other elements like heavy metals, have been also shown to be excellent candidates for this purpose, like for instance gold or bismuth [80], due to their good X-ray absorption properties and chemical stability. In order to facilitate the surface functionalization, or their protection, stability, metal nanocrystals are often embedded into polymeric NPs, directly improving their *in vivo* behavior like

the circulation time in blood pool, described in literature [67] to give significant contrast up to 4 h after injection. The first bismuth sulphide (Bi_2S_3) nanoparticles (10-50 nm), coated with polyvinylpyrrolidone (PVP) were developed by Rabin *et al.* [24]. One great advantage of using heavy metal is their X-ray adsorption coefficient definitively higher than the one of iodine, conferring them better properties for a same concentration. This is the case with PVP-bismuth sulphide NPs, along with a blood opacification, persisting until 140 min after injection. A commercially available example (ExiTron nano 12000®) is a polymeric nanoparticulate system formulated with alkaline earth metal. A significant blood contrast enhancement is observed (see Fig. 1 D from Ref. [81]) with half life in blood around 3 h, before its accumulation in liver for more than 100 days.

On the other hand, the coating of inorganic nanoparticles with macromolecules like polymers is a definite necessity in order to stabilize the NPs suspension, to prevent the fast recognition by immune system, by also to induce a specific targeting with the appropriate functionalization. More than half of the published example for that purpose of X-ray imaging concerns gold nanoparticles [80] since they have excellent X-ray attenuation properties and they are considered to be biocompatible and nontoxic *in vivo* [70, 82–88]. Coated gold nanoparticles found numerous application for targeted imaging, here is a panel of the representative examples and possibilities. Liver-specific contrat agent: heparin-coated gold nanoparticles [89] showed a maximum accumulation in liver tissue at 2 h post injection into mice. Lymph node targeting: mixed PEG / antibody (anti CD4) coating gave efficient result in targeted imaging of lymph node [90]. Tumor targeting: mixed PEG / peptide (bombesin) showed a specific targeting of human prostate tumor cells [91]. Bone targeting: glutamic acid coated gold nanoparticles were efficient for targeting micro-damaged bone tissue [92].

3.4. Polymeric micelles

Polymeric micelles are formed from self-assembly of amphiphilic block polymers when dispersed in aqueous media, typically with diameters below 100 nm [93, 94]. One main characteristic is their low critical micelle concentration (CMC), lower than conventional detergents in order to avoiding their disruption when they will be diluted in bloodstream. This is a fundamental criterion in pharmaceutical applications. Such micellar polymer-based system can be used as micro-CT blood pool contrast agents with the incorporation of contrasting materials. Polymeric micelles have an inner hydrophobic core and an outer hydrophilic shell, allowing incorporation of various hydrophobic compounds, which may be drugs, or molecules extending the stability of the micelle for modifying the biodistribution pattern [38, 73, 95]. Contrast agents can be incorporated within the core and/or covalently grafted onto the polymers itself [38].

Torchilin and coworkers [25, 96] reported synthesis of iodine-containing amphiphilic bock-copolymer (MPEG-iodolysine), the hydrophilic part being methoxypolyethyleneglycol (MPEG) (hydrophilic cloud around the micelle) and the lipophilic one is a poly[ϵ,N-(triiodobenzoyl)]-L-lysine (PLL) (inner hydrophobic core of the micelle). The block-copolymer micelles exhibits a size around 80 nm in water, with a iodine content higher 30 wt.% (of the polymer molecular weight). These iodinated micellar contrast agent injected intravenously gave significant contrast enhance-

ment of aorta, heart, liver and spleen. In addition, the contrast in blood pool does not show sign of decrease during 3 hours. However, due to the low iodine content compared to other systems (like nano-emulsions), the injected volume have to be high in respect to the vascular volume in small animals and this appears as a limitation for their use and commercial development of preclinical imaging.

3.5. Other nanoparticles

Finally, another type of formulations can be classified as nanoparticles like the crystalline nano suspension of iodinated compounds, like ethyl-3,5-bis(acetylamino)-2,4,6-triiodobenzoate [97, 98]. These NPs were described to be selectively recognized by macrophages, and thus were injected into hypercholesterolemia rabbits to allow the specific detection of atherosclerotic plaques in the aorta, by micro-CT [97, 98]. Through different experimental models, both ruptured and non-ruptured atherosclerotic plaques can be visualized.

4. Passive targeted imaging

The preferential passive accumulation in tissues is related to the surface properties and size of nanoparticles. In that way, this phenomenon can induce differences in the accumulation of NPs contrast agent between healthy and damaged tissues, and therefore can reveal structural information on lesions. This section presents the state-of-the-art of the using of nanoparticulate X-ray contrast agents for the imaging of lesions, according to their spontaneous accumulation into the specific sites. Passive accumulation of NPs is performed following different mechanisms described below, either mediated by the reticuloendothelial system up to the targeted tissue, or passively accumulated due to cells uptake or due to specific accumulation based on affinities of the NPs for the targeted sites.

4.1. Uptake of nanoparticulate contrast agents by reticuloendothelial system (RES)

The liver is a common site of metastases [99] due to its high volume of blood flow, suitable size of sinusoids for trapping metastatic cells, and rich environment for rapid growth [89]. Non-stealth (*i.e.* non-PEGylated) nanoparticulate X-ray contrast agents will be rapidly sequestered by the reticuloendothelial system (RES) and in particular by Kupffer cells [89, 100]. It is noteworthy that even stealth particles can gradually concentrate in liver for the same reasons, at the end of life course in bloodstream. In the case of presence of hepatic tumor nodules, and since they are devoid of RES, they should appear negatively contrasted thanks to the privileged accumulation of NPs contrast agents in the healthy tissues. Compared to the use of hydrophilic iodinated molecules, this NPs-based technology allows the detection of lesions with fewer doses [101] and better sensitivity [102, 103].

In this respect, non-PEGylated iodinated liposomes or nanoemulsions are specifically formulated to accumulate in liver [56, 104, 105], in order to give a hepatic opacification following i.v. injection. Results showed persistent X-ray contrast of the liver tissues, reached for a lower dosage compared to conventional contrast agents. An example is given by liposomes composd of iodolipid and lipiodol, encapsulating a water soluble iodinated compound (iopamidol), to be a RES targeted contrast agents [106]. As a result, their i.v. administration in rats (tail vein) led to a very fast liver

contrast enhancement, at 6 min post-injection. Moreover, by lasting up to 24 h, this contrast effect was considered clinically relevant. Likewise, contrast enhancement in spleen appeared immediately after administration, but reached a maximum of persistence at around 90 min [106].

Similar results are obtained with iodinated copolymeric nanoparticles for hepatic tumors by negative imaging, *i.e.* using their specific accumulation in liver healthy tissues to visualize the lesions. Poly-[2-methacryloyloxyethyl(2,3,5-trriodobenzoate)]-(glycidyl methacrylate) (P(MAOETIB-GMA)) [107, 108] were prepared by emulsion copolymerization of 2-methacryloyloxyethyl (2,3,5-triiodobenzoate) (MAOETIB) using a low proportion of glycidyl methacrylate (GMA). Significant contrast enhancements of the blood pool, lymph nodes, liver and spleen were observed after intravenous injection of the NPs suspension in rats. Upon intravenous injection of 300 μL of the suspension, a strong enhancement of healthy liver tissue rapidly occurred and provided a negative contrast of cancerous liver tissue.

Actually all the other alternatives for liver and spleen imaging take benefit of this passive transport by the RES system to reach their target. Numerous examples are provided in literature, notably encapsulating heavy metal as X-ray contrasting materials [69, 84, 89]. As introduced above for their efficiency as blood pool contrast agent, commercial products consisting in NPs encapsulating alkaline earth metal-based contrast agents (ExiTron nano 6000® and ExiTron nano 12000®) are also used as liver and spleen targeted contrast agent for micro-CT [81]. The former, ExiTron nano 6000®, undergoes a quick uptake by macrophages in the liver and spleen, allowing their visualization for several months after a single injection of only 100 μL. Illustration of this contrast enhancement using ExiTron nano 6000® is reported in Fig. 2 A. A_1 shows the contrast before injection and A_2 24 h after a single i.v. administration. On the other hand, ExiTron nano 12000®, has the same composition than ExiTron nano 6000®but twice more concentrated, improving the blood pool contrast and circulation time with half life around 3 h after i.v. injection in mice (as shown in Fig. 1 D). Interestingly, ExiTron nano 12000® also accumulated in lymph nodes and in adrenal glands, inducing a significant X-ray contrast enhancement of these zones illustrated in Fig. 2 B_1 and B_2, respectively. This is likely due to a macrophage uptake of the NPs before reaching the targeted sites.

The same authors took benefit of this RES uptake and NPs liver accumulation in order to detect hepatic metastases by negative contrast (illustrated in Fig. 3 A). This method allows measuring tumors regions (non-contrasted within the contrasted organ) as small as 300 μm, and following their growth over time, *e.g.* shown Fig. 3 A_1 to A_4, respectively 9, 12, 14 and 19 days after intrasplenic injection of cancer cells (MC38 colon tumor cells). Comparable results, reported in Fig. 3 B, were observed with iodinated nano-emulsions (Fenestra LC®) by Almajadub and coworkers [18]. They observed a significant contrast between healthy tissues (contrasted) and tumor (non-contrasted) in spleen and liver. Fig. 3 B_1 and B_2 show healthy spleen, and Fig. 3 B_3 to B_6 emphasize the presence of tumor region. Generally authors consider that lipid nano-emulsions are exclusively taken up by hepatocytes, associating them to remnant chylomicron taken up by the liver through a receptor-mediated apoliporpotein-E process. This example proves that the RES system also plays a non negligible role in the nano-droplet clearance. It could be more adequate to consider that these different elimination mechanisms occurs simultaneously.

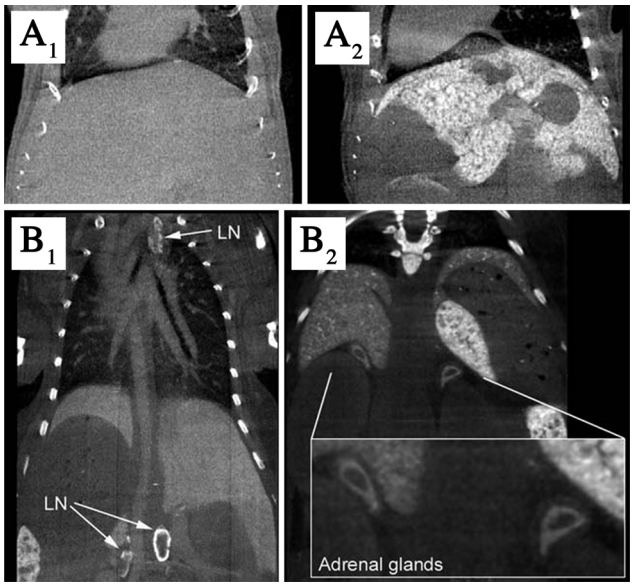

Figure 2: Micro-CT reticuloendothelial uptake of CT-contrast agent, from Ref. [81]. (A) micro-CT scan of the murine liver before (A_1) and 24 h after (A_2) i.v. administration of ExiTron nano 6000®. (B) Contrast enhancement of the abdominal and mediastinal lymph nodes (LN) and of the adrenal glands. (B_1) was acquired 4 h after i.v. injection of ExiTron nano 12000®, (B_2) was acquired 22 days after i.v. injection of ExiTron nano 12000®.

4.2. Uptake of nanoparticulate contrast agents by hepatocytes

While macrophages (such as Kupfer cells) are abundant in the liver, hepatocytes are the constitutive cells of the liver. In that way, if the nanoparticles are hepatocyte-selective like are recognized ITG lipid emulsions (*e.g.* Fenestra LC® discussed above [47, 101]), they will provided different kinds of results that the ones systems described in the previous sections, *i.e.* toxicity, elimination routes, specific organ imaging. Generally, ITG nano-emulsions showed a blood pool effect at early time points after injection, avoiding the reticuloendothelial system (even if it can be observed in some examples discussed in the previous seciont), and then is taken up into hepatocytes through a high-volume receptor-mediated process for metabolization by lipolytic enzymes [109]. ITG metabolites are ultimately eliminated through the bile [110]. This pathway results in a prolonged and marked liver X-ray opacification [111, 112].

On the other hand, the properties of the liver-specific contrast agent (contrast and elimination time) were observed to be strongly dependent to the chemical nature of the compounds, likely due to their affinities for the tissues. Actually, from the administration, the time needed for the contrast agents to show the maximum accumulation in liver, depends on the NPs surface properties and size. However, numerous examples prove that the NPs liver clearance will rather depend on their chemical composition. Indeed, the two examples of Fig. 1 A (from Ref. [41], made with iodinated vitamin E) and the one form Fig. 1 B (from Ref. [40], made with Lipiodol®), have exactly the same composition (made with the same surfactant, Cremophor ELP® from BASF) and physicochemical properties (similar size range, similar surface properties), but only differing in the composition of the oily core. These two examples show similar contrast enhancement of blood pool with half life of 10 h and 4 h respectively, followed by a hepatic uptake. However,

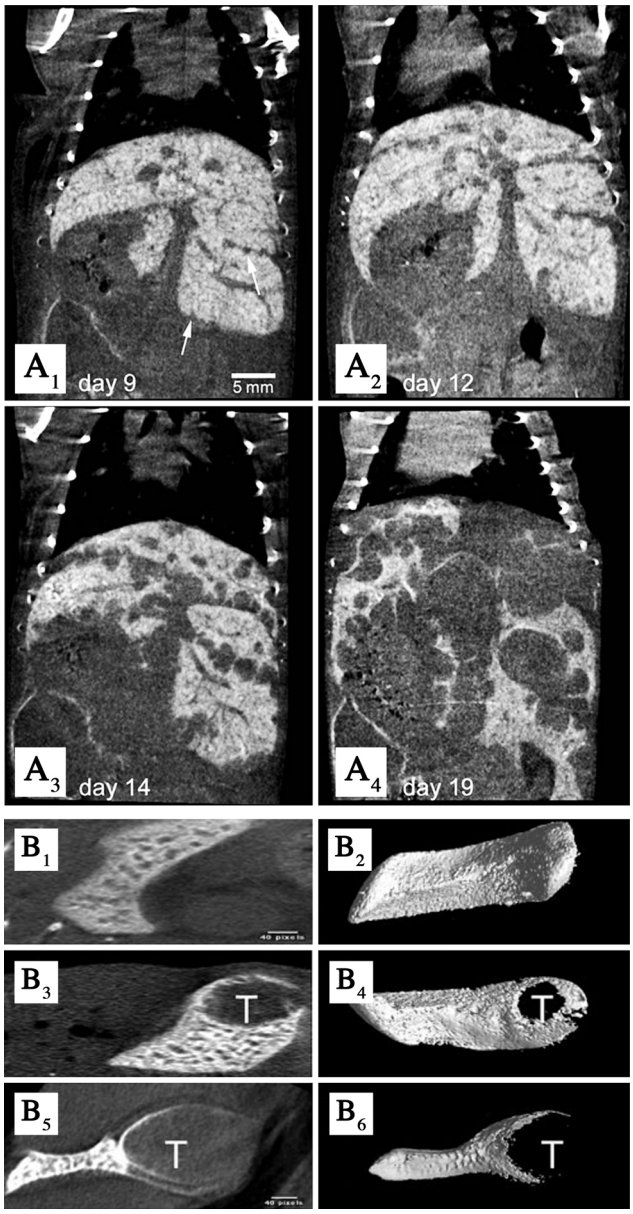

Figure 3: Micro-CT tumors imaging by negative contrast through the reticuloendothelial uptake of CT-contrast agent. (A) from Ref. [81]: micro-CT scan after a single injection of ExiTron nano 6000® in mouse. (A_1) to (A_4) illustrate development of liver metastases 9, 12, 14 and 19 days after intrasplenic injection of MC38 colon tumor cells. (B) from Ref. [18]: tumor imaging in spleen after injection of iodinated nano-emulsions (Fenestra VC®). (B_1) (B_3) (B_5) are axial views and (B_2) (B_4) (B_6) are the corresponding 3D reconstructions. (B_1)-(B_2) is the control mouse (without tumor), (B_3)-(B_4) show the spleen tumor 15 days after injection of STC1 tumor cells in the spleen, and (B_5)-(B_6) show the tumor growth 30 days after the tumor cells injection.

the former (iodinated vitamin E based product) remains accumulated liver 130 days offering a significant contrast during this prolonged period (illustrated in Fig. 4, 48 h post injection), while the second one (Lipiodol based) is totally eliminated form the mice body in 2 days. It shows that the *in vivo* behavior of the nanoparticulate contrast

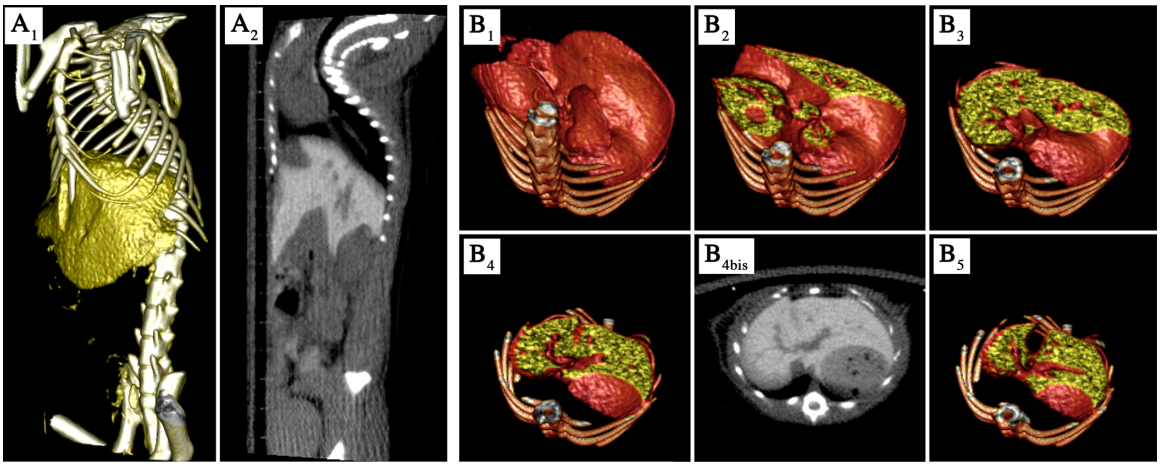

Figure 4: Micro-CT liver imaging with hepatocytes-specific contrast agent: vitamin E nano-emulsions, from Ref. [41]. (A_1) Left lateral view, 3D rendering, (A_1) Sagittal view, maximal intensity projection. (B_1) to (B_5) show 3D rendering of liver sections, emphasizing the clear contrast different between the liver tissues and its vascularization. ($B_4 bis$) is the transverse view of maximal intensity projection corresponding to (B_4).

agents not only depends of the physico-chemical properties of the formulation itself, but is strongly related to the chemical nature of the compound, their affinities for the targeted tissues, and their metabolism. Furthermore, these two examples can be completed with numerous others like the formulation describe in Ref. [39] made with iodinated macrogol nano-emulsified with nonionic surfactants, eliminated from the mice body in two days. This passive uptake and accumulation is illustrated in Fig. 4. Fig. 4 A_1 and A_2 represent the whole body with a clear delineation of the hepatic region. Fig. 4 B_1 to B_5 show the tri-dimensional view and cuts of liver, highlighting the accurate and specific contrast difference between the hepatic tissue and its irrigation. This result evidences the high potential of the nano-emulsions technology as targeted CT contrast agents, that allows a clear differentiation between the soft tissues each other and between soft tissues and biological fluids.

In addition, similarly to the methods worked out with RES-recognized contrast agents, these hepatocyte-selectives systems can allows detection of tumors by negative staining. Indeed, primary and secondary liver tumor cells do not internalize ITG like normal liver cells, inducing a significant difference in their attenuation compared to healthy liver tissue. In fact, tumors cells are deficient in hepatic lipase and then cannot uptake iodinated lipids [18–20, 42]. Here alse, efficacy of micro-CT lies in its resolution allowing to detect tumor as small as 300 μm, with a tumor detectability was superior to 80% [19, 45]. Combining micro-CT with a suitable hepatocyte-selective contrast agent is a solution for detecting and monitoring multiple liver tumors in mice as early as 7 days after implantation of the cancer cells [19]. Figure 5 A illustrates this method of detection of liver tumor from Ref. [23], showing acquisition 3 h post injection of Fenestra LC® in nude mice. The tumors appears negatively contrasted and the 3D reconstruction (Fig. 5 A_3) shows their spacial repartitions in the organ. It is important to note that liver vasculature also appear negatively contrasted (in red in Fig. 5 A_3). This vasculature was also detected in healthy organ like in Fig. 4, and can induce confusion. A simple solution to this problem is the concomitant use of hepatocyte-selective contrast agent with blood pool contrast agents,

finally giving rise to the exclusive imaging of hepatic tumors regions [42]. Following this methodology, Aprahamian and coworkers [113] followed the evolution of hepatic tumor (see Fig. 5 B) without treatment, and treated with a new antitumoral molecules (Myo-inositol trispyrophosphate). This powerful method allows a very accurate observation of the tumor location and size, a quantitative *in vivo* following-up and its potential response to applied treatments.

4.3. Accumulation of nanoparticulate contrast agents through enhanced permeation and retention effect (EPR)

This passive retention effect is based to the fact that tumor vessels are structurally and functionally different to normal vessels. They are tortuous, dilated and their endothelium are porous owing to the their unregulated angiogenesis. These are typical characteristics of tumors or various ischemic and inflammatory diseases [114], and can be exploited for drug targeting and targeted imaging. However, it is to be noted that the limited size of tumor vessels only induce slight contrast enhancement, which makes difficult their direct image directly using classical X-ray based techniques. Due to their size in nanoscale, nanoparticles show a preferential accumulation in tumors [115–119]. Since nanoparticulate contrast agents consist of discrete distribution of highly concentrated contrasting atoms, their self-accumulation in the tumor sites result in a local high contrast enhancement.

Numerous example of efficient use of EPR effect for targeted imaging are reported. The main reason of their passive accumulation in tumors is their size in the nanoscale.

Liposome containing hydrophilic iodinated molecules (iohexol and gadoteridol) were intravenously administrated to VX2 sarcoma bearing rabbits [63], see Fig. 6 A. Passive accumulation at tumor sites was achieved through the EPR effect due to their colloidal size, and lack of effective lymphatic drainage at lesion sites. In Fig. 6 A_1 the region of interest (ROI) is placed in liver as a reference, and in Fig. 6 A_2 ROI is located in the tumor site. The related graphics show similar X-ray attenuation values between both cases, with a maximum arising around 48 h post-administration, and a contrast enhancement sustained for 10 days. Another example [120] showed that, a dose of 455 mg iodine per kilogram of body weight of liposomal probe, too low to produce blood vessel visibility in the normal tissue, is able to accumulate at the tumor sites providing a detectable contrast (illustrated in Fig. 6 B). Likewise, different other examples are reported highlighting EPR for liposomal CT contrast agent, in small animals bearing breast cancer [21, 121]. In Fig. 6 C, from Ref. [21], shows The tumor vasculature with a liposomal CT nanoprobe, enhancing contrast in vessels as small as 200-300 microns (C_2). Then, in function of time (C_3 to C_5) the contrast agent gradually accumulate in the tumor itself by the ERP effect.

5. Active targeted imaging

The more convenient approach lies in a direct visualization of the tumor sites, which is actually linked to the nature and location of the tumor, and the available contrast agents [122]. We saw in the previous section that the accumulation into the lesion sites can be passively performed through EPR effect, and allow the direct visualization or tumor area. In the present section, we will see how this direct accumulation can be induced using specific ligand / receptor

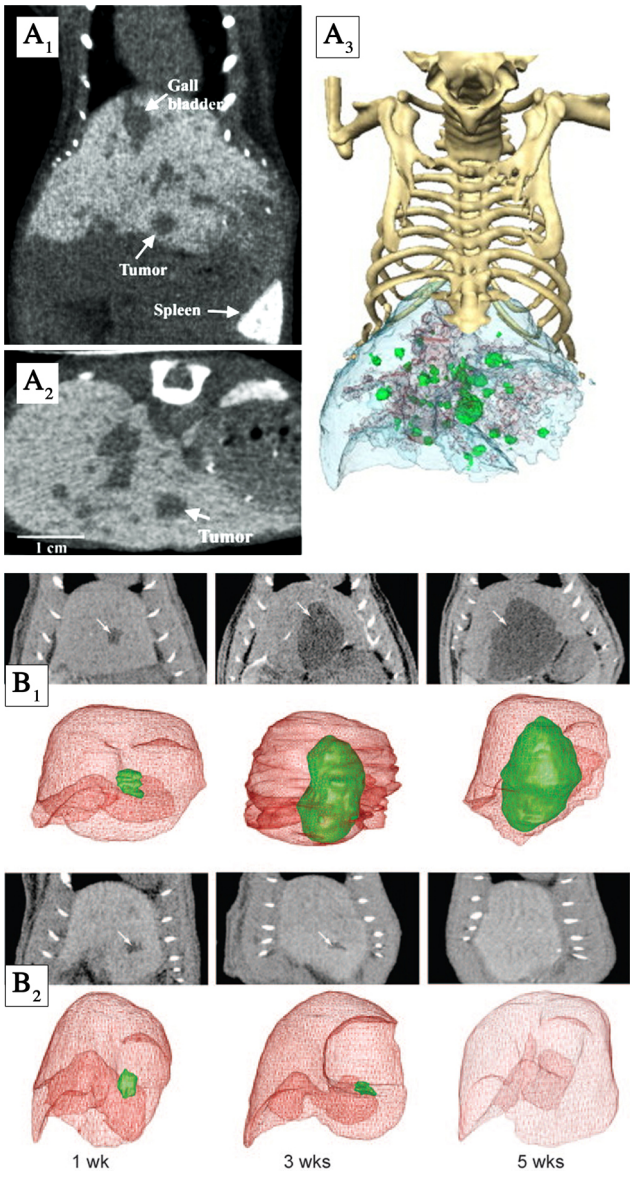

Figure 5: Micro-CT tumors imaging by negative contrast through the hepatocyte-specific uptake of CT-contrast agent. (A) From Ref. [23]: micro-CT scan acquired 3 h after injection of Fenestra LC® in nude mice with developed liver lesions. (A_1) Coronal and (A_2) sagittal views. The arrow points the same lesion in all views. (A_3) Anterior 3D surface rendering image. The significant contrast difference allow a clear characterization of the tumors (green), liver lobes (blue) and liver vessels (red). (B) From Ref. [113]:Detection of liver tumors by negative contrast using smultaneously hepotocyte-selective contrast agent Fenestra LC®, and also blood pool contrast agent Fenestra VC® injected at the interval of two days, in order to exclusively see the contrast difference in the tumor site. (B_1) untreated rats and (B_2) treated with Myo-inositol trispyrophosphate. The tumor in 2D slices is indicated by an arrow (monochrome images). 3D transparent simulations created by 3D virtual-reality and rendering software (color images).

interactions, so-called active targeting. Nanoparticles contrast agents are suited for this targeting purpose since their surface can be easily functionalized with selected ligands, corresponding to receptors over-expressed by malignant

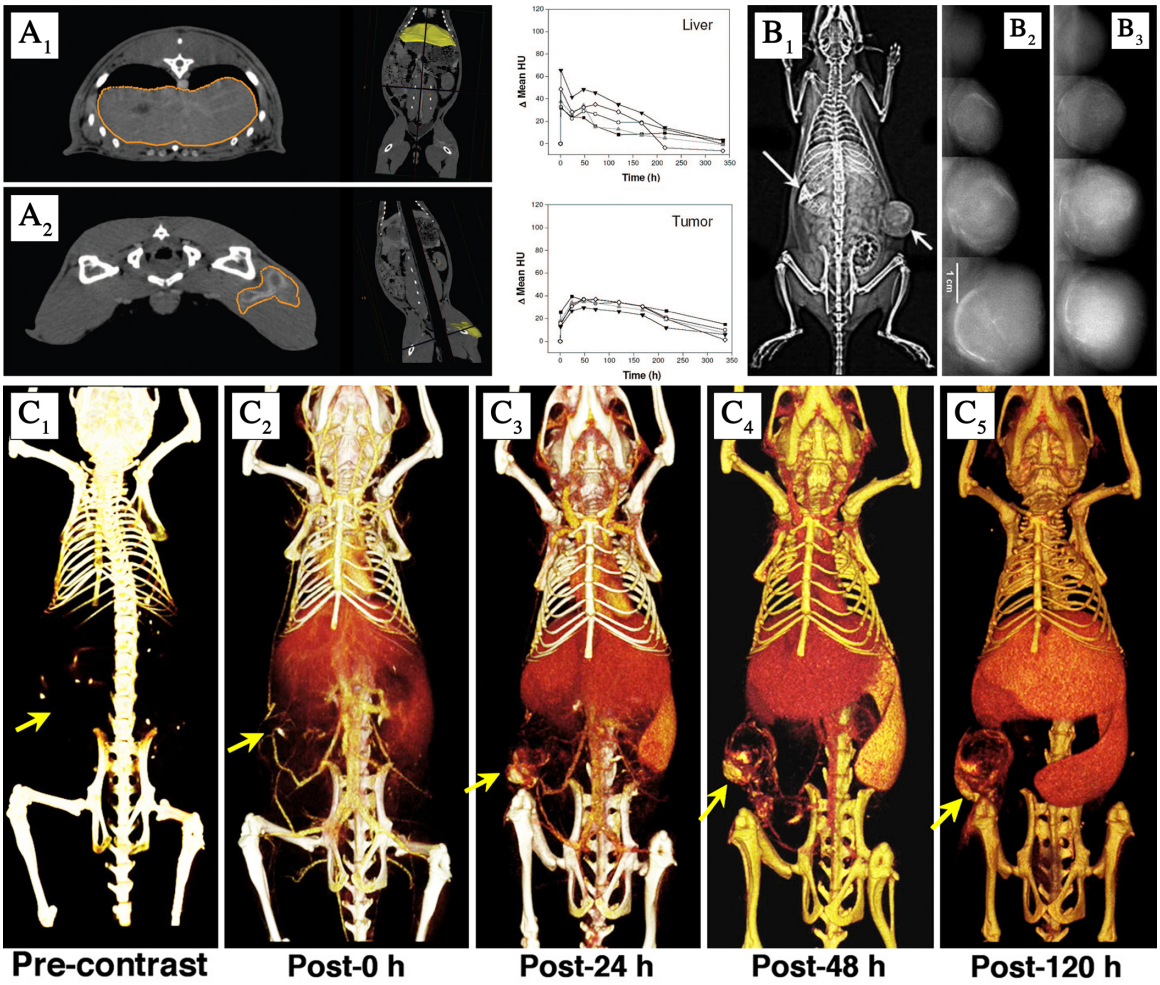

Figure 6: Micro-CT imaging of enhanced permeation and retention effect. (A) From Ref. [63]: Visual illustration of transverse (left) CT slices of the rabbit liver (A_1) and tumor (A_2) acquired at 48 h post-injection. These images are acquired at submillimeter resolution, and they demonstrate potential for quantification of intraorgan heterogeneity. Bulk organ analysis (middle) was performed on the contoured organ/tissue volumes (in yellow). The differential mean HU measured in each region of interest at selected time points are reported in the graphs (right). (B) From Ref. [120]: (B_1) X-ray images display 5 days intratumoral fate of probe in rat breast tumor model before 72 h after administration of probe at dose of 455 mg of iodine per kilogram. After injection, images showed that no blood vessels were visible in normal tissue; spleen, liver, and tumor were clearly seen. (B_2) and (B_3) X-ray images of two tumors before (top) and after (others) injection of probe at dose of 455 mg of iodine per kilogram. (C) Fron Ref. [21]: Dynamics of tumor signal enhancement. Coronal three-dimensional volume-rendered images demonstrating the extravasation and accumulation of nanoparticle contrast agent within the tumor (yellow arrow). Immediately after administering the nanoparticle contrast agent, the overall body and tumor vasculature is nicely demonstrated. Tumor accumulation of nanoparticle contrast agent was observed as early as 24 h. No image-detectable nanoparticle contrast agent signal was observed from the blood-pool at post-120 h (C_5) as confirmed by the absence of any vessels or heart signal on post-120 h image. However, the tumor is clearly enhanced. The only other organs enhanced are the liver and spleen, which are the organs for nanoparticle contrast agent clearance.

cells [123]. Effective ligand / receptor interactions allow enhancing accumulation and residence time of NPs and contrast-agent in malignant tissues.

Studies proving the potentials of active targeted imaging were recently published, showing that targeting solution can be found with functionalizing the NPs surface with monoclonal antibodies [124, 125], peptides [126, 127] or small molecules like folic acid [128, 129]. This technology allowed visualization, characterization and quantification of the biological processes at the molecular and cellular levels in human and other animal models [130, 131], and confers an high contrast to targeted cells [132, 133]. It remains, still today, a promising and complex technology gathering a high number of interdependent parameter described above in this review, eventually aiming a simple result.

Starting from the contrast agent-loaded functionalizable NPs, a panel of ligands, already proved to be effective as cancer targeting ligands, can be grafted onto the surface at high concentrations. Typical examples can be found in peptides like cyclic pentapeptide c(RGDfk) recently showed to be efficient to target $\alpha_v\beta_3$ integrin over-expressed in cancer cells *in vivo* [134]. In that case, anticancer loaded polymeric NPs have been fabricated with their external surrounding layer composed of carboxylic acid function. In substance, this chemical platform allows a general surface functionalization with a very wide range of molecules like peptides (the case here), proteins, antibodies, etc. *In vivo* results showed that active targeting significantly enhanced anticancer activity. The idea developed through this present section, is that the existing technologies developed for the active targeting for drug delivery are very easily transposable to targeted imaging. Nevertheless, only a few examples are recently proposed by literature, and some representative are detailed below.

Peptides represent an important and efficient family of ligands used for improving the targeted accumulation of nanocarriers in tumor sites. Grafting of thioctic-acid-modified bombesin peptide on starch-coated gold NPs induces their specific accumulation on cancer cells *in vivo* (in prostate-tumor-bearing mice), thanks to their high affinity toward gastrin-releasing peptide receptors *in vivo* that are over-expressed in prostate, breast, and small-cell lung carcinoma [91].

Another example of peptide driven active targeted imaging is described using E-selectin-binding peptide, which have a specific affinity toward E-selectin expressed on activated endothelial cells, and notably in leukocyte rolling during inflammatory processes or angiogenesis [135, 136]. As illutrated in Fig. 7, from Ref. [137], E-selectin-binding peptide (ESBP)-targeted iodine containing liposomes were shown by micro-CT imaging to induce a privileged targeting to small subcutaneous tumors if compared to the same non-targeted (control) liposomes. A significant contrast enhancement between targeted and control is visible over time, evidencing the clear role of peptide / receptor interactions. Finally, the residency time of ESBP coated liposomes inside the tumor was about 314 min, whereas it was only about 90 min for the non-targeted ones.

Active targeted imaging with similar results were obtained with the conjugation of antibodies to the contrast agent nanocarriers. For example, as illustrated in Fig. 8 from Ref. [138], gold nanoparticles coated with polyethylene glycol and anti-Her2+ antibody (Herceptin) showed a specific targeted binding to human breast cancer cells over-expressed Her2+ receptors. After intravenous injection in mice, the highest uptake was showed in the periphery of the tumors, 1.6 fold higher than that another tumor expressing Her2- receptor (control) and 22 fold higher than surrounding muscle.

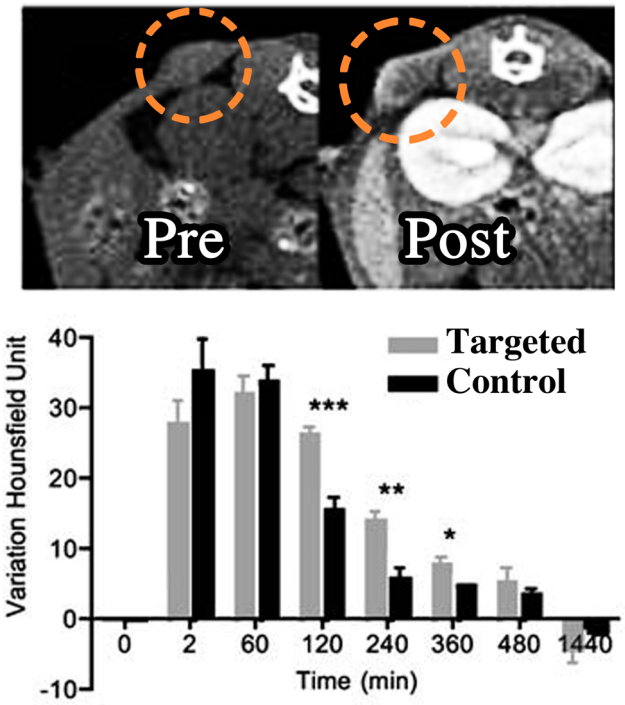

Figure 7: Active targeted CT imaging of tumor with iodinated liposome decorated with E-selectin-binding peptide, from Ref. [137]. Colon adenocarcinoma cell line HT-29 were injected subcutaneously and allowed to grow for 5-6 days. The transverse view in the tumor region (top) show a clear contrast enhancement in the tumor region (arrow) and the comparison with non-labeled liposomes (bottom) reveal a statistical difference at 120, 240, and 360 min post-injection. The determination of the blood half-lives gives 121 min for ESBP-liposomes and 71 min for non-labeled liposomes.

In another example, Anti-CD4 targeted gold nanoparticles exhibited a specific accumulation in the periphery of lymph nodes in mice, revealed by micro-CT imaging [90]. Functional coating was performed from a PEG (spacer) with a COOH termination, on which is grafted the antibody. Here also, long circulating properties induced by the PEG is of prime importance since it prevents the rapid NPs elimination favoring the contact with the targeted tumor sites. 200 μL of a dispersion of gold nanoparticle-anti-mouse CD4 conjugates were injected into mice. As illustrated in Fig. 9 from Ref. [90], anti-CD4 targeted gold NPs provided higher X-ray opacification of lymp nodes in comparison to similar gold NPs only coated with PEG, or as well, coated with another (control) antibody IgG2b.

Different other types of biological molecules equally provide interesting results for developing targeted imaging technologies. Folic acid coated silica / gold nanorods showed promising *in vivo* results in that sense [139]. The silica shell decreases the cytotoxicity, improves the biocompatibility, and facilitates the chemical grafting of folic acid, connected with 3-aminopropyltrimethoxysilane. Nanorod-SiO_2-NH_2 is then covalently linked to folic acid. Once injected in mice, as illustrated in Fig. 10 from Ref. [139], these functional NPs specifically target folic acid receptors over-expressed in xenografted gastric cancer MGC803 cells [90, 140]. Compared to healthy tissues, strong contrast was displayed in tumor lesions during 12 h after a single injection, which constitutes direct evidences of the efficiency

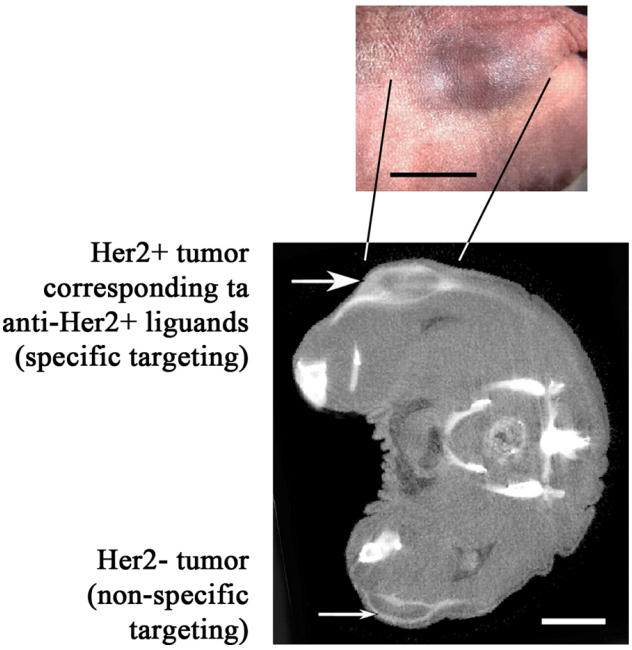

Figure 8: Active targeted CT imaging of tumor with gold nanoparticles decorated with anti-Her2+ antibody, from Ref. [138]. Micro-CT sections from five different mice bearing Her2+ (top large arrow) and Her2- tumours (bottom small arrow) growing in opposite thighs imaged 20 h after i.v. injection of 15 nm anti-Her2+ gold nanoparticles. Dose applied was 0.86 g Au/kg. Bar = 5 mm.

of active tumor targeting enhanced by folic acid coating.

To finish, different other examples of targeted imaging are reported in literature, based on the affinities between density lipoprotein (LDL) encapsulating ITG, and LDL cell surface receptor (LDLR) [141] over-expressed in several tumor types [142–145]. Another targeting strategy took benefit of the avidity of cancer cells for glucose (energy consumption) to induce the NPs targeting. 2-deoxy-D-glucose (2-DG)-labeled gold nanoparticles showed a preferential accumulation (three time higher than non-coated NPs) toward human alveolar epithelial cancer cell line (A-549) [142–145].

6. Perspectives: evolution toward theranostic

Nanoparticulate contrast agents for micro-CT play an important role on the detection of structural and functional abnormalities and for characterizing tumor aggressiveness in small animals. These nanoparticulate contrast agents presented long circulation time in blood stream and made possible the detection of early metastasis and small lesions in CT imaging using their passive transport to the targeting sites. Nanoparticulate contrast agents can also be designed to selectively accumulate into desired tissues or tumor sites by conjugation of tissue-targeting molecules. Besides targeted imaging, the next step is incorporation in the same functionalized nanocarrier, additional bioactive molecules. The objective is to perform a simultaneous imaging and drug delivery, in that way offering a very accurate control of the drug amount delivered, kinetics, with the possibility of adapting the therapy to the patient response [140]. This

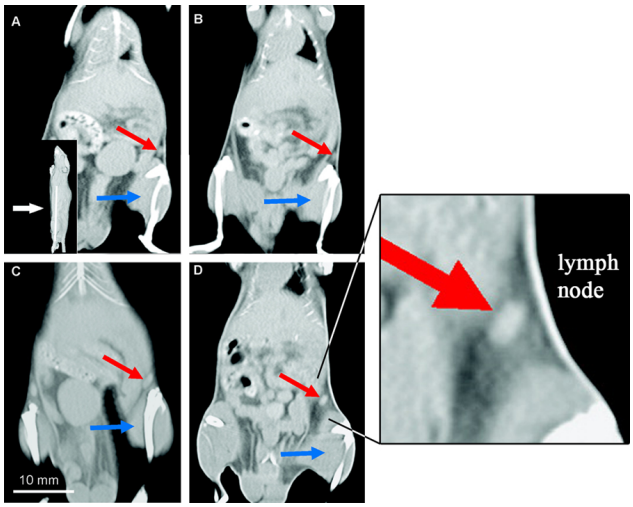

Figure 9: Active targeted CT imaging of tumor with gold nanoparticles decorated with anti-CD4 IgG antibody, from Ref. [90]. X-ray CT images of mice before (A, B) and 1 h after (C, D) injection of gold nanoparticles (38 nm individual diameter) conjugated to unspecic IgG (C) and anti-CD4 IgG (D). The inlay in A provides orientation of the reformatted plane of the abdomen of the mice, where the arrow points along the viewing direction. The targeted (anti-CD4 IgG) nanoparticles show clear contrast enhancement of inguinal lymph nodes (red arrows in B and D), whereas virtually no change is visible for the nonspecic controls (red arrows in A and C). For better visual comparability of X-ray densities, the hind limb muscles have been labeled and set to a standard brightness value (blue arrows). Average measured X-ray densities of the individual lymph nodes (red arrows) in Hounseld units (HU) are 47 HU (A), 26 HU (B), 52 HU (C), 121 HU (D).

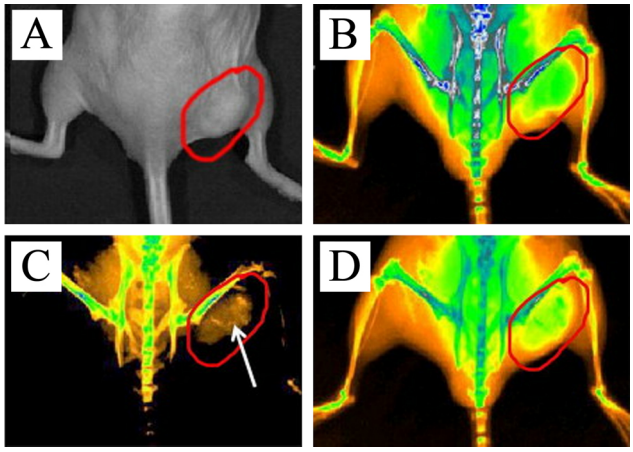

Figure 10: Active targeted CT imaging of tumor with gold nanorods/silica decorated with folic acid, from Ref. [139]. X-ray images after intravenous injection of gold nanorod-SiO2-folic acid in nude mice at different time points. (A) Picture of the tumor tissue; (B) X-ray projection at 0 h; (C) X-ray projection at 12 h, (D) X-ray projection at 24 h.

new concept has been named theranostic. Literature proposes some recent studies in that field, like the work of Kim *et al.* [146] in which the authors present a hybrid gold NPs targeting prostate cancer cells, and also encapsulating anticancer molecules (doxorubicin). As a result, the cancer cells were significantly targeted, and as well, specifically destroyed.

7. Conclusion

Micro-CT is a widely used, cost-effective, fast, and accurate three-dimensional radiographic imaging technology for small animal models. However, the main limitation of micro-CT lies in the poor efficacy or toxicity of the contrast agents currently available. Efficient contrast agents for micro-CT have to be stealth nanoparticulate systems for preventing their rapid renal clearance, highly loaded in X-ray contrasting materials, stable, and with controlled surface properties. Through the present article, we review the state-of-the-art of targeted imaging technologies, from blood pool properties as a prerequisite, to the influence of the composition and physicochemical properties on the *in vivo* becoming of the contrast agent. We discussed the different passive targeted imaging through representative examples of the literature, and likewise we present the first examples of active targeted imaging only recently published.

References

[1] L. R. Desnoyers, R. Pai, R. E. Ferrando, K. Hötzel, T. Le, J. Ross, D. A. Carano, R. and, J. Qing, I. Mohtashemi, A. Ashkenazi, D. M. French, Targeting fgf19 inhibits tumor growth in colon cancer xenograft and fgf19 transgenic hepatocellular carcinoma models, Oncogene 27 (2008) 85–97.

[2] C. T. Badea, M. Drangova, D. W. Holdsworth, G. A. Johnson, In vivo small-animal imaging using micro-ct and digital subtraction angiography, Phys. Med. Biol. 53 (2008) R319–R350.

[3] S. J. Schambach, S. Bag, C. Groden, L. Schilling, M. A. Brockmann, Vascular imaging in small rodents using micro-ct, Methods 50 (2010) 26–35.

[4] L. Zagorchev, P. Oses, Z. W. Zhuang, K. Moodie, M. Mulligan-Kehoe, M. Simons, T. Couffinhal, Micro computed tomography for vascular exploration, J. Angiogenesis Res. 2 (2010) 7–17.

[5] R. A. de Kemp, F. H. Epstein, C. Catana, B. M. W. Tsui, E. L. Ritman, Small-animal molecular imaging methods, J. Nucl. Med. 51 (2010) 18–32.

[6] J. French, N. Gingles, J. Stewart, N. Woodhouse, Use of magnetic resonance imaging (mri) and micro-computed tomography (micro-ct) in the morphological examination of rat and rabbit fetuses from embryo-fetal development studies, Reprod. Toxicol. 30 (2010) 292–300.

[7] B. M. Patterson, C. E. Hamilton, Dimensional standard for micro x-ray computed tomography, Anal. Chem. 82 (2010) 8537–8543.

[8] E. L. Ritman, Small-animal ct: Its difference from, and impact on, clinical ct, Nucl. Instrum. Methods Phys. Res. A 580 (2007) 968–970.

[9] J. C. Williams, J. A. McAteer, A. P. Evan, J. E. Lingeman, Micro-computed tomography for analysis of urinary calculi, Urol. Res. 38 (2010) 477–484.

[10] B. M. W. Tsui, D. L. Kraitchman, Recent advances in small-animal cardiovascular imaging, J. Nucl. Med. 50 (2009) 667–670.

[11] A. J. Burghardt, T. M. Link, S. Majumdar, High-resolution computed tomography for clinical imaging of bone microarchitecture, Clin. Orthop. Relat. Res. 469 (2011) 2179–2193.

[12] E. Weber, M. Fernandez, P. Wapner, W. Hoffman, Comparison of x-ray micro-tomography measurements of densities and porosity principally to values measured by mercury porosimetry for carbon-carbon composites, Carbon 48 (2010) 2151–2158.

[13] J. Li, A. Chaudhary, S. J. Chmura, C. Pelizzari, T. Rajh, C. Wietholt, M. Kurtoglu, B. Aydogan, A novel functional ct contrast agent for molecular imaging of cancer, Phys. Med. Biol. 55 (2010) 4389–4397.

[14] K. C. Graham, L. A. Wirtzfeld, L. T. MacKenzie, C. O. Postenka, A. C. Groom, I. C. MacDonald, A. Fenster, J. C. Lacefield, A. F. Chambers, Three-dimensional high-frequency ultrasound imaging for longitudinal evaluation of liver metastases in preclinical models, Cancer Res. 65 (2005) 5231–5237.

[15] K. H. Bae, H. J. Chung, T. G. Park, Nanomaterials for cancer therapy and imaging, Mol. Cells 31 (2011) 295–302.

[16] H. Maeda, Tumor-selective delivery of macromolecular drugs via the epr effect: background and future prospects, Bioconjugate Chem. 21 (2010) 797–802.

[17] D. Peer, J. M. Karp, S. Hong, O. C. Farokhzad, R. Margalit, R. Langer, Nanocarriers as an emerging platform for cancer therapy, Nat. Nano. 2 (2007) 751–760.

[18] M. Almajdub, M. Nejjari, G. Poncet, L. Magnier, E. Chereul, C. Roche, M. Janier, In-vivo high-resolution x-ray microtomography for liver and spleen tumor assessment in mice, Contrast Media Mol. Imaging 2 (2007) 88–93.

[19] H. W. Kim, Q.-Y. Cai, H. Y. Jun, K. S. Chon, S. H. Park, S. J. Byun, M. S. Lee, J. M. Oh, H. S. Kim, K.-H. Yoon, Micro-ct imaging with a hepatocyte-selective contrast agent for detecting liver metastasis in living mice, Acad. Radiol. 15 (2008) 1282–1290.

[20] S. Ohta, E. W. Lai, J. C. Morris, D. A. Bakan, B. Klaunberg, S. Cleary, J. F. Powers, A. S. Tischler, M. Abu-Asab, D. Schimel, K. Pacak, Microct for high-resolution imaging of ectopic pheochromocytoma tumors in the liver of nude mice, Int. J. Cancer 119 (2006) 2236–2241.

[21] K. B. Ghaghada, C. T. Badea, L. Karumbaiah, N. Fettig, R. V. Bellamkonda, G. A. Johnson, A. Annapragada, Evaluation of tumor microenvironment in an animal model using a nanoparticle contrast agent in computed tomography imaging, Acad. Radiol. 18 (2011) 20–30.

[22] C.-Y. Kao, E. A. Hoffman, K. C. Beck, R. V. Bellamkonda, A. V. Annapragada, Long-residence-time nano-scale liposomal iohexol for x-ray-based blood pool imaging, Acad. Radiol. 10 (2003) 475–483.

[23] L. Martiniova, D. Schimel, E. W. Lai, A. Limpuangthip, R. Kvetnansky, K. Pacak, In vivo micro-ct imaging of liver lesions in small animal models, Methods 50 (2010) 20–25.

[24] O. Rabin, J. Manuel Perez, J. Grimm, G. Wojtkiewicz, R. Weissleder, An x-ray computed tomography imaging agent based on long-circulating bismuth sulphide nanoparticles, Nat. Mater. 5 (2006) 118–122.

[25] V. P. Torchilin, M. D. Frank-Kamenetsky, G. L. Wolf, Ct visualization of blood pool in rats by using long-circulating, iodine-containing micelles, Acad. Radiol. 6 (1999) 61–65.

[26] O. van Tellingen, J. Beijnen, J. Verweij, E. Scherrenburg, W. Nooijen, A. Sparreboom, Rapid esterase-sensitive breakdown of polysorbate 80 and its impact on the plasma pharmacokinetics of docetaxel and metabolites in mice, Clin. Cancer Res. 5 (1999) 2918–2924.

[27] G. Storm, S. O. Belliot, T. Daemen, D. D. Lasic, Surface modification of nanoparticles to oppose uptake by the mononuclear phagocyte system, Adv. Drug Deliv. Rev. 17 (1995) 31–48.

[28] I. Brigger, C. Dubernet, P. Couvreur, Nanoparticles in cancer therapy and diagnosis, Adv. Drug Deliv. Rev. 54 (2002) 631–651.

[29] B. Haley, E. Frenkel, Nanoparticles for drug delivery in cancer treatment, Urol. Oncol. 26 (2008) 57–64.

[30] R. Singh, J. W. Lillard Jr., Nanoparticle-based targeted drug delivery, Exp. Mol. Pathol. 86 (2009) 215–223.

[31] V. P. Torchilin, V. S. Trubetskoy, Which polymers can make nanoparticulate drug carriers long-circulating?, Adv. Drug Deliv. Rev. 16 (1995) 141–155.

[32] N. Anton, J.-P. Benoit, P. Saulnier, Design and production of nanoparticles formulated from nano-emulsion templates – a review, J. Control. Release 128 (2008) 185–199.

[33] N. Anton, T. F. Vandamme, The universality of low-energy nano-emulsification, Int. J. Pharm. 377 (2009) 142–147.

[34] N. Anton, H. Mojzisova, E. Porcher, J.-P. Benoit, P. Saulnier, Reverse micelle-loaded lipid nano-emulsions: New technology for nano-encapsulation of hydrophilic materials, Int. J. Pharm. 398 (2010) 204–209.

[35] N. Anton, T. Vandamme, Nano-emulsions and micro-emulsions: Clarifications of the critical differences, Pharm. Res. 28 (2011) 978–995.

[36] M. Fryd, T. Mason, Advanced nanoemulsions, Annu. Rev. Phys. Chem. 63 (2012) 493–518.

[37] D. McClements, Nanoemulsions versus microemulsions: Terminology, differences, and similarities, Soft Matter 8 (2012) 1719–1729.

[38] F. Hallouard, N. Anton, P. Choquet, A. Constantinesco, T. Vandamme, Iodinated blood pool contrast media for preclinical x-ray imaging applications, Biomaterials 31 (2010) 6249–6268.

[39] F. Hallouard, N. Anton, G. Zuber, P. Choquet, X. Li, Y. Arntz, G. Aubertin, A. Constantinesco, T. Vandamme, Radiopaque iodinated nano-emulsions for preclinical x-ray imaging, RSC Advances 1 (2011) 792–801.

[40] F. Hallouard, S. Briançon, N. Anton, X. Li, T. Vandamme, H. Fessi, Iodinated nano-emulsions as contrast agents for preclinical x-ray

imaging, impact of the free surfactants on the pharmacokinetics, Eur. J. Pharm. Biopharm. in press (2012).

[41] X. Li, N. Anton, G. Zuber, M. Zhao, F. Hallouard, H. Fessi, N. Messaddeq, G. Bour, L. Soler, T. Vandamme, Iodinated vitamin e nanoemulsions: A novel efficient and non-toxic contrast agent for preclinical x-ray imaging, Submitted (2012).

[42] J. P. Weichert, F. T. Lee, S. G. Chosy, M. A. Longino, J. E. Kuhlman, D. M. Heisey, G. E. Leverson, Combined hepatocyte-selective and blood-pool contrast agents for the ct detection of experimental liver tumors in rabbits, Radiology 216 (2000) 865–871.

[43] C. T. Badea, L. W. Hedlund, M. de Lin, J. F. Boslego Mackel, G. A. Johnson, Tumor imaging in small animals with a combined micro-ct/micro-dsa system using iodinated conventional and blood pool contrast agents, Contrast Media Mol. Imaging 1 (2006) 153–164.

[44] D. A. Bakan, M. A. Longino, J. P. Weichert, R. E. Counsell, Physicochemical characterization of a synthetic lipid emulsion for hepatocyte-selective delivery of lipophilic compounds: Application to polyiodinated triglycerides as contrast agents for computed tomography, J. Pharm. Sci. 85 (1996) 908–914.

[45] S. M. Weber, K. A. Peterson, B. Durkee, C. Qi, M. Longino, T. Warner, F. T. Lee Jr, J. P. Weichert, Imaging of murine liver tumor using microct with a hepatocyte-selective contrast agent: accuracy is dependent on adequate contrast enhancement, J. Surg. Res. 119 (2004) 41–45.

[46] J. P. Weichert, M. P. Groziak, M. A. Longino, S. W. Schwendner, R. E. Counsell, Potential tumor- or organ-imaging agents. 27. polyiodinated 1,3-disubstituted and 1,2,3-trisubstituted triacylglycerols, J. Med. Chem. 29 (1986) 2457–2465.

[47] J. P. Weichert, M. A. Longino, D. A. Bakan, M. G. Spigarelli, T. Chou, S. W. Schwendner, R. E. Counsell, Polyiodinated triglyceride analogs as potential computed tomography imaging agents for the liver, J. Med. Chem. 38 (1995) 636–646.

[48] J. P. Weichert, M. A. Longino, S. W. Schwendner, R. E. Counsell, Potential tumor- or organ-imaging agents. 26. polyiodinated 2-substituted triacylglycerols as hepatographic agents, J. Med. Chem. 29 (1986) 1674–1682.

[49] D. A. Bakan, Imaging efficacy of a hepatocyte-selective polyiodinated triglyceride for contrast-enhanced computed tomography, Am. J. Ther. 8 (2001) 359–365.

[50] A. de Vries, E. Custers, J. Lub, S. van den Bosch, K. Nicolay, H. Grüll, Block-copolymer-stabilized iodinated emulsions for use as ct contrast agents, Biomaterials 31 (2010) 6537–6544.

[51] D. Y. Jiang, G. Scott Gazelle, G. L. Wolf, A model of focal cancer in rabbit lymph nodes, Acad. Radiol. 3 (1996) 159–162.

[52] G. L. McIntire, E. R. Bacon, J. L. Toner, J. B. Cornacoff, P. E. Losco, K. J. Illig, K. J. Nikula, B. A. Muggenburg, L. Ketai, Pulmonary delivery of nanoparticles of insoluble, iodinated ct x-ray contrast agents to lung draining lymph nodes in dogs, J. Pharm. Sci. 87 (1998) 1466–1470.

[53] E. R. Wisner, R. W. Katzberg, S. M. Griffey, C. M. Drake, P. J. Haley, A. R. Vessey, Indirect computed tomography lymphography using iodinated nanoparticles: Time and dose response in normal canine lymph nodes, Acad. Radiol. 2 (1995) 985–993.

[54] E. R. Wisner, J. P. Weichert, M. A. Longino, R. E. Counsell, S. E. Weisbrode, Percutaneous ct lymphography using a new polyiodinated biomimetic microemulsion, Acad. Radiol. 9 (2002) S191–S193.

[55] M. H. Oh, N. Lee, H. Kim, S. P. Park, Y. Piao, J. Lee, S. W. Jun, W. K. Moon, S. H. Choi, T. Hyeon, Large-scale synthesis of bioinert tantalum oxide nanoparticles for x-ray computed tomography imaging and bimodal image-guided sentinel lymph node mapping, J. Am. Chem. Soc. 133 (2011) 5508–5515.

[56] T. S. Desser, D. L. Rubin, H. Muller, G. L. McIntire, E. R. Bacon, J. L. Toner, Blood pool and liver enhancement in ct with liposomal iodixanol: Comparison with iohexol, Acad. Radiol. 6 (1999) 176–183.

[57] A. Sachse, J. U. Leike, T. Schneider, S. E. Wagner, G. L. Rling, W. Krause, M. Brandl, Biodistribution and computed tomography blood-pool imaging properties of polyethylene glycol-coated iopromide-carrying liposomes, Invest. Radiol. 32 (1997) 44–50.

[58] U. P. Schmiedl, W. Krause, J. Leike, A. Sachse, Ct blood pool enhancement in primates with lopromide-carrying liposomes containing soy phosphatidyl glycerol, Acad. Radiol. 6 (1999) 164–169.

[59] P. Leander, P. Höglund, A. Borseth, Y. Kloster, A. Berg, A new liposomal liver-specific contrast agent for ct: first human phase-i clinical trial assessing efficacy and safety, Eur. Radiol. 11 (2001) 698–704.

[60] A. Spinazzi, S. Ceriati, P. Pianezzola, V. Lorusso, F. Luzzani, X. Fouillet, S. Alvino, E. J. Rummeny, Safety and pharmacokinetics of a new

liposomal liver-specific contrast agent for ct: Results of clinical testing in nonpatient volunteers, Invest. Radiol. 35 (2000) 1–7.

[61] S. Mukundan Jr., K. B. Ghaghada, C. T. Badea, C.-Y. Kao, L. W. Hedlund, J. M. Provenzale, G. A. Johnson, E. Chen, R. V. Bellamkonda, A. Annapragada, A liposomal nanoscale contrast agent for preclinical ct in mice, Am. J. Roentgenol. 186 (2006) 300–307.

[62] S. J. Burke, A. Annapragada, E. A. Hoffman, E. Chen, K. B. Ghaghada, J. Sieren, E. J. R. van Beek, Imaging of pulmonary embolism and t-pa therapy effects using mdct and liposomal iohexol blood pool agent. preliminary results in a rabbit model, Acad. Radiol. 14 (2007) 355–362.

[63] J. Zheng, D. Jaffray, C. Allen, Quantitative ct imaging of the spatial and temporal distribution of liposomes in a rabbit tumor model, Mol. Pharm. 6 (2009) 571–580.

[64] D. B. Elrod, R. Partha, D. Danila, S. W. Casscells, J. L. Conyers, An iodinated liposomal computed tomographic contrast agent prepared from a diiodophosphatidylcholine lipid, Nanomed.-Nanotechnol. Biol. Med. 5 (2009) 42–45.

[65] Y. Fu, D. E. Nitecki, D. Maltby, G. H. Simon, K. Berejnoi, H.-J. Raatschen, B. M. Yeh, D. M. Shames, R. C. Brasch, Dendritic iodinated contrast agents with peg-cores for ct imaging: synthesis and preliminary characterization, Bioconjugate Chem. 17 (2006) 1043–1056.

[66] A. Yordanov, N. Mollov, A. Lodder, E. Woller, M. Cloninger, S. Walbridge, D. Milenic, M. Brechbiel, A water-soluble triiodo amino acid and its dendrimer conjugate for computerized tomography (ct) imaging, J. Serb. Chem. Soc. 70 (2005) 163–170.

[67] W. Ho Kong, W. Jae Lee, Z. Yun Cui, K. Hyun Bae, T. Gwan Park, J. Hoon Kim, K. Park, S. Won Seo, Nanoparticulate carrier containing water-insoluble iodinated oil as a multifunctional contrast agent for computed tomography imaging, Biomaterials 28 (2007) 55555561.

[68] J. M. Ashcroft, K. B. Hartman, K. R. Kissell, Y. Mackeyev, S. Pheasant, S. Young, P. A. W. Van der Heide, A. G. Mikos, L. J. Wilson, Single-molecule i2@us-tube nanocapsules: a new x-ray contrast-agent design, Adv. Mater. 19 (2007) 573–576.

[69] E. Boote, G. Fent, V. Kattumuri, S. Casteel, K. Katti, N. Chanda, R. Kannan, K. Katti, R. Churchill, Gold nanoparticle contrast in a phantom and juvenile swine: models for molecular imaging of human organs using x-ray computed tomography, Acad. Radiol. 17 (2010) 410–417.

[70] V. Kattumuri, K. Katti, S. Bhaskaran, E. J. Boote, S. W. Casteel, G. M. Fent, D. J. Robertson, M. Chandrasekhar, R. Kannan, K. V. Katti, Gum arabic as a phytochemical construct for the stabilization of gold nanoparticles: in vivo pharmacokinetics and x-ray-contrast-imaging studies, Small 3 (2007) 333–341.

[71] K. E. de Krafft, Z. Xie, G. Cao, S. Tran, L. Ma, O. Z. Zhou, W. Lin, Iodinated nanoscale coordination polymers as potential contrast agents for computed tomography, Angew. Chem.-Int. Edit. 48 (2009) 9901–9904.

[72] A. W. Bosman, H. M. Janssen, E. W. Meijer, About dendrimers: structure, physical properties, and applications, Chem. Rev. 99 (1999) 1665–1688.

[73] O. M. Koo, I. Rubinstein, H. Onyuksel, Role of nanotechnology in targeted drug delivery and imaging: a concise review, Nanomed.-Nanotechnol. Biol. Med. 1 (2005) 193–212.

[74] R. Guo, H. Wang, C. Peng, M. Shen, M. Pan, X. Cao, G. Zhang, X. Shi, X-ray attenuation property of dendrimer-entrapped gold nanoparticles, J. Phys. Chem. C 114 (2009) 50–56.

[75] C. Kojima, Y. Umeda, M. Ogawa, A. Harada, Y. Magata, K. Kono, X-ray computed tomography contrast agents prepared by seeded growth of gold nanoparticles in pegylated dendrimer, Nanotechnology 21 (2010) 245104.

[76] C. Peng, H. Wang, R. Guo, M. Shen, X. Cao, M. Zhu, G. Zhang, X. Shi, Acetylation of dendrimer-entrapped gold nanoparticles: Synthesis, stability, and x-ray attenuation properties, J. Appl. Polym. Sci. 119 (2011) 1673–1682.

[77] R. Guo, H. Wang, C. Peng, M. Shen, L. Zheng, G. Zhang, X. Shi, Enhanced x-ray attenuation property of dendrimer-entrapped gold nanoparticles complexed with diatrizoic acid, J. Mater. Chem. 21 (2011) 5120–5127.

[78] C. Peng, L. Zheng, Q. Chen, M. Shen, R. Guo, H. Wang, X. Cao, G. Zhang, X. Shi, Pegylated dendrimer-entrapped gold nanoparticles for in vivo blood pool and tumor imaging by computed tomography, Biomaterials 33 (2012) 1107–1119.

[79] H. Wang, L. Zheng, C. Peng, R. Guo, M. Shen, X. Shi, G. Zhang, Computed tomography imaging of cancer cells using acetylated dendrimer-entrapped gold nanoparticles, Biomaterials 32 (2011) 2979–2988.

[80] A. Jakhmola, N. Anton, T. Vandamme, Inorganic nanoparticles based contrast agents for x-ray computed tomography, Adv. Healthcare Mater. in press (2012).

[81] H. Boll, S. Nittka, F. Doyon, M. Neumaier, A. Marx, M. Kramer, C. Groden, M. A. Brockmann, Micro-ct based experimental liver imaging using a nanoparticulate contrast agent: A longitudinal study in mice, PLoS ONE 6 (2011) e25692–e25697.

[82] E. E. Connor, J. Mwamuka, A. Gole, C. J. Murphy, M. D. Wyatt, Gold nanoparticles are taken up by human cells but do not cause acute cytotoxicity, Small 1 (2005) 325–327.

[83] J. L. Dalsin, B.-H. Hu, B. P. Lee, P. B. Messersmith, Mussel adhesive protein mimetic polymers for the preparation of nonfouling surfaces, J. Am. Chem. Soc. 125 (2003) 4253–4258.

[84] J. F. Hainfeld, D. N. Slatkin, T. M. Focella, H. M. Smilowitz, Gold nanoparticles: a new x-ray contrast agents, Br. J. Radiol. 79 (2006) 248–253.

[85] L. Hiebert, The uptake of heparin by liver sinusoidal cells in normal and atherosclerotic rabbits, Thromb Res. 21 (1981) 383–390.

[86] D. Kim, S. Park, J. H. Lee, Y. Y. Jeong, S. Jon, Antibiofouling polymer-coated gold nanoparticles as a contrast agent for in vivo x-ray computed tomography imaging, J. Am. Chem. Soc. 129 (2007) 7661–7665.

[87] K. Park, K. Kim, I. C. Kwon, S. K. Kim, S. Lee, D. Y. Lee, Y. Byun, Preparation and characterization of self-assembled nanoparticles of heparin-deoxycholic acid conjugates, Langmuir 20 (2004) 11726–11731.

[88] R. Shukla, V. Bansal, M. Chaudhary, A. Basu, R. R. Bhonde, M. Sastry, Biocompatibility of gold nanoparticles and their endocytotic fate inside the cellular compartment: a microscopic overview, Langmuir 21 (2005) 10644–10654.

[89] I. Sun, D. Eun, J. H. Na, S. Lee, I. Kim, I. Youn, C. Ko, H. Kim, D. Lim, K. Choi, P. B. Messersmith, T. G. Park, S. Y. Kim, I. C. Kwon, K. Kim, C. Ahn, Heparin-coated gold nanoparticles for liver-specific ct imaging, Chem.-Eur. J. 15 (2009) 13341–13347.

[90] W. Eck, A. I. Nicholson, H. Zentgraf, W. Semmler, S. Bartling, Anti-cd4-targeted gold nanoparticles induce specific contrast enhancement of peripheral lymph nodes in x-ray computed tomography of live mice, Nano Lett. 10 (2010) 2318–2322.

[91] N. Chanda, V. Kattumuri, R. Shukla, A. Zambre, K. Katti, A. Upendran, R. R. Kulkarni, P. Kan, G. M. Fent, S. W. Casteel, C. J. Smith, E. Boote, J. D. Robertson, C. Cutler, J. R. Lever, K. V. Katti, R. Kannan, Bombesin functionalized gold nanoparticles show in vitro and in vivo cancer receptor specificity, Proc. Natl. Acad. Sci. U. S. A. 107 (2010) 8760–8765.

[92] Z. Zhang, R. D. Ross, R. K. Roeder, Preparation of functionalized gold nanoparticles as a targeted x-ray contrast agent for damaged bone tissue, Nanoscale 2 (2010) 582–586.

[93] V. P. Torchilin, Structure and design of polymeric surfactant-based drug delivery systems, J. Control. Release 73 (2001) 137–172.

[94] V. P. Torchilin, Polymeric micelles in diagnostic imaging, Colloid Surf. B-Biointerfaces 16 (1999) 305–319.

[95] A. N. Lukyanov, V. P. Torchilin, Micelles from lipid derivatives of water-soluble polymers as delivery systems for poorly soluble drugs, Adv. Drug Deliv. Rev. 56 (2004) 1273–1289.

[96] V. S. Trubetskoy, G. S. Gazelle, G. L. Wolf, V. P. Torchilin, Block-copolymer of polyethylene glycol and polylysine as a carrier of organic iodine: design of long-circulating particulate contrast medium for x-ray computed tomography, J. Drug Target. 4 (1997) 381–388.

[97] J. L. Herck, G. R. Y. Meyer, W. Martinet, R. A. Salgado, B. Shivalkar, R. Mondt, H. Ven, A. Ludwig, P. Veken, L. Vaeck, H. Bult, A. G. Herman, C. J. Vrints, Multi-slice computed tomography with n1177 identifies ruptured atherosclerotic plaques in rabbits, Basic Res. Cardiol. 105 (2009) 51–59.

[98] F. Hyafil, J.-C. Cornily, J. E. Feig, R. Gordon, E. Vucic, V. Amirbekian, E. A. Fisher, V. Fuster, L. J. Feldman, Z. A. Fayad, Noninvasive detection of macrophages using a nanoparticulate contrast agent for computed tomography, Nat. Med. 13 (2007) 636–641.

[99] Y. Liu, O. Matsui, Changes of intratumoral microvessels and blood perfusion during establishment of hepatic metastases in mice, Radiology 243 (2007) 386–395.

[100] G. Scott Gazelle, G. L. Wolf, G. L. McIntire, E. R. Bacon, N. George, E. F. Halpern, J. L. Toner, Hepatic imaging with iodinated nanoparticles: A comparison with iohexol in rabbits, Acad. Radiol. 2 (1995) 700–704.

[101] J. P. Weichert, M. A. Longino, M. G. Spigarelli, F. T. Lee Jr, S. W. Schwendner, R. E. Counsell, Computed tomography scanning of morris hepatomas with liver-specific polyiodinated triglycerides, Acad. Radiol. 3 (1996) 412–417.

[102] A. Bergman, A. Sundin, A. Magnusson, An iodinated lipid emulsion for ct of the liver: Comparison with iohexol in the detection of experimental hepatic metastases, Acta Radiol. 38 (1997) 55–60.

[103] W. Krause, K. Handreke, G. Schuhmann-Giampieri, K. Rupp, Efficacy of the iodine-free computed tomography liver contrast agent, dy-eob-dtpa, in comparison with a conventional iodinated agent in normal and in tumor-bearing rabbits, Invest. Radiol. 37 (2002) 241–247.

[104] S.-J. Lim, J. S. Lim, J. Choi, J.-Y. Choi, W. J. Hyung, H. S. Kim, J. Suh, K. W. Kim, Nanoscaled iodized oil emulsion as a ct contrast agent for the detection of experimental liver tumors in a rat model, Acad. Radiol. 17 (2010) 985–991.

[105] E. J. Rummeny, W. Berning, M. Fuest, U. Bick, B. Niggemann, P. Tournier, X. Fouillet, New res-specific contrast agents for ct, Acad. Radiol. 9 (2002) S185–S190.

[106] S. Kweon, H.-J. Lee, W. J. Hyung, J. Suh, J. S. Lim, S.-J. Lim, Liposomes coloaded with iopamidol/lipiodol as a res-targeted contrast agent for computed tomography imaging, Pharm. Res. 27 (2010) 1408–1415.

[107] H. Aviv, S. Bartling, F. Kieslling, S. Margel, Radiopaque iodinated copolymeric nanoparticles for x-ray imaging applications, Biomaterials 30 (2009) 5610–5616.

[108] A. Galperin, D. Margel, J. Baniel, G. Dank, H. Biton, S. Margel, Radiopaque iodinated polymeric nanoparticles for x-ray imaging applications, Biomaterials 28 (2007) 4461–4468.

[109] A. D. Cooper, Hepatic uptake of chylomicron remnants, J. Lipid Res. 38 (1997) 2173–2192.

[110] D. A. Bakan, F. T. Lee Jr, J. P. Weichert, M. A. Longino, R. E. Counsell, Hepatobiliary imaging using a novel hepatocyte-selective ct contrast agent, Acad. Radiol. 9 (2002) S194–S199.

[111] T. Henning, A. W. Weber, J. S. Bauer, R. Meier, J. M. Carlsen, E. J. Sutton, S. Prevrhal, S. I. Ziegler, H. Feussner, H. E. Daldrup-Link, E. J. Rummeny, Imaging characteristics of dhog, a hepatobiliary contrast agent for preclinical microct in mice, Acad. Radiol. 15 (2008) 342–349.

[112] C. E. Suckow, D. B. Stout, Microct liver contrast agent enhancement over time, dose, and mouse strain, Mol. Imaging. Biol. 10 (2008) 114–120.

[113] M. Aprahamian, G. Bour, C. Y. Akladios, K. Fylaktakidou, R. Greferath, L. Soler, J. Marescaux, J. M. Egly, J. M. Lehn, C. Nicolau, Myo-inositoltrispyrophosphate treatment leads to hif-1α suppression and eradication of early hepatoma tumors in rats, ChemBioChem 12 (2011) 777–783.

[114] P. Carmeliet, R. K. Jain, Angiogenesis in cancer and other diseases, Nature 407 (2000) 249–257.

[115] M. Hiroshi, Smancs and polymer-conjugated macromolecular drugs: advantages in cancer chemotherapy, Adv. Drug Deliv. Rev. 46 (2001) 169–185.

[116] T. K. T. I. K. U. M. Maeda, H.; Matsumoto, Tailor-making of protein drugs by polymer conjugation for tumor targeting: A brief review on smancs, Journal of Protein Chemistry 3 (1984) 181–193.

[117] H. Maeda, J. Wu, T. Sawa, Y. Matsumura, K. Hori, Tumor vascular permeability and the epr effect in macromolecular therapeutics: a review, J. Control. Release 65 (2000) 271–284.

[118] Y. Noguchi, J. Wu, R. Duncan, J. Strohalm, K. Ulbrich, T. Akaike, H. Maeda, Early phase tumor accumulation of macromolecules: a great difference in clearance rate between tumor and normal tissues, Cancer Sci. 89 (1998) 307–314.

[119] B. P. Schneider, K. D. Miller, Angiogenesis of breast cancer, J. Clin. Oncol. 23 (2005) 1782–1790.

[120] E. Karathanasis, S. Suryanarayanan, S. R. Balusu, K. McNeeley, I. Sechopoulos, A. Karellas, A. V. Annapragada, R. V. Bellamkonda, Imaging nanoprobe for prediction of outcome of nanoparticle chemotherapy by using mammography, Radiology 250 (2009) 398–406.

[121] E. Samei, R. S. Saunders, C. T. Badea, K. B. Ghaghada, L. W. Hedlund, Y. Qi, H. Yuan, R. C. Bentley, S. Mukundan Jr, Micro-ct imaging of breast tumors in rodents using a liposomal, nanoparticle contrast agents, Int. J. Nanomed. 4 (2009) 277–282.

[122] T. Helmberger, R. C. Semelka, New contrast agents for imaging the liver, Magn. Reson. Imaging Clin. N. Am. 9 (2001) 745–766.

[123] C. Sun, J. S. H. Lee, M. Zhang, Magnetic nanoparticles in mr imaging and drug delivery, Adv. Drug Deliv. Rev. 60 (2008) 1252–1265.

[124] J. W. M. Bulte, Y. Hoekstra, R. L. Kamman, R. L. Magin, A. G. Webb, R. W. Briggs, K. Gwan Go, C. E. Hulstaert, S. Miltenyi, T. Hauw The, L. De Leij, Specific mr imaging of human lymphocytes by monoclonal antibody-guided dextran-magnetite particles, Magn. Reson. Med. 25 (1992) 148–157.

[125] S. Cerdan, H. R. Lötscher, B. Künnecke, J. Seelig, Monoclonal antibody-coated magnetite particles as contrast agents in magnetic resonance

imaging of tumors, Magn. Reson. Med. 12 (1989) 151–163.

[126] P. Wunderbaldinger, L. Josephson, R. Weissleder, Tat peptide directs enhanced clearance and hepatic permeability of magnetic nanoparticles, Bioconjugate Chem. 13 (2002) 264–268.

[127] S. A. Lyons, J. O'Neal, H. Sontheimer, Chlorotoxin, a scorpion-derived peptide, specifically binds to gliomas and tumors of neuroectodermal origin, Glia 39 (2002) 162–173.

[128] C. Sun, R. Sze, M. Zhang, Folic acid-peg conjugated superparamagnetic nanoparticles for targeted cellular uptake and detection by mri, J. Biomed. Mater. Res. Part A 78A (2006) 550–557.

[129] Y. Zhang, C. Sun, N. Kohler, M. Zhang, Self-assembled coatings on individual monodisperse magnetite nanoparticles for efficient intracellular uptake, Biomed. Microdevices 6 (2004) 33–40.

[130] H. Hong, Y. Zhang, J. Sun, W. Cai, Molecular imaging and therapy of cancer with radiolabeled nanoparticles, Nano Today 4 (2009) 399–413.

[131] R. Weissleder, Molecular imaging: exploring the next frontier, Radiology 212 (1999) 609–614.

[132] N. Chanda, R. Shukla, A. Zambre, S. Mekapothula, R. R. Kulkarni, K. Katti, K. Bhattacharyya, G. M. Fent, S. W. Casteel, E. J. Boote, J. A. Viator, A. Upendran, R. Kannan, K. V. Katti, An effective strategy for the synthesis of biocompatible gold nanoparticles using cinnamon phytochemicals for phantom ct imaging and photoacoustic detection of cancerous cells, Pharm. Res. 28 (2010) 279–291.

[133] D. Danila, R. Partha, D. B. Elrod, M. Lackey, S. W. Casscells, J. L. Conyers, Antibody-labeled liposomes for ct imaging of atherosclerotic plaques, Tex. Heart Inst. J. 36 (2009) 393–403.

[134] N. Graf, D. R. Bielenberg, N. Kolishetti, C. Muus, J. Banyard, O. C. Farokhzad, S. J. Lippard, $\alpha_v\beta_3$ integrin-targeted plga-peg nanoparticles for enhanced anti-tumor efficacy of a pt(iv) prodrug, ACS Nano 6 (2012) 4530–4539.

[135] F. Austrup, D. Vestweber, E. Borges, M. Lohning, R. Brauer, U. Herz, H. Renz, R. Hallmann, A. Scheffold, A. Radbruch, A. Hamann, P- and e-selectin mediate recruitment of t-helper-1 but not t-helper-2 cells into inflamed tissues, Nature 385 (1997) 81–83.

[136] B. J. Graves, R. L. Crowther, C. Chandran, J. M. Rumberger, S. Li, K.-S. Huang, D. H. Presky, P. C. Familletti, B. A. Wolitzky, D. K. Burns, Insight into e-selectin/ligand interaction from the crystal structure and mutagenesis of the lec/egf domains, Nature 367 (1994) 532–538.

[137] C. Wyss, S. C. Schaefer, L. Juillerat-Jeanneret, L. Lagopoulos, H.-A. Lehr, C. D. Becker, X. Montet, Molecular imaging by micro-ct: specific e-selectin imaging, Eur. Radiol. 19 (2009) 2487–2494.

[138] J. F. Hainfeld, M. J. O'Connor, F. A. Dilmanian, D. N. Slatkin, D. J. Adams, H. M. Smilowitz, Micro-ct enables microlocalisation and quantification of her2-targeted gold nanoparticles within tumour regions, Br. J. Radiol. 84 (2011) 526–533.

[139] P. Huang, L. Bao, C. Zhang, J. Lin, T. Luo, D. Yang, M. He, Z. Li, G. Gao, B. Gao, S. Fu, D. Cui, Folic acid-conjugated silica-modified gold nanorods for x-ray/ct imaging-guided dual-mode radiation and photo-thermal therapy, Biomaterials 32 (2011) 9796–9809.

[140] S. S. Kelkar, T. M. Reineke, Theranostics: combining imaging and therapy, Bioconjugate Chem. 22 (2011) 1879–1903.

[141] M. L. Hill, I. R. Corbin, R. B. Levitin, W. Cao, J. G. Mainprize, M. J. Yaffe, G. Zheng, In vitro assessment of poly-iodinated triglyceride reconstituted low-density lipoprotein: initial steps toward ct molecular imaging, Acad. Radiol. 17 (2010) 1359–1365.

[142] S. R. Graziani, F. A. F. Igreja, R. Hegg, C. Meneghetti, L. I. Brandizzi, R. Barboza, R. F. Amancio, J. A. Pinotti, R. C. Maranhao, Uptake of a cholesterol-rich emulsion by breast cancer, Gynecol. Oncol. 85 (2002) 493–497.

[143] A. Niendorf, H. Nägele, D. Gerding, U. Meyer-Pannwitt, A. Gebhardt, Increased ldl receptor mrna expression in colon cancer is correlated with a rise in plasma cholesterol levels after curative surgery, Int. J. Cancer 61 (1995) 461–464.

[144] A. Stranzl, H. Schmidt, R. Winkler, G. M. Kostner, Low-density lipoprotein receptor mrna in human breast cancer cells: Influence by pkc modulators, Breast Cancer Res. Treat. 42 (1997) 195–205.

[145] L. Tatidis, M. Masquelier, S. Vitols, Elevated uptake of low density lipoprotein by drug resistant human leukemic cell lines, Biochem. Pharmacol. 63 (2002) 2169–2180.

[146] D. Kim, Y. Y. Jeong, S. Jon, A drug-loaded aptamer-gold nanoparticle bioconjugate for combined ct imaging and therapy of prostate cancer, ACS Nano 4 (2010) 3689–3696.

The overview of the existing nanoparticulate contrast agent systems has presented the general context of this study:

- Different types of nanoparticles were studied as contrast agent systems.
- Hydrophilic commercial contrast agents or synthesized contrast molecules were incorporated into nanoparticles to show the *in vivo* prolonged contrast enhancements in different organs.
- Nanoparticulate contrast agents showed not only prolonged contrast enhancement in bloodstream but also tissue-specific imaging by passive targeting strategy or by active targeting strategy on linking targeted molecules.

In order to develop new iodinated nanoparticulate contrast agents having a long circulation time in bloodstream, in this study, we decided to focus on the nano-emulsion template. The formulation strategy regards firstly, the synthesis of high iodine-containing oils, and secondly, the formulation of this oil in the form of nano-emulsion nanodroplets dispersed in water. Nano-emulsions were selected owing to their simple preparation process, good stability during several months, suitable structures to encapsulate hydrophobic molecules and finally prolonged circulation time and targeted delivery properties. In this work we choose the low-energy nano-emulsification method, namely the spontaneous nano-emulsification. This method allows the generation of nanometric-scaled droplets without energy supply.
The following paragraph will discuss the theory of nano-emulsions, their characterization methods and different types of emulsification process, especially the spontaneous emulsification method.

Nano-emulsions: Overview and Applications

Xiang Li, Nicolas Anton and Thierry Vandamme

University of Strasbourg, Faculty of Pharmacy, CNRS 7199, Laboratoire de Conception et Application de Molécules Bioactives Equipe de Pharmacie Biogalénique, 74 route du Rhin, BP 60024, F-67401 Illkirch Cedex, France

1. Introduction

Nanotechnology, also called nanoscience, is research focused on multifunctional devices at nanoscale from tens to hundred nanometers. Nanotechnology application in medicine is called nanomedicine, referring to nanoparticle based drug delivery systems. Scientifically defined nanoparticles are colloidal particles of less than 1 μm in diameter. These nanodevices can carry detection signals and/or therapeutic cargos to sites of interest[1, 2]. Many drug candidates present multiple delivery problems *in vivo* such as low solubility or stability, poor pharmacokinetics, adverse effects or undesired toxicity. Formulation scientists have struggled to overcome these problems with nanotechnology. Nanoparticle based drug delivery systems showed to improve efficacy, reduce toxicity, enhance biodistribution, present targeted drug delivery and improve patient compliance compared with conventional dosage forms[3]. These nano-systems with different compositions and biological reactivity have been extensively investigated for drug and gene delivery applications. For example, several anti-cancer drugs are successfully incorporated into nanocarriers. Brain cancer is one of the most difficult malignancies to be detected and treated due to the difficulty of penetrating the blood-brain barrier. However, nanoparticle based anti-cancer drug delivery systems are shown to cross the intact blood-brain barrier and release at therapeutic concentrations in the brain[3, 4]. Nanovehicles in nanomedicine include liposomes, polymeric micelles, nano-emulsions, nanocapsules, dendrimers and nanocrystals etc. In this chapter, we will focus on one of the most important nanovehicles nano-emulsions. Nano-emulsions are suitable systems for drug delivery, given their large surface area, low surface tension and small droplet sizes, which can enhance the penetration and absorption of hydrophobic active compounds. Submicron droplet sizes and great stability of nano-emulsions make them as a promising candidate for practical applications in chemical, pharmaceutical, cosmetic and agro-alimentary fields.

2. Nano-emulsions

2.1. Definition of nano-emulsions

"In an emulsion, liquid droplets and/or liquid crystals are dispersed in a liquid" is the definition of emulsions given by the International Union of Pure and Applied Chemistry (IUPAC) states[5]. Nano-emulsions are nano-sized emulsions, the upper limit of diameter is 500nm[5, 6]. They are transparent or

translucent systems as shown in Fig.1, named also mini-emulsions[8], ultrafine emulsions or sub-micrometer emulsions[7].

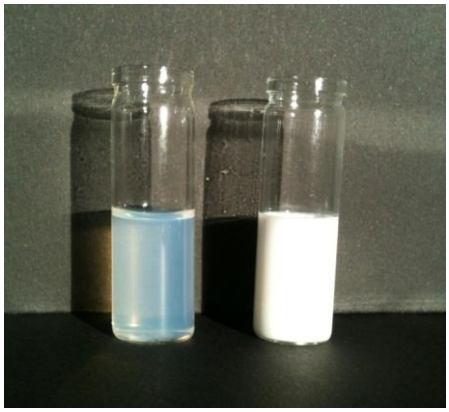

Fig.1. Nano-emulsions with droplet size of 35nm on the left and macro-emulsions with droplet size of 1μm on the right.

Unlike micro-emulsions, nano-emulsions are not thermodynamically but kinetically stable systems. They can remain stable for several months, because their small droplet sizes and narrow size distribution reduce the gravity force and prevent sedimentation and creaming[9, 10]. The trend of the interfacial area minimization is the main physical destabilization of nano-emulsions. This phenomenon is caused by flocculation and Ostwald ripening. Coagulation is naturally prevented by steric stabilization because of the nano-meter droplet sizes of nano-emulsions. The minimum energy of interaction U_T between particles can be reached when $h=2\delta$ (h is inter-droplet distance, δ is interfacial layer thickness), mentioned as U_0, presented in Fig.2 [6]. This energy is directly related to the stability of emulsions. The higher the δ/r ratio is, the lower the value of U_0 and the higher the stability of emulsion systems would be. In the case of nano-emulsions, the ratio of δ/r is much higher than that of macro-emulsions, which prevents the flocculation phenomenon[6, 9].

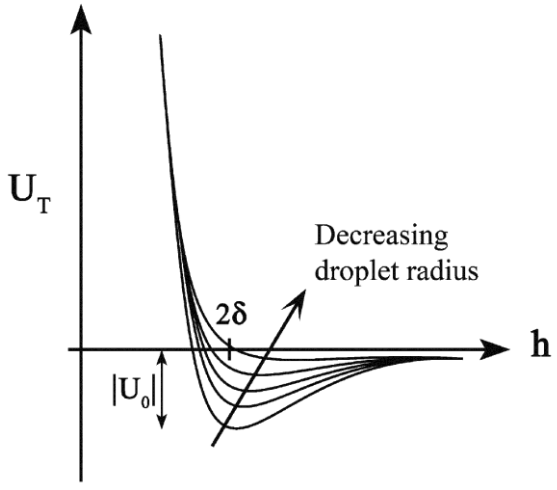

Fig.2. Influence on steric stabilization by emulsion droplet radius[6].

Ostwald ripening is the main mechanism for nano-emulsion breakdown. Small droplets have different interfacial tension than bigger ones, which causes the diffusion of oil molecules from small droplets to bigger droplets[9, 11]. Ostwald ripening rate can be reduced by adding small amounts of additives depending on the different solubility between dispersed components and additives to the bulk phase. Surfactants and co-surfactants can also enhance the stability of nano-emulsion systems and reduce the ripening rate. Because the polymeric emulsifiers increase the layer density in the interfacial zone and the thickness of barrier at the droplet interface, the diffusion rate of the component from droplets is decreased[6].

2.2. Different types of emulsification methods

Since nano-emulsions are not equilibrium systems, they can only be formed with an input energy. In general, methods can be classified based on mechanical devices or the chemical potential of components[7]. Nano-emulsion preparation methods can be divided into two groups: high-energy emulsification methods and low-energy emulsification or condensation methods. High-energy emulsification methods include high shear stirring, high pressure homogenizers or ultrasounds generators. Low-energy emulsification methods make use of phase transitions taking place during the emulsification process. There are two routes: the phase inversion method (PIT) and the spontaneous emulsification method[7, 10, 12, 13].

2.2.1. High-energy emulsification methods

In this part, emulsion formation can be considered as a mixing process by different equipment, including high-pressure, ultrasonic or rotor-stator, etc[14].

1) Rotor-stator systems

Coarse emulsions are passed through a narrow gap between a rotor and a stator[14, 15]. The emulsification process is carried out by rotor rotating, which creates a lower pressure to draw the liquid in and out. This technique is generally used for high viscosity liquids. The dispersion of droplet size is larger than the nano-emulsions formed by sonication and high-pressure homogenizers systems. Emulsion droplet size less than 1μm cannot be achieved by these systems[14, 16].

2) High-pressure systems

Microfluidizer is the most important homogenizer in this device. Macro-emulsions are passed through two opposite narrow gaps. A great shearing action is created by high pressure up to 150MPa and provides an exceptionally fine emulsion[14]. The operating pressure and number of passes of the coarse emulsion through the interaction chamber of microfluidizer determine the particle size. Smaller emulsions can be obtained by increasing the operating pressure or the pass numbers. Microfluidizer

can work with small sample volumes for expensive drugs. But, the production is expensive and the contamination of the different chambers in the microfluidizer is questionable for its application[14, 15, 17].

3) Ultrasonic systems

Ultrasonic emulsification is an efficient method by reducing droplet size for nano-emulsion formation in small batches[7]. The main mechanism for this device is the cavitation. Nano-emulsions formed by sonication need lower amount of surfactant and lower input energy, but are more stable for a given desired diameter[9, 17]. Their droplet size can achieve 0.2μm. Ultrasonic systems are the most popular systems for nano-emulsion production for research purposes.

4) Advantages and disadvantages of high-energy emulsification methods

High-energy emulsification methods present several advantages in industrial applications, such as the flexible control of droplet size distributions and the ability to produce submicron emulsions from a large variety of materials[18]. The amount of surfactant is lower than that produced by low-energy emulsification methods. The main problem of high-energy emulsification methods on nano-emulsion production is "over-processing", which refers to increase in emulsion size by supplying more energy due to a high rate of re-coalescence of new droplets[14]. For ultrasonic systems, only the volume near the sonifer is affected by ultrasonic waves, and a weak mechanical stirring in the other part of samples, which need the additional mechanism to homogenize the droplet size and generate nano-emulsions for high volumes[6].

2.2.2. Low-energy emulsification methods

By taking intrinsic physicochemical properties of components into the formulation, nano-emulsions can be produced almost spontaneously[12, 19]. Two different methods are described in the literature: (i) phase inversion temperature (PIT) method, in which the composition is maintained but has a change in temperature. (ii) spontaneous emulsification method[6, 7, 10].

1) Phase inversion temperature (PIT) method

This method is based on the change in solubility of polyethoxylated nonionic surfactants with different temperatures. Surfactants undergo a partitioning coefficient change in function of the temperature, including under stirring caused by a phase inversion, the so-called transitional emulsion phase inversion.

This process is generally performed with ethoxylated type nonionic surfactants, which is composed of one alkyl chain and one polyethylene oxide chain, which is either hydrophilic or lipophilic according to different temperatures. Polyethoxylated type nonionic surfactants become lipophilic when temperature increases, as a consequence of the dehydration of the polyoxyethylene chains. The

surfactant has more affinity with the aqueous phase at low temperature, inducing the formation of oil-in-water (O/W) emulsion upon stirring and when the temperature rises, the nonionic surfactant becomes lipophilic and water-in-oil (W/O) emulsion is generated. At the HLB temperature, the spontaneous curvature becomes close to zero and at equilibrium a bicontinuous micro-emulsion phase can be established[7].

The determination of HLB temperature or phase inversion temperature (PIT) is very important for the study of nano-emulsion formation. This is carried out by following-up the conductivity of emulsions at different temperatures. The conductivity rises when the temperature increases, until it reaches a maximum and then suddenly decreases. The PIT temperature is defined as the average between the highest and the lowest conductivity values. This temperature varies with different concentration of surfactant, is reduced when the surfactant concentration increases. Because the molecules of polyethoxylated surfactant present a wide distribution of alkyl chain length and ethylene oxide (EO) units, the chains with the lower EO percentage have more affinity with the oily phase. When the concentration of surfactant becomes higher, the content of chains with low EO percentage increases and the PIT temperature decreases[20].

The minimum interfacial tension is achieved at PIT temperature between 10^{-2} and 10^{-5} mNm^{-1} [7], when the affinity of the surfactant for each phase is similar. However the system is not stable and the coalescence rate is very high. Nano-emulsions are produced by rapidly cooling or heating the emulsion system at a temperature much higher than HLB temperature, causing sudden breaking-up of the homogeneous oil/surfactant rich phase. Such thermal shock induces a sudden change in the surfactant solubility and results in the separation of the oil nano-droplets which are immediately stabilized by the surfactant. The obtained nano-emulsions present small droplet sizes and a narrow size distribution. By increasing the surfactant concentration, the emulsion droplet sizes decrease. The PIT method is considered easy to adapt and forms small and uniform droplet size nano-emulsions at low energy cost, free from the toxicity of organic solvent, with a potentially low amount of surfactant[7, 21].

2) Spontaneous emulsification method

The process of spontaneous emulsification method can be described as adding a mixture of surfactant, oil and water-miscible solvent into the aqueous phase[22]. The initial assumption of spontaneous emulsification is that if two bulk liquids are not initially in equilibrium, it is conceivable that dynamic processes such as diffusion could produce emulsification when two liquids are brought into contact without stirring. The energy source of the spontaneous emulsification method is mainly from the interfacial turbulence, the convection driven by interfacial tension gradients which often accompanies diffusion of a solute between phases. Interfaces are subject to capillary waves by thermal fluctuations, whose amplitude is increased when the surface tension decreases[23]. The break-off of droplets is possible for sufficiently large amplitudes.

The establishment of phase diagrams is very important to disclose potential feasibility areas for the emulsification and their optimization[22]. The phase diagram can help to predict the behavior of the liquid at the interface of two immiscible phases brought into contact without stirring. The simplest ternary system consists in water, alcohol and oil, mentioned in Fig.3 [6]. A single-phase region and a two-phase region where the aqueous and oily phase coexist are demonstrated in Fig.3. The evolution of the concentration within each phase is knowen as the "diffusion path". The aqueous phase (point 1) is in contact with the mixture of oil and alcohol (point 4). The dotted segment (2-3) shows the local equilibrium at the interface. The difference between Fig.3a and b demonstrates the spontaneous emulsification region (1'-2), which depends on the composition and natural properties of the alcohol. The depth of the spontaneous emulsification region has a great influence on the intensity of the process. Higher the interfacial turbulences and dispersion can be achieved when the diffusion path of the spontaneous emulsification region is deeper. As mentioned above, the stirring doesn't influence the mechanism of spontaneous emulsification itself but greatly increases the rate of emulsification process. The emulsification process in surfactant free systems is caused solely by the diffusion process. Droplets generated in this model are quickly destabilized; therefore newly formed interfaces have to be stabilized by surfactant adsorption[6].

Fig.3. Ternary diagram of water/alcohol/oil system. Segment (1-2), diffusion path of aqueous phase. Segment (3-4), diffusion path of oily phase. Segment (2-3), interfacial local equilibrium. (a) No spontaneous emulsification region. (b) Segment (1'-2), spontaneous emulsification region[6].

Quaternary systems are established and a more complex of the diffusion path has to be considered between the different phases potentially formed in the interfacial region. Fig.4[6] presents the surfactant with a negative and positive Winsor R, defined as the ratio between the inter-molecular interactions per unit interfacial area, surfactant-oil/surfactant-water. The liquid crystalline (LC) phase plays a decisive role in the spontaneous emulsification process. In Fig.4a, the case of hydrophilic surfactant (R >1), spontaneous emulsification of hydrophilic droplets is the segment (5-5'). For the lipophilic surfactant (R<1) in Fig. 4b, spontaneous emulsification region of oily droplets in water is the segment (1'-2).

Fig.4. Diffusion path of water/alcohol+surfactant/oil system. (a) Hydrophilic surfactant (R >1). Segment (2-3), aqueous sub-phase. Segment (5-5'), spontaneous emulsification region. (b) Hydrophobic surfactant (R<1). Segment (1'-2), spontaneous emulsification region[6].

The process of O/W nano-emulsion preparation by spontaneous emulsification method can be described as slowly adding the mixture of surfactant and oil into the magnetically stirring aqueous phase, normally distilled water or buffer solutions. The rapid diffusion of the hydrophilic surfactant from the oily phase to the aqueous phase induces a dramatic increase of the interfacial area and forms the metastable emulsion state. The proportion of different components influences the nano-emulsion properties, such as size, polydispersity index (PDI) and droplet concentration. Main factors influencing nano-emulsion properties are as followed, (i) solvent/oil weight ratio (SOR), SOR = $100*W_{surfacntant} / (W_{surfactant}+W_{oil})$, which influences the size of nano-emulsions. When the SOR becomes higher, the quantity of surfactant rises and the size of nano-emulsions decreases. However, when the SOR achieves 75-80%, the decrease of droplet size will be stopped. (ii) surfactant-oil/water weight ratio, SOWR = $100*W_{surfactant+oil} / (W_{surfactant+oil} + W_{water})$. The SOWR only has influence on the droplet concentration of nano-emulsions but no influence on nano-emulsion formation. (iii) polydispersity index (PDI), demonstrates the size distribution and the quality of nano-emulsions ranged between 0 and 1. The lower is the PDI, the narrower the size distribution and the better is the quality of nano-emulsions. The nature of surfactant and its affinity between the oily phase and the aqueous phase are also determining factors on nano-emulsion formations. Surfactants have better affinity with aqueous phase, ensuring quick and complete diffusion from the oily phase to the aqueous phase, which is the basis of this process[22].

3) Advantages and disadvantages of low-energy emulsification methods

Low-energy emulsification methods divert intrinsic physicochemical properties of components in the nano-emulsion formulation and expend very low energy on the nano-emulsion formation process. The nano-emulsions generated present submicron sizes and narrow size distributions. These methods are easy to scale-up in pharmaceutical or cosmetic industries and favor work for fragile or thermo-sensitive drugs. But by using low-energy emulsification methods, we should have a careful selection

of surfactant and co-surfactant combination and a carful control of the temperature for the PIT method[17].

3. Nano-emulsion characterization methods

Nano-emulsions and micro-emulsions are both systems ranging in size in the nanometric scale. These systems are self-emulsifying drug delivery systems, present simple formation process, and need very low amounts of supplied energy. However, these systems of micro-emulsion and nano-emulsion are fundamentally different.

Micro-emulsions are thermodynamically stable systems. Their morphology type and size is strongly affected and even destroyed by the change of temperatures or sample dilutions, such as reaching the limit of micro-emulsion stability domain (presented in the phase diagram of micro-emulsions in the literature) by increasing temperature; strong dilution can cause micelle sizes lower than the CMC concentration and destroy the micro-emulsion system. Compared to micro-emulsions, nano-emulsions are thermodynamically unstable but kinetically stable systems, which can remain in stable state in such stress conditions[24].

The formulation process of these two systems is also different. For nano-emulsions, the order of formulation is very important. They can be only formed if surfactants are first mixed with the oily phase and then adding the aqueous phase into the mixture. On the contrary only “macroscopic” emulsions can be formed in the opposite procedure, in which surfactants are mixed with aqueous phase before adding the oily phase. In the case of micro-emulsions, they are strictly identical no matter what order in which the compounds are mixed. This point constitutes a preliminary test for characterizing the nature of the dispersion obtained[24].

To clarify the confusion between nano-emulsion and micro-emulsion systems, two main experimental procedures can serve to identify the nature of nano-systems: (1) the size distribution of nano-systems can be measured by the dynamic light scattering (DLS), which requires a sample dilution (water) before starting the measurement. This dilution can result its change of size of the swollen micelles in micro-emulsion systems, which invalidates the result of characterization or even destroys the micelles. But this procedure is suitable for nano-emulsion systems, because the dilution does not influence the droplet size and size distribution of nano-emulsions. (2) changing the temperature presents a great effect on structure and size of micro-emulsions, which can even cross a boundary when rising the temperature. However, the rise of temperature has no immediate effect on the state of nano-emulsions[24].

4. Parenteral nano-emulsions

More than 40% active substances are hydrophobic bioactive compounds, which are difficult to formulate using conventional approaches[25]. In the case of nano-emulsions, the hydrophobic substance is dissolved in an oily phase dispersed in an aqueous phase as nano-droplets with narrow size distributions[17]. These systems are considered as new vehicles for hydrophobic bioactive compound administration because they provide safer and more patient-compliant dosage forms with enhanced dissolution, improved efficacy and reduced side effects[26].

Parenteral administration is one of the most important routes in drug research. The development of the parenteral formulation of new chemical molecules is necessary for understanding the behavior of new chemical molecules inside the body. Parenteral administration is the best route for emergency cases, due to its direct access to the bloodstream and rapid onset of action as well as targeting specific organs and tissues[27, 28].

Conventional approaches for parenteral formulation of hydrophobic bioactive compounds are the use of co-solvents or oily vehicles. Co-solvent systems present several limitations for parenteral administration, such as the precipitation of the drug upon dilution[27, 28], pain at the moment of injection and hemolysis in some cases. The oily vehicle systems using fixed oil or medium chain triglycerides are only suitable for intramuscular administration but not for intravenous administration and rapid onset of action[27].

Modern approaches for parenteral delivery of hydrophobic bioactive compounds are nanoparticles, such as micelles, liposomes and micro- or nano-emulsions. As a new vehicle for hydrophobic bioactive compounds delivery by parenteral administration, nano-emulsions have interesting features, such as submicron droplet sizes, greater surface area, ability to solubilize considerable amounts of drugs, good physical stability, ease of manipulation, scale-up and low cost[27]. However, nano-emulsions bring the risk of emboli formation after administration, rapid growth of microorganisms and few excipients are available for parenteral administration.

Suitable excipients for parenteral administration have to be biocompatible, sterilizable, non-pyrogenic grade, non-irritant and non-hemolytic. In the case of nano-emulsion systems, components in two phases and properties of surfactant are considered as the main factors for an available parenteral formulation.

1) Oily phase of nano-emulsions

The selection of appropriate oil for nano-emulsion formulation is very important. The rule of the oil selection is based on (i) the solubility of drug in the oily phase. A good solubility helps to achieve larger drug loading in nano-emulsions. Drug solubility can be increased by increasing the chain length

of oily phase[29]. (ii) The properties of the selected oil for the emulsification process. Shorter chain triglycerides and fatty acid esters such as Labrafac® CC (Caprylic/Capric Triglyceride) or vitamin E are easier to emulsify than longer chain triglycerides such as soybean oil or olive oil. A qualified oily phase of nano-emulsion systems presents a good solubility of the drugs and ease to emulsify[27].

2) Surfactants

A suitable surfactant can make the emulsification process easier and enhance the nano-emulsion stability. The selected surfactant should be compatible with the drug and has a good solubility for the drug. Natural surfactants are better than synthetic surfactants, since the nocuous of several surfactants, such as Cremophor EL, a PEG 35 castor oil, could cause anaphylactic shocks and histamine release[30]. The selection of the surfactant is based on the concentration and the type of the nano-emulsion to be formulated. The quantity of surfactant should be as low as possible due to the nocuous properties. Low HLB surfactant or high HLB surfactants are selected for the W/O and O/W types of nano-emulsions, respectively. Some surfactants are considered as suitable components for parenteral administration, such as Tween® 80 (Polysorbate 80), Tween® 20 (Polysorbate 20), Span® 20 (Sorbitan monolaurate), Brij® 96 (Polyoxyethylene 10 oleoyl ether), Cremophor® ELP (Polyoxyl 35 castor oil), Solutol® HS 15 (Macrogol 15 Hydroxystearate) and lcithins etc[27].

3) Aqueous phase

A proper nano-emulsion formulation should be iso-osmotic to the blood and have a neutral pH. In general, the aqueous phase of nano-emulsions is a buffer solution with the blood osmolarity (280-320mOsm/kg) and suitable pH (4-11) for injection.

The size of nano-emulsions for parenteral route should be smaller than the red cells to avoid capillary embolism *in vivo*. The submicron droplet sizes of nano-emulsions could achieve long blood circulation time *in vivo*. Nano-emulsion systems are interesting parenteral delivery systems for hydrophobic drugs, owing to its good solubilization, low-viscosity, less pain at the injection site and the availability to filtrated sterilization technique.

5. Conclusion

Early and accurate diagnosis of clinical conditions and an efficient treatment without side effects are the major goal of medicine. Nanotechnology makes the medicines closer to this purpose. Nano-emulsions can improve the solubility of hydrophobic compounds and their bioavailability. These nano-systems increase the circulation time of hydrophobic bioactive compounds *in vivo* and can have targeted delivery. The design of multifunctional nano-emulsions should be developed in potential therapy areas, where one particle is suitable for both diagnosis and therapy purposes. The same particle may contain an imaging agent to monitor the drug transport process, a function to evaluate the

therapeutic efficacy of a drug, a specific cellular penetration moiety and a therapeutic agent simultanously[31]. Another crucial factor of nano-emulsion evaluation for *in vivo* applications is the toxicity studies. Their submicron droplet sizes, large surface area, chemical composition and geometry could also be factors for potential hazard to human health. Further studies are required to demonstrate the risks associated with exposure to nanoparticles. An ideal nano-emulsion system should be secreted or degraded without any toxic side effects[32]. Nano-emulsions are excellent potential drug delivery systems in nanomedicine field.

References

(1) Park, K. Nanotechnology: What it can do for drug delivery. *Journal of Controlled Release* **2007**, *120*, 1-3.
(2) Wang, M.; Thanou, M. Targeting nanoparticles to cancer. *Pharmacological Research* **2010**, *62*, 90-99.
(3) Ravichandran, R. Nanotechnology-based drug delivery systems. *Nanobiotechnology* **2009**, *5*, 17-33.
(4) Tosi, G.; Costantino, L.; Rivasi, F.; Ruozi, B.; Leo, E.; Vergoni, A.; Tacchi, R.; Bertolini, A.; Vandelli, M.; Forni, F. Targeting the central nervous system: In vivo experiments with peptide-derivatized nanoparticles loaded with Loperamide and Rhodamine-123. *Journal of Controlled Release* **2007**, *122*, 1-9.
(5) Gutiérrez, J.; González, C.; Maestro, A.; Solè, I.; Pey, C.; Nolla, J. Nano-emulsions: New applications and optimization of their preparation. *Current Opinion in Colloid and Interface Science* **2008**, *13*, 245-251.
(6) Anton, N.; Benoit, J.; Saulnier, P. Design and production of nanoparticles formulated from nano-emulsion templates-A review. *Journal of Controlled Release* **2008**, *128*, 185-199.
(7) Solans, C.; Izquierdo, P.; Nolla, J.; Azemar, N.; Garcia-Celma, M. Nano-emulsions. *Current Opinion in Colloid and Interface Science* **2005**, *10*, 102-110.
(8) El-Aasser, M.; Sudol, E. Miniemulsions: Overview of research and applications. *Journal of Coatings Technology Research* **2004**, *1*, 20-31.
(9) Tadros, T.; Izquierdo, P.; Esquena, J.; Solans, C. Formation and stability of nano-emulsions. *Advances in Colloid and Interface Science* **2004**, *108-109*, 303-318.
(10) Solè, I.; Pey, C.; Maestro, A.; González, C.; Porras, M.; Solans, C.; Gutiérrez, J. Nano-emulsions prepared by the phase inversion composition method: Preparation variables and scale up. *Journal of Colloid and Interface Science* **2010**, *344*, 417-423.
(11) Huynh, N.; Passirani, C.; Saulnier, P.; Benoit, J. Lipid nanocapsules: A new platform for nanomedicine. *International Journal of Pharmaceutics* **2009**, *379*, 201-209.
(12) Shinoda, K.; Saito, H. The effect of temperature on the phase equilibria and the types of dispersions of the ternary system composed of water, cyclohexane, and nonionic surfactant. *Journal of Colloid And Interface Science* **1968**, *26*, 70-74.
(13) Calderó, G.; García-Celma, M.; Solans, C. Formation of polymeric nano-emulsions by a low-energy method and their use for nanoparticle preparation. *Journal of Colloid and Interface Science* **2011**, *353*, 406-411.
(14) Jafari, S.; Assadpoor, E.; He, Y.; Bhandari, B. Re-coalescence of emulsion droplets during high-energy emulsification. *Food Hydrocolloids* **2008**, *22*, 1191-1202.
(15) Pinnamaneni, S.; Das, N.; Das, S. Comparison of oil-in-water emulsions manufactured by microfluidization and homogenization. *Pharmazie* **2003**, *58*, 554-558.
(16) Schultz, S.; Wagner, G.; Urban, K.; Ulrich, J. High-pressure homogenization as a process for emulsion formation. *Chemical Engineering and Technology* **2004**, *27*, 361-368.
(17) Wulff-Pérez, M.; Torcello-Gómez, A.; Gálvez-Ruíz, M.; Martín-Rodríguez, A. Stability of emulsions for parenteral feeding: Preparation and characterization of o/w nanoemulsions with natural oils and Pluronic f68 as surfactant. *Food Hydrocolloids* **2009**, *23*, 1096-1102.

(18) Seekkuarachchi, I.; Tanaka, K.; Kumazawa, H. Formation and charaterization of submicrometer oil-in-water (O/W) emulsions, using high-energy emulsification. *Industrial and Engineering Chemistry Research* **2006**, *45*, 372-390.
(19) Rang, M.; Miller, C. Spontaneous emulsification of oils containing hydrocarbon, nonionic surfactant, and oleyl alcohol. *Journal of Colloid and Interface Science* **1999**, *209*, 179-192.
(20) Izquierdo, P.; Esquena, J.; Tadros, T.; Dederen, C.; Garcia, M.; Azemar, N.; Solans, C. Formation and stability of nano-emulsions prepared using the phase inversion temperature method. *Langmuir* **2002**, *18*, 26-30.
(21) Izquierdo, P.; Esquena, J.; Tadros, T.; Dederen, J.; Feng, J.; Garcia-Celma, M.; Azemar, N.; Solans, C. Phase behavior and nano-emulsion formation by the phase inversion temperature method. *Langmuir* **2004**, *20*, 6594-6598.
(22) Anton, N.; Vandamme, T. The universality of low-energy nano-emulsification. *International Journal of Pharmaceutics* **2009**, *377*, 142-147.
(23) Miller, C. Spontaneous Emulsification Produced by Diffusion - A Review. *Colloids and Surfaces* **1988**, *29*, 89-102.
(24) Anton, N.; Vandamme, T. Nano-emulsions and Micro-emulsions: Clarifications of the Critical Differences **2010**.
(25) Merisko-Liversidge, E.; Liversidge, G. Drug nanoparticles: Formulating poorly water-soluble compounds. *Toxicologic Pathology* **2008**, *36*, 43-48.
(26) Kelmann, R.; Kuminek, G.; Teixeira, H.; Koester, L. Carbamazepine parenteral nanoemulsions prepared by spontaneous emulsification process. *International Journal of Pharmaceutics* **2007**, *342*, 231-239.
(27) Date, A.; Nagarsenker, M. Parenteral microemulsions: An overview. *International Journal of Pharmaceutics* **2008**, *355*, 19-30.
(28) Constantinides, P.; Chaubal, M.; Shorr, R. Advances in lipid nanodispersions for parenteral drug delivery and targeting. *Advanced Drug Delivery Reviews* **2008**, *60*, 757-767.
(29) Vandamme, T. Microemulsions as ocular drug delivery systems: Recent developments and future challenges. *Progress in Retinal and Eye Research* **2002**, *21*, 15-34.
(30) Ten Tije, A.; Verweij, J.; Loos, W.; Sparreboom, A. Pharmacological effects of formulation vehicles: Implications for cancer chemotherapy. *Clinical Pharmacokinetics* **2003**, *42*, 665-685.
(31) Sanvicens, N.; Marco, M. Multifunctional nanoparticles - properties and prospects for their use in human medicine. *Trends in Biotechnology* **2008**, *26*, 425-433.
(32) Cormode, D.; Skajaa, T.; Fayad, Z.; Mulder, W. Nanotechnology in medical imaging: Probe design and applications. *Arteriosclerosis, Thrombosis, and Vascular Biology* **2009**, *29*, 992-1000.

3. Conclusion

Ce chapitre bibliographique a permis d'introduire le contexte de ce travail de thèse et les principaux concepts théoriques, principalement focalisé sur des agents de contraste iodés sous la forme de nano-émulsions lipidiques. L'objectif de l'étude a été de synthétiser des huiles iodées constituant la phase huileuse de nano-émulsions et ensuite de les utiliser pour formuler des nano-émulsions par la méthode d'émulsification spontanée. Les propriétés les plus recherchées pour de tels agents de contrastes, concernent principales les une action prolongé au niveau sanguin et/ou spécifique du foie. Comme décrit ci-dessus, le surfactant PEGylé, disposé à l'interface des gouttes de nano-émulsions permet d'éviter la reconnaissance des nano-émulsions par le système immunitaire et donc leur confère une longue rémanence vasculaire *in vivo*. De plus, la nature chimique des composants de ces nanoparticules peut leur permettre de s'accumuler spécifiquement au niveau hépatique selon un phénomène d'accumulation passive. Les chapitres suivants visent à présenter les différentes études expérimentales réalisées dans ce cadre.

Chapter 2.
Blood Pool Contrast Agents based on Iodinated Nano-Emulsions

Dans ce chapitre nous nous intéresserons aux agents de contraste iodé à longue rémanence vasculaire sous forme de nano-émulsions. Les nano-émulsions iodées de type huile-dans-eau sont fabriqués par la méthode d'émulsification spontanée. La phase huileuse consiste en un composé lipophile contenant des molécules capables d'atténuer les rayons X (il va s'agir d'huile iodée). Dans ce chapitre, deux nouvelles huiles iodées ont été développées par notre équipe. La première huile iodée a été effectuée à partir d'une huile commercialisée de type macrogol (le Labrafil® M 1944 CS). La deuxième huile iodée est une huile iodée synthétisée, dont la structure chimique est basée sur celle du Labrafil® M 1944 CS, mais qui contiendra davantage de molécules d'iodes que pour ce premier exemple.

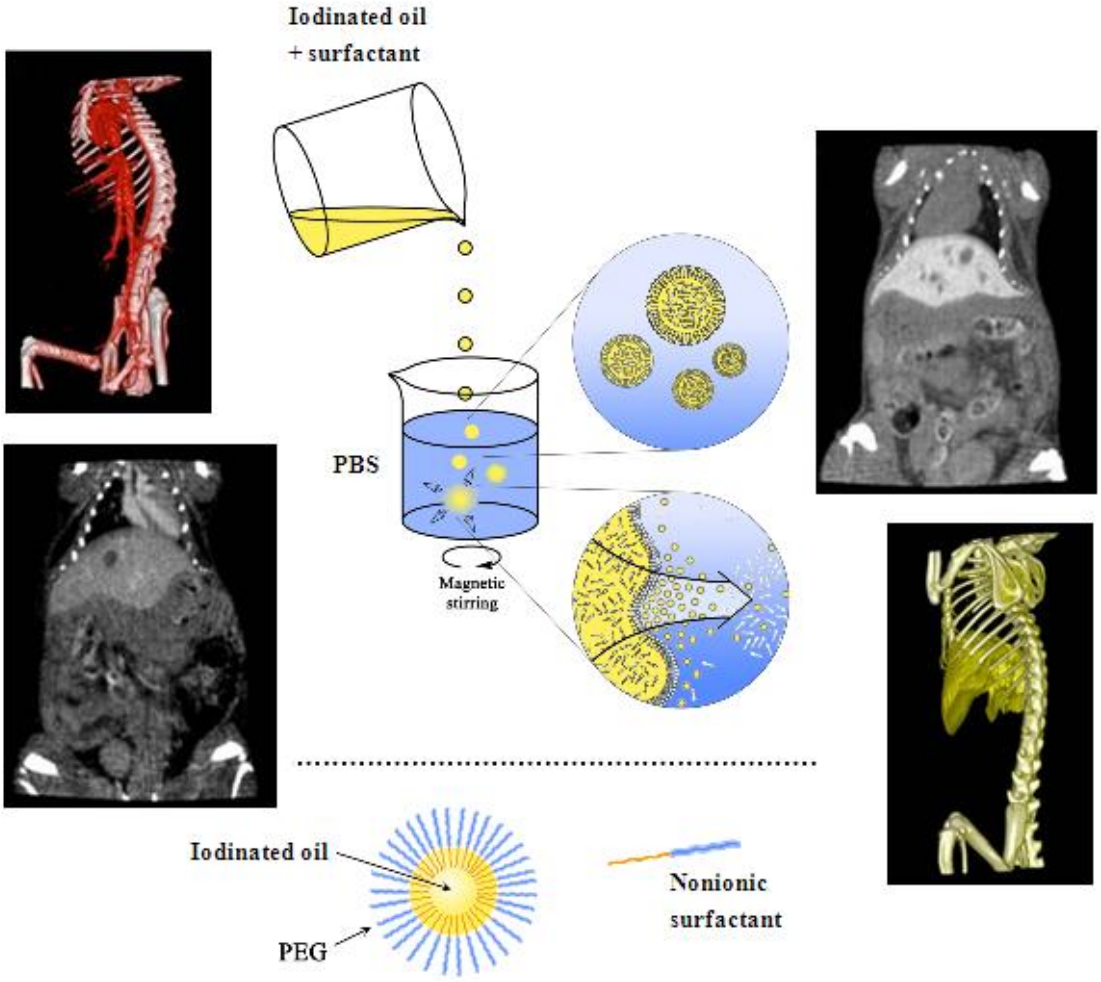

2.1. Agent de Contraste à Longue Rémanence Vasculaire – Nano-émulsions de Labrafil® M 1944 CS iodé

La première partie de ce chapitre est focalisée sur l'étude de nano-émulsions contenant le Labrafil® M 1944 CS iodé. Le Labrafil® M 1944 CS est une huile commercialisée ayant une structure appropriée pour former des nano-émulsions par la méthode d'émulsification spontanée. L'iode a été ensuite introduit par la réaction de Wijs en qui consiste à fixer du chlorure d'iode ICl sur les doubles liaisons des chaînes d'acides gras du Labrafil® M 1944 CS. Les nano-émulsions de Labrafil® M 1944 CS iodé ont une teneur en iode était environ de 85 mg I/mL, ce qui est remarquable comparé aux produits sur le marché. La couche hydrophile autour des gouttes d'huile iodée a été réalisée en associant un surfactant PEGylé, le Cremophor® ELP, qui permet d'éviter la reconnaissance des nano-émulsions par le système immunitaire, et ainsi de leur conférer une longue rémanence vasculaire *in vivo*.

RSC Advances

Cite this: *RSC Advances*, 2011, **1**, 792–801

www.rsc.org/advances

PAPER

Radiopaque iodinated nano-emulsions for preclinical X-ray imaging†

François Hallouard,[a] Nicolas Anton,*[a] Guy Zuber,[a] Philippe Choquet,[b] Xiang Li,[a] Youri Arntz,[c] Gaëlle Aubertin,[b] André Constantinesco[b] and Thierry F. Vandamme[a]

Received 15th April 2011, Accepted 20th July 2011
DOI: 10.1039/c1ra00048a

The context of the this research is the development of nanoparticulate systems exhibiting long circulation times in the blood pool, loaded with X-ray contrasting compounds, to be used as blood pool contrast agents in computed tomography. This study presents an original, new and simple formulation of radiopaque nano-emulsions composed of iodinated oil, formed by a spontaneous emulsification method. As a result, extremely monodisperse, iodinated nano-droplets were generated, ranging in size from 20 to 190 nm, presenting an iodine concentration of around 85 mg I/mL, and coated with a polyethylene glycol shell which ensured their stealth properties against the immune system in the blood stream. *In vivo* assays demonstrated a significant contrast effect, along with a long residence in the blood pool. This study highlights novel nano-formulations used as efficient contrast agents for preclinical X-ray imaging applications, along with simple and efficient alternatives for the generation of iodinated nano-emulsions.

1 Introduction

Micro-computed tomography (micro-CT), is a very powerful and non-invasive tool used to establish high-resolution images with isotropic voxels in relatively short scan times. This technology is particularly suitable for visualizing and differentiating bones and related inorganic constituents from the organic (soft tissue). It is possible to extend the scope of micro-CT application to soft tissue by using X-ray opaque, exogeneous compounds to provide contrast by their selective biodistribution.

Radiopacity is achieved using atoms with high atomic number. Most contrasting agents are composed of iodine because this specie offers a good compromise between contrasting power, safety and cost.[1] Contrast agents used for human applications are hydrosoluble, organic, iodinated molecules. Even if these contrast agents are cleared very quickly from large and small animals, they are effective in humans since clinical CT scanners for human are very fast (*e.g.* five seconds to acquire 15 cm thick volume). However, their use appear limited with micro-CT systems since they tend to be very slow in comparison (*e.g.* ten minutes to scan a mouse). Hence the need to have long circulating agents.[2]

We recently reviewed in detail[1] the different strategies for the formulation of blood pool contrast agents as well as the potential and methods for improving their biocompatibility and pharmacokinetic properties. We then presented an overview of the toxicology of these nanoparticulate contrast agents. Formulations are mainly constituted of liposomes,[3,4] chylomicrons,[5] micelles,[6] dendrimers[7] or polymeric nanoparticles.[8,9]

The general methods used to confer long-circulating properties to contrast agents involve the control of nanoparticle stability and surface properties.[10–17] Although the results are promising, it is worth noting the complexity of the chemistry involved in such formulations, which greatly limits their transposition in this specific field, posing problems even when it comes to potential industrial scale-ups and commercialization (only 2 are available).

Associated with the use of biocompatible excipients, nano-emulsions are prime candidates for our imaging aims and specifications. Not only are these dispersions extremely homogeneous, but they also present very useful stability properties and can remain stable for months.[18]

Nano-emulsion generating processes are generally divided into two groups. The first one comprises "high-energy" processes based on the use of specific devices (high pressure homogenizers, sonifiers, rotor/stator apparatus and so on), supplying enough energy to increase the water/oil interface in order to attain nanometric range droplet sizes. Due to the simplicity of the process, such methods are the most widespread in nano-emulsion formulation. Nevertheless, they are limited by significant inherent drawbacks such as very low energy yields which present a potential problem for industrial scale-up, or difficult conditions of formulation, likely to induce the degradation of fragile molecules during the encapsulation process.

[a]*University of Strasbourg, Faculty of Pharmacy; CNRS 7199, Laboratoire de Conception et Application de Molécules Bioactives, équipe de Pharmacie Biogalénique, 74 route du Rhin, F-67400, Illkirch, France. E-mail: nanton@unistra.fr; Fax: +33 3 6885 4306; Tel: +33 3 6885 4213*
[b]*Service de Biophysique et Médecine Nucléaire, CHRU Strasbourg, Hôpital de Hautepierre; IMFS CNRS 3240, Université de Strasbourg, Laboratoire de biomécanique, 1 avenue Molière, F-67098, Strasbourg, France*
[c]*University of Strasbourg, Faculty of Pharmacy; CNRS 7213, Laboratoire de Biophotonique et Pharmacologie, équipe de biophotonique, 74 route du Rhin, F-67400, Illkirch, France*

† Electronic supplementary information (ESI) available. See DOI: 10.1039/c1ra00048a

In this study, we have chosen to focus on the second group of nano-emulsion generating methods using "low-energy" processes. The principle is very simple, based on spontaneous emulsification mechanisms described elsewhere.[19] It consists in bringing into contact two liquid phases, both at thermodynamic equilibrium. One is an organic phase solubilizing hydrophilic compounds (surfactants, solvents *etc.*) and the other is an aqueous medium. When mixed, the system is in a state of non-equilibrium, resulting in very rapid diffusion of the surfactants and/or solvents (hydrophilic species) from the organic to the aqueous phase. This then generates nano-emulsion droplets. It is worth noting that, unlike microemulsions, nano-emulsions are not thermodynamically stable, but present great kinetic stability.[20] Nano-emulsion droplets are similar to Brownian particles in that they are stable for months, destabilized only by the very slow Ostwald ripening.[18] To summarize, the formulation of nano-emulsions by means of this method is extremely straightforward, simply involving the mixing of two liquids with no need for energy or specific devices. It is a solvent-free process requiring a low amount of surfactant, and results in very stable nanodispersion. The simplicity of the process makes it suitable for quick formulation just prior to administration. It would be easy, for instance, to mix two ampoules containing these two phases. This premise is the basis of the present study. Here we present an original formulation of nano-emulsions based on a novel approach, involving extremely simple spontaneous emulsification of iodinated amphiphiles. The low-energy nano-emulsification process is used, with an iodinated oil as the hydrophobic phase. Oil iodination is performed following the one-step Wijs reaction, in which the oil molecules with non-conjugate double bonds take up the amount of iodine chloride in a short time, forming iodochloro compounds. In addition to the simplicity of the whole process, this study aims to highlight another salient point: the particular location of the iodine atoms, right in the middle of each hydrophobic chain. So here is a solution that potentially influences the physicochemical properties of the iodinated compounds and is very simple to use. Despite these advantages, it is hardly dealt with in the literature, where it is more common to read about iodine binding at the extremities of the molecule. In this work, we therefore wanted to point out the potential and efficiency of this chemical configuration. After in-depth chemical characterization and studying the influence of the formulation parameters on the nano-emulsion features and stability, an *in vivo* evaluation of this iodinated nanoparticle contrast agent is performed in mice.

2 Materials and methods

2.1 Materials

The chemicals used in this study were purchased from commercial sources, in accordance with European Pharmacopoeia, and were used without further purification. Iodine monochloride (98%), $Na_2S_2O_3$ (99%), cyclohexane (99.9%) and sodium hydroxide (99%) were obtained from Sigma (Saint Louis, USA). Potassium iodide (99%) was purchased from Fluka (Saint Louis, USA), NaH_2PO_4-$2H_2O$ (98%) from Merck (Darmstadt, Germany) and dichloromethane (99.95%) from Carlo Erba (Val-de-Reuil, France). Nonionic surfactant from BASF (Ludwigshafen, Germany), *i.e.* Cremophor ELP, batch 29054609T0, was kindly provided by Laserson (Etampes, France) and used as received. This nonionic highly polyethoxylated surfactant is a polyoxiethylated-35 castor oil with a number of ethylene oxide groups given around 35, that is to say with a molecular weight around 1500 $g{\cdot}mol^{-1}$. This surfactant is be a mixture of different oligomers of molecular weights following a Poisson-like distribution centered on the one of announced by the manufacturer. These amphiphiles exhibit a hydrophilic-lipophilic balance, HLB, around ~12–14, and create the PEG layer surrounding the nano-emulsions droplets from their hydrophilic PEG moiety. Finally, the hydrophobic phase, *i.e.* Labrafil M 1944 CS® (Oleoyl Macrogolglycerides), batch 0807541, was obtained from Gattefossé (Saint-Priest, France).

2.2 Methods

2.2.1 Synthesis of iodinated oil. As presented above, the covalent incorporation of iodine into the oil molecules was performed by the Wijs reaction.[21] The hydrophobic phase, Labrafil M 1944 CS® (20 g), was first dispersed in cyclohexane (80 mL). Iodine monochloride (0.09 mol) was then added to this mixture. The dark red solution was magnetically stirred, protected from light and maintained at (40 ± 1) °C for 1 h. Next and with continued stirring, the excess of Wijs reagent was deactivated by mixing it with an aqueous solution of potassium iodide (100 mL at 0.06 mol). This resulted in the formation of an I_2 precipitate, which was eliminated and converted into hydrophilic iodides by adding sodium thiosulfate. The organic phase was washed 3 times with 300 mL of deionized water before removing the organic solvent by rotary evaporation (MD 4C + AK + EK, Vacuubrand, Wertheim, Germany) at (40 ± 1) °C. A light brown iodinated oil was finally obtained. Elemental analysis: C, 50.70%; H, 7.87%; O, 10.04%; I, 24.53%; Cl, 6.86%. The NMR analysis (the spectra are provided as Supplementary Information, ESI†) was reported as follows: ^{1}H NMR ($CDCl_3$) δ 0.84 (t, 6H, CH_3), δ 1.20 to 1.22 (m, 35H, the other CH_2 of fatty acid), δ 1.48 (m, 4H, CH_2 in β of COOR), δ 1.55 (m, 4H, CH_2 in α of CHCl and CHI), δ 2.25 (t, 4H, CH_2 of fatty acid in α of COOR), δ 3.61 (m, 9H, the other CH_2 of poly(ethylene glycol)), δ 4.08 (m, 6H, CH_2 of poly(ethylene glycol) in α of COOR and CHCl), 4.45 (m, 1H, CHI). ^{13}C NMR ($CDCl_3$) δ 14.121 (C-18), δ 22.659 (C-17), δ 24.923 (C-3), δ 26.7 (C-7 and C-12), δ 31.0 (other C of the fat acid), δ 34.054 (C-2), δ 34.415 (C-8), δ 37.532 (C-11), δ 42.435 (C-9), δ 63.377 (C-1′), δ 65.604 (C-10), δ 70.4 (other C of the poly(ethylene glycol)), δ 173.721 (C-1). For the ^{13}C NMR, carbon assignments were done according the two following criteria: (i) C correspond to fatty acids carbons and C′ to poly(ethylene glycol) carbons, and (ii) C carbons numbering goes from COOR (number 1) to CH_3 (number 18). HRMS (ES+): two predominant products were found with a Gaussian distribution of three times 44 Da (corresponding to an ethylene glycol monomer) on both sides *m/z* 1217.39497 ($M+K^+$, 15.58) and 791.27352 ($M+K^+$, 84.42).

2.2.2 Formulation of iodinated nano-emulsions. First, various amounts of iodinated oil and nonionic surfactant were mixed at a controlled temperature of (70 ± 1) °C. Their respective proportions were an important parameter for the control of the droplet size and polydispersity index, PDI, (see below). Next,

this mixture was added to the aqueous phase (a phosphate buffer) and magnetically stirred until a homogeneous, bluish, translucent suspension was obtained (*i.e.* in a few seconds). The mechanism on which the method was based is described in detail in our recent work.[19] The formulation parameters were rationalized through the (i) surfactant/oil weight ratio: SOR = $100 \times w_{surfactant}/(w_{surfactant} + w_{oil})$, and (ii) surfactant-oil/water weight ratio: SOWR = $100 \times w_{surfactan+oil}/(w_{surfactan+oil} + w_{water})$. The value of the SOWR was kept constant at 40% throughout this study, since its influence on nano-emulsion formation is negligible (it only influences droplet concentration[19]). In addition, the pH and osmolarity of the suspension were strictly controlled and adapted for compatibility with parenteral administration. Finally, sample sterilization was performed by filtration through a 0.22μm fluoride of polyvinylidene hydrophilic (PVDF) membrane (Millipore, Molsheim, France). All the formulations were repeated five times.

2.2.3 Characterization. Elemental analysis was performed with an appropriate instrument and approximately 20 mg of dried samples. For the ^{1}H and ^{13}C NMR spectra, chloroform-d chemical shifts were expressed in ppm downfield from tetramethylsilane used as an internal standard. Mass spectra were obtained by the electro-spray method (University of Strasbourg, Service Commun d'Analyses Chimiques).

The hydrodynamic diameters and PDI of the nano-droplets were obtained by dynamic light scattering (DLS) using a Malvern NanoZS instrument (Orsay, France). The helium/neon laser, 4 mW, operated at 633 nm, with the scatter angle fixed at 173° and the temperature maintained at 25 °C. PDI is a measure of the broadness of size distribution derived from the cumulant analysis of DLS data according to ISO 13321 : 1996; for a single Gaussian population with standard deviation, σ, and mean size, x_{PCS}, thus PDI = σ^2/x_{PCS}^2 is the relative variance of the distribution. In other words, it shows the quality of the dispersion. Values $\leqslant 0.1$ reflect very good monodispersity and quality of the nanoparticulate suspensions. Zeta potential measurements were performed with the same apparatus. Measurements were performed three times for each point.

The viscosity of iodinated oil was measured with a rotational viscometer (DV I+, Brookfield, Boston, Massachusetts, USA) at 25 °C, whereas for nano-emulsions, it was determined by means of a capillary Ostwald viscometer, at 37 °C.

The reproducibility of the nano-emulsion formulations was studied by repeating the experiments five times. The pH, osmolarity, size, zeta potential and PDI were determined for each sample.

AFM measurements were performed using a commercial microscope (the Solver Pro-M, from NT-MDT Inc., Moscow). Sample preparation protocol was following: 100 μL of a diluted iodinated nano-emulsion suspensions (oil concentration ~0.3 wt.%) was deposited on the freshly cleaved mica substrate, followed by the addition of 10 μL of a $MgCl_2$ stock solution to obtain a final concentration of 10 nM. The measurements were performed 10 min after sample preparation to allow the interactions between oil droplets and mica. All measurements were conducted in liquid phase (MilliQ water) by using the tapping mode. The cantilevers used were NSG03 type (NT-MDT Inc., Moscow) with a typical spring constant of 1.7 N/m, a resonance frequency of 32 kHz in liquid, and a tip curvature radius of 10 nm. Images were acquired with a resolution of 512 × 512 and a scan rate of 2 Hz.

2.2.4 Stability study. The *in vitro* stability study of iodinated nano-emulsions was performed by following-up the pH, osmolarity, size and PDI of samples stored at (4 ± 2) °C. At each point (0, 1, 2, 3, 14, 30, 60 and 90 days), the formulations were visually observed in order to detect possible creaming. Then they were stirred for 30 s using a Vortex device prior to measuring.

2.2.5 Nano-emulsion stability in FBS. The incubation with fetal bovin serum (FBS) was performed by mixing 0.1 mL of selected nano-emulsions with 1 mL of FBS. The mixture was homogenized and incubated at (37 ± 1) °C under gentle agitation. Visual observation were performed 5 min, 12 h, and 24 h after mixing. Two formulations of iodinated nano-emulsions were tested, SOR = 15% and SOR = 30%.

2.2.6 Micro-CT imaging. The micro-CT scanner used in this study was a GE Healthcare apparatus, eXplore speCZT

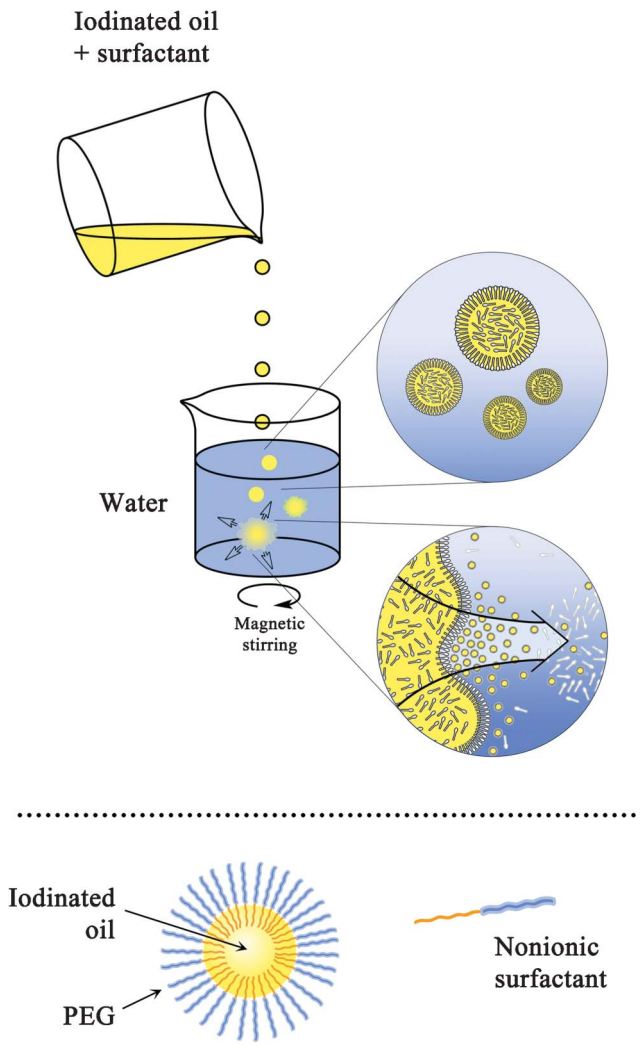

Fig. 1 Diagram of the nano-emulsion formulation process (top), and morphology of the nano-droplets formed (bottom).

Vision® (Waukesha, USA). Parameters for X-ray imaging were: 70 kV, 32 mA and 10 ms. The quantification, in Hounsfield units (HU), was performed by the image-processing software, MicroView by GE Healthcare (Waukesha, USA).

In vitro measurements were performed on iodinated oil and nano-emulsions. An *in vivo* evaluation of the products was carried out using a *nude* mice model (weight *ca.* around 20 g), anaesthetized with isoflurane during administration of the product and throughout the CT scans. 200 µL of nano-emulsions were intravenously injected in the tail-vein, and CT scans were performed at 5, 75 and 210 min after administration. The whole experiment were repeated with five different mice.

The experiments were performed in accordance with the Committee on Animal Research and Ethics of the University of Lyon-1.

3 Results

3.1 Iodinated nano-emulsions

The principle of generating nano-emulsions, illustrated in Fig. 1, shows the simplicity of the process. Once the organic and aqueous phases were in contact with each other, the hydrophilic species solubilized in oil (*i.e.* nonionic surfactants) underwent a very rapid diffusion towards water. This resulted in a demixing of the lipophilic molecules in the form of nanometric-scaled droplets, immediately stabilized by the surfactants. The morphology of the resulting droplets (bottom part of Fig. 1) was simply an iodinated oily core surrounded by a nonionic surfactant layer, thus developing a "hairy" surface due to the PEG moiety of the amphiphiles.

In order to grasp and optimize the formulation of nano-emulsions, it was necessary to study the influence of the formulation parameters on the resulting nano-emulsion properties. This is illustrated in Fig. 2, by showing the relationship between both SOR and size, and SOR and PDI. The nano-emulsification of iodinated and non-iodinated Labrafil M 1944 CS® was also compared, using the same surfactant (Cremophor ELP®) and aqueous phase. This is reported in Fig. 2.

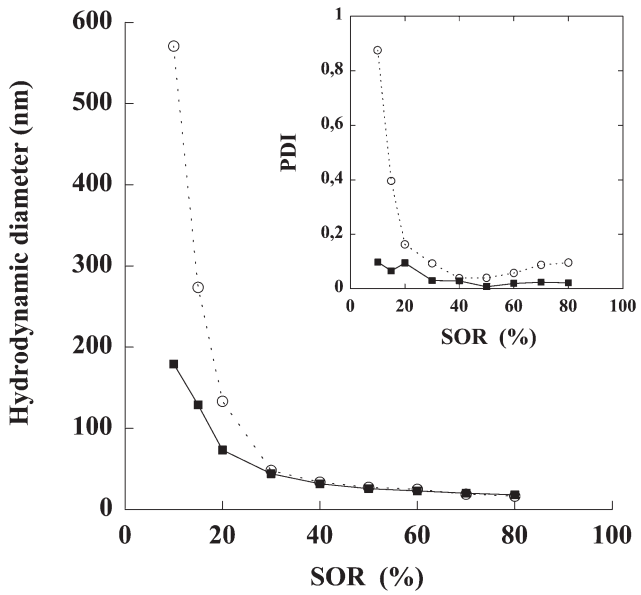

Fig. 2 Nano-emulsions formulated with non-iodinated oil (open circles) and iodinated oil (filled squares). Surfactant = Cremophor ELP®, oil = (native or iodinated) Labrafil M 1944 CS®. Hydrodynamic diameters are plotted against the surfactant oil weight ratio (SOR). *Inset*: The corresponding polydispersity indices are plotted *vs.* SOR.

Table 1 Data on the reproducibility of representative (SOR = 15%, SOWR = 40%) nano-emulsion features. *Size*, *PDI*, *pH*, *osmolarity*: Nano-emulsions were formulated using iodinated Labrafil M 1944 CS®, Cremophor ELP® and phosphate buffer as the aqueous phase.

	Mean value	Standard deviation (%)
Size (nm)	120	2
PDI	0.066	0.032
pH	7.26	0.12
Osmolarity (mOsm/L)	277	1
ζ potential[a] (mV)	−33.3	0.5
ζ potential[b] (mV)	−35.2	0.7

[a] Formulation using iodinated Labrafil M 1944 CS®, Cremophor ELP®. [b] Formulation using *non*-iodinated Labrafil M 1944 CS®, Cremophor ELP®.

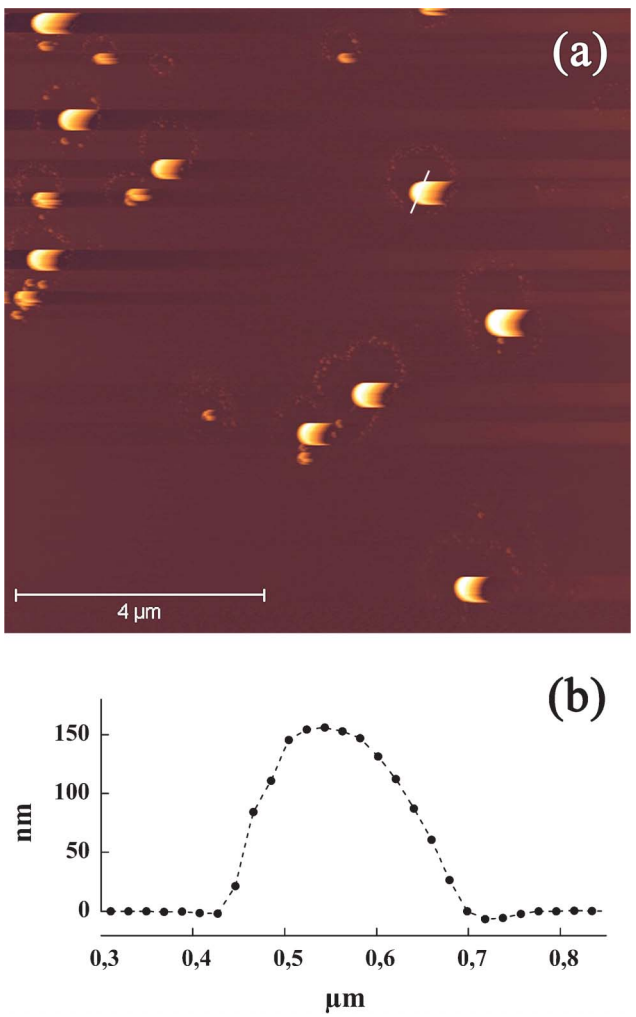

Fig. 3 (a) AFM tapping mode images in liquid phase of iodinated nano-emulsions (SOR = 15%). Nano-emulsion droplets were deposed on mica substrate. (b) Section of a nano-emulsion droplet corresponding to the white line in (a).

The formulation chosen to be used as the blood pool contrast agent was a compromise between the quality of the dispersion (*i.e.* low size and PDI) and amount of surfactant. The formulation parameters were SOR = 15% and SOWR = 40%, and the result of its characterization is reported in Table 1, showing a significant reproducibility of the experiments. The very low PDI values indicate the extreme monodispersity of the nano-emulsion. Zeta potentials measured on iodinated and non-iodinated nano-emulsions disclose a significant negative surface charge as well as similar values for both systems. This is finally coherent with the chemical nature of the compounds used (oil can contain free fatty acid) and with the fact that chemical bounding of iodine has not influence on the surface charge.

Further characterization of these nano-emulsions (SOR = 15%) were conducted using the AFM microscopy (atomic force microscopy) in liquid conditions and tapping mode for less invasive imaging. Fig. 3 presents a typical topographical image of nano-emulsion droplets deposed on atomic flat mica surface. The oil droplets appear regular in shape and size, which is actually coherent with the log-normal distribution and low PDI values disclosed by the dynamic light scattering measurements ($\leqslant 0.1$, see Fig. 4). As well, the droplet size given by the AFM picture is coherent with the DLS results (dh = (120 $\pm$ 2) nm). The images were acquired in low force mode to minimize the morphological distortion of the sample, we observed a surface shadowing effect induced by the interactions between the tip with a soft sample. Section analysis show a typical diameter around (150 $\pm$ 20) nm.

3.2 Stability study

An *in vitro* stability study was performed for 90 days at (4 $\pm$ 2) °C, on two representative iodinated nano-emulsions sized 120 and

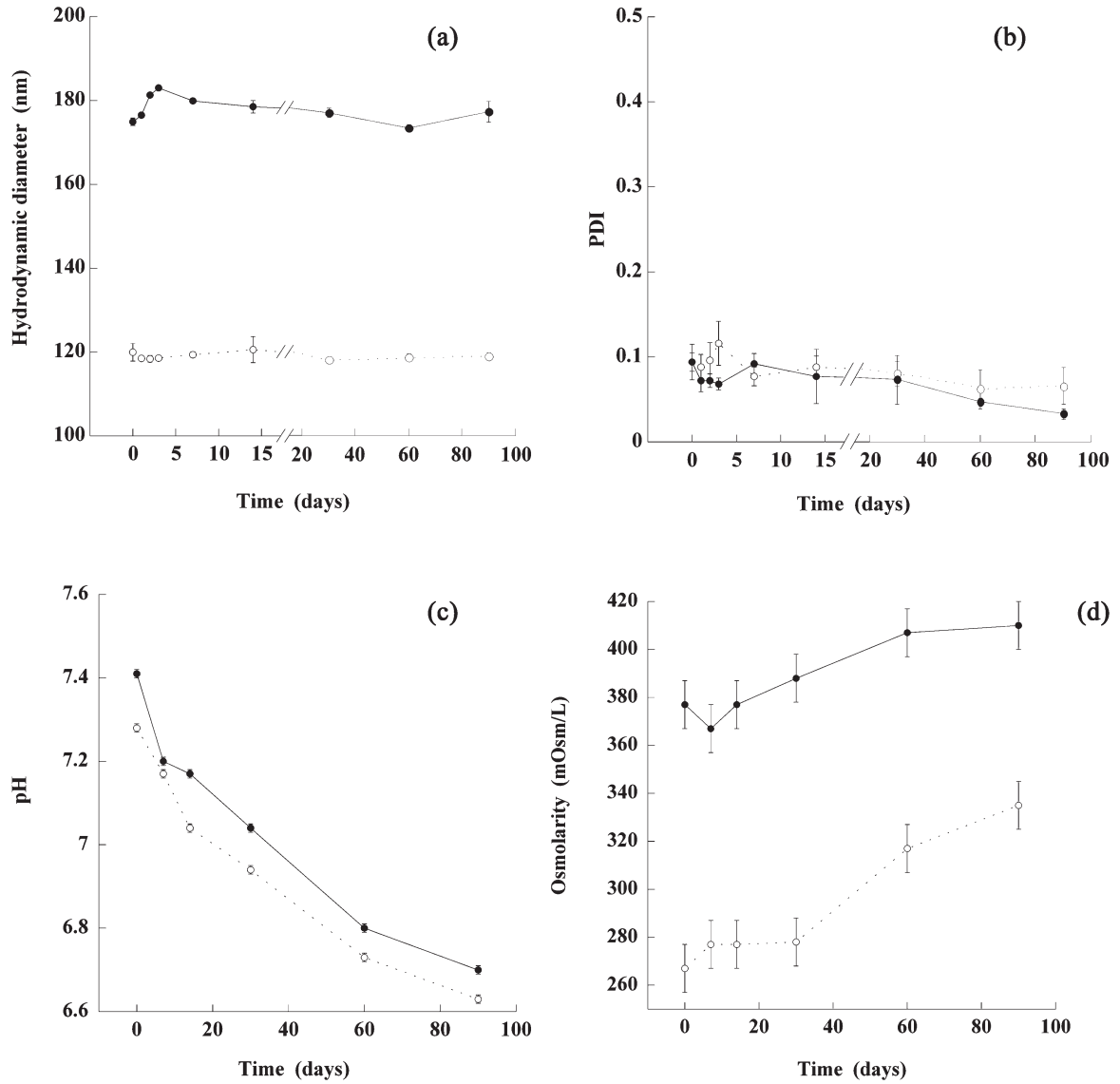

Fig. 4 *In vitro* stability at (4 $\pm$ 2) °C for 3 months of nano-emulsions formulated with iodized/chlorinated Labrafil M 1944 CS®, Cremophor ELP® (non-ionic surfactant) using phosphate buffer as the aqueous phase. Nano-emulsion 1 (filled circles) was formulated with a SOR of 10% and a phosphate buffer with an osmolarity of 330 mOsm/L and nano-emulsion 2 (open circles) was formulated with a SOR of 15% and a phosphate buffer with an osmolarity of 270 mOsm/L. The size (a) and PDI (b) of both emulsions were measured at 0, 1, 2, 3, 7, 14, 30, 60 and 90 days and pH (c) and osmolarity (d) were measured at 0, 7, 14, 30, 60 and 90 days.

180 nm, formulated with controlled pH and osmolarity-compatible with the parenteral administration route. This study includes the follow-up of the hydrodynamic diameter, PDI, pH and osmolarity, and the results are reported in Fig. 4.

The samples exhibit a great stability in time, which is totally coherent with the expected behavior for nano-emulsions. The sizes are centered around the initial one, along with low and constant PDI values lower than 0.1. However, in both formulations we observed similarly fall of the pH and osmolarity: A slow decrease of the pH values appeared, reaching about 6.8 pH at 90 days, along with an increase in osmolarity around 40 mOsm/L, after having been stable for one month. These results reveal a slight, gradual, regular release from the nano-emulsion droplets, of a substance impacting on the pH, and thus also resulting in an increase in osmolarity. This may be a leakage of iodine.

3.3 *In vitro* evaluation

In this section, the *in vitro* X-ray attenuation of our iodinated nano-emulsion and of commercial nano-emulsions (Fenestra VC®), were evaluated by establishing a calibration curve. A commercial hydrophilic contrast agent, XenetiX®, was used as a reference, at a concentration of 300 mg I/mL. The results are shown in Fig. 5 and the corresponding values reported in Table 2.

These results confirm the significant attenuation induced by iodinated nano-emulsions, providing values even higher than 53%, more than for the commercial products (Fenestra VC® at around 55 mg I/mL,[22] which we confirmed, see Table 2).

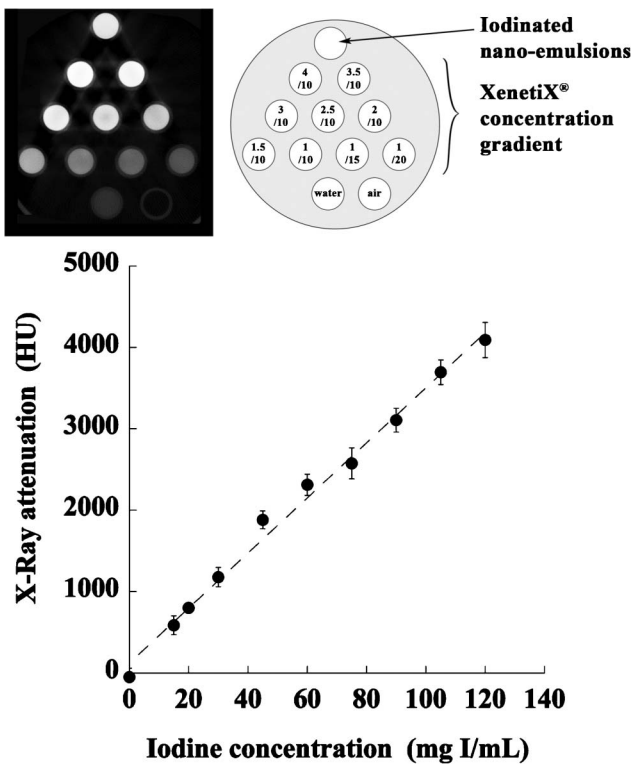

Fig. 5 *In vitro* X-Ray visibility of the iodinated nano-emulsions (120 nm), water, air, and various dilutions of a commercial hydrophilic contrast agent, XenetiX® at 300 mg I/mL. (Top) raw data from the microCT apparatus, and a diagram of the dilutions. (Bottom) resulting calibration curve established with XenetiX®.

Table 2 Values of X-ray attenuation corresponding to the samples presented in Fig. 5. The Iodine concentration was determined using the calibration curve, see details in the text

	Opacification (HU)	Iodine concentration (mg I/mL)
Water	−50.75 ± 109.24	—
Air	−1007.04 ± 114.86	—
Iodinated nano-emulsion	3083.28 ± 130.03	85.52 ± 0.51
Fenestra VC®	2003.55 ± 120.95	55.63 ± 0.24

The higher attenuation is due to higher iodine content. The stability of iodinated nano-emulsions in fetal bovine serum was evaluated and reported in Table 3. The samples appear very stable and homogeneous up to 12 h, and the bigger nano-emulsion (SOR = 15%) shows the first signs of destabilization (slight precipitation) around 24 h, whereas the smaller nano-emulsion remains very stable.

3.4 *In vivo* evaluation of iodinated nano-emulsions

The selected iodinated nano-emulsions described above (SOR = 15% and SOWR = 40%, sized 120 nm see Table 1) were intravenously injected in mice. The results presented in Fig. 6 and Fig. 7, show pictures focused respectively on the heart and kidney, acquired 75 min after injecting the nano-emulsions. A clear vascular contrast is obtained, providing clear images of the blood pool and thus proving the potentials of such iodinated nano-emulsions as blood pool contrast agents for preclinical imaging by disclosing their significant X-ray attenuation power.

Fig. 8 reports the temporal evolution profile of X-ray attenuation in the heart and liver, through three representative acquisitions to the point when the signal is no longer detectable. The mean attenuation is calculated using a cylindrical volume (region of interest) placed inside the left ventricle and the hepatic parenchyma (in yellow on the figure).

4 Discussion

The main challenge for this study is to achieve a simple and efficient chemical iodination, with a negligible impact on both the physico-chemical properties of the oil and the emulsification process.

In the literature, the solution to this problem has generally been to graft iodine atoms to the extremities of the oily molecules using multi-step chemistry,[22] in order to avoid the potential change in their solubility and their interaction with the different compounds of the formulation. Iodinated triglycerides (ITG) were formulated with this aim in mind, and used as the iodinated hydrophobic phase in the formulation of blood pool contrast agents. As regards the application of nano-emulsions as blood pool contrast agents, only a few formulations are proposed,

Table 3 *In vitro* stability of iodinated nano-emulsions in fetal bovine serum. "++" = the sample appears homogeneous without visual aggregation, "−" = a slight precipitation is observed

	5 min	12 h	1 day
Iodinated NE SOR 15%	++	++	−
Iodinated NE SOR 30%	++	++	++

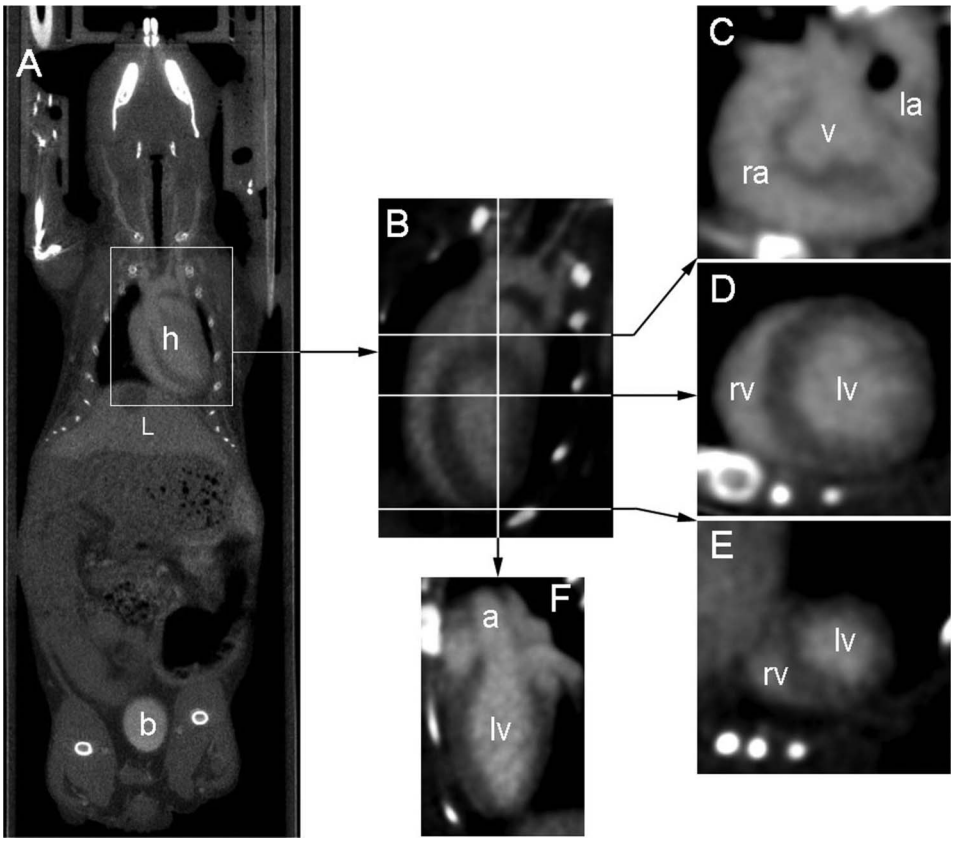

Fig. 6 Images illustrating the contrast enhancement obtained 75 min after IV injection. (A) Whole body coronal view crossing heart (h), liver (L) and bladder (b), showing the dual elimination route. (B) Four cavity slice through the heart (obtained after reorientation), lines indicate positions of corresponding transverse slices (see below). (C) Transverse slice through the base of the heart: right atrium (ra), aortic valve plane (v), left atrium (la). (D) Transverse slice through the middle of the heart : right ventricle (rv) and left ventricle (lv). (E) Transverse slice through the apex of the heart. (F) Slice through the left ventricle showing the beginning of the aortic cross (a).

commercialized and registered, such as for example Fenestra VC® and Fenestra LC®.[5] These products are chylomicron-like in design and either include a specific PEG coating (for blood pool contrast agents) or not (for hepatocyte-selective contrast agents). The oily core of the nano-droplet comprises ITG, synthesized using multi-step chemistry, binding the tri-iodobenzene functions to the hydrophobic extremity of medium chain triglycerides. The nano-emulsions are thus generated using a high-energy process.

The current study proposes a simpler and more efficient alternative, combining (i) one-step chemistry, and (ii) a quick, spontaneous nano-emulsification process. The chemical characterization confirms complete iodination of the unsaturated sites by Wijs reaction. In this study, the hydrophobe used as the oil core for nano-emulsion droplets was selected by means of the two following criteria: (i) good compatibility with the low-energy spontaneous nano-emulsification method (before and after iodination), and (ii) the presence of non-conjugate double bonds in its chemical structure to facilitate iodine incorporation. Labrafil M 1944 CS®, a mixture of PEGylated fatty acids, totally suits these requirements, allowing full iodination following Wijs reaction and thus producing the iodinated oily compounds illustrated in Fig. 9.

According to the European Pharmacopoeia, Labrafil M 1944 CS® iodine value is between 24 and 38 g expecting a theoretical maximum range of iodine between 19 to 27.5 wt%. Now as seen before, iodinated Labrafil M 1944 CS® contains 24.53% of iodine and according to the ^{1}H NMR and ^{13}C NMR, it does not have any double-bound. Thus, we can conclude that Wijs reaction is complete.

Although the iodine is in the middle of each oily chain, its impact on the nano-emulsion formulation process, as shown in Fig. 2, appears to be relatively reduced. The spontaneous emulsification process is not affected by the new properties of the oil and seems, in fact, to be more efficient, giving rise to smaller droplets with a thinner size distribution. This may be due to the slight modifications in the oil hydrophobicity caused by the presence of iodine, which in turn results in slight changes in the affinities between the oil and the surfactants, a critical point of the nano-emulsification process.[19] These appear to be minor variations, probably due to the length of the fatty chains, which counterbalance the chemical perturbation. The lower the oil proportion in the oil/surfactant mixture (*i.e.* the higher the SOR), the lower the resulting nano-emulsion droplet size and PDI. Since the affinities between the oil and the surfactants during the emulsification process impact on the transfer velocity of the diffusing molecules, closely linked to the droplet size, the iodinated oily molecules can be said to show an enhanced hydrophobicity compared to native ones. This then results in inducing a faster diffusion of the surfactants during the

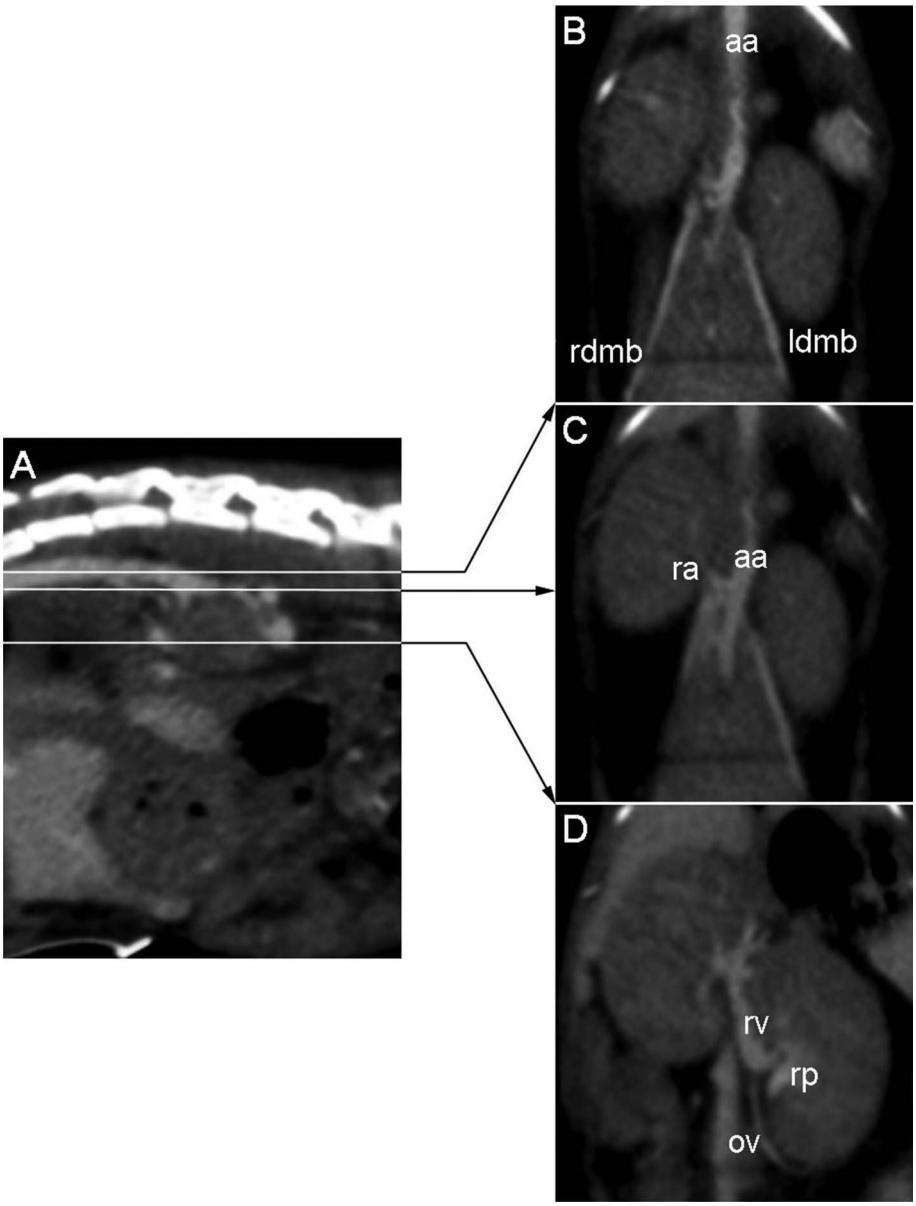

Fig. 7 Anatomical details of kidney vascularization at 75 min after IV injection: (A) Sagittal slice through the lombar spine, lines indicate positions of corresponding coronal slices. (B) Coronal slice through the dorsal part of the kidneys, showing the abdominal course of the aorta (aa) and the right and left dorsal muscular branches (rdmd and ldmb respectively). (C) Coronal slice 1.5 mm lower than (B) showing the right renal artery (ra). (D) Coronal slice 5 mm lower than (C) showing the venous side of kidney vascularization: left renal vein (rv) and left ovarian vein (ov), as well as the contrasted urine in the renal pelvis (rp).

emulsification process, resulting in smaller nano-emulsion droplets. However, the formulation of nano-emulsions is not conditioned by a specific organization of lipids (as is the case for liposome formulation for instance) and this explains the robustness of the process against such chemical modifications.

The stability of the nano-suspensions formed, presented in Fig. 4, shows how compatible the results are with the target applications. Furthermore, the simplicity of the formulation process renders this technology suitable for extemporaneously prepared applications. In other words, users will easily be able to formulate the nano-emulsification on their own, by simply mixing the two pre-sterilized and appropriately packaged phases (organic and aqueous), and then following the appropriate protocol. It will thus be possible to create nano-emulsions just before use. Finally, as shown in Fig. 4, the formulated nano-emulsions remain very stable for the first month of storage, the pH overall is $\geqslant$7.0 and the osmolarity remains stable. This concretely means that once formulated by users, the iodinated suspensions remain stable for a reasonable period and may be used for performing experiments.

To summarize, in comparison to the other types of iodinated contrast agents these low-energy iodinated nano-emulsions offered many advantages, but also, they can be complementary and considered as alternatives to metal nanoparticle (*e.g.* gold or bismuth nanoparticles[23–27]) contrast agents. However, the great advantage of the nano-emulsified forms remains in the stability

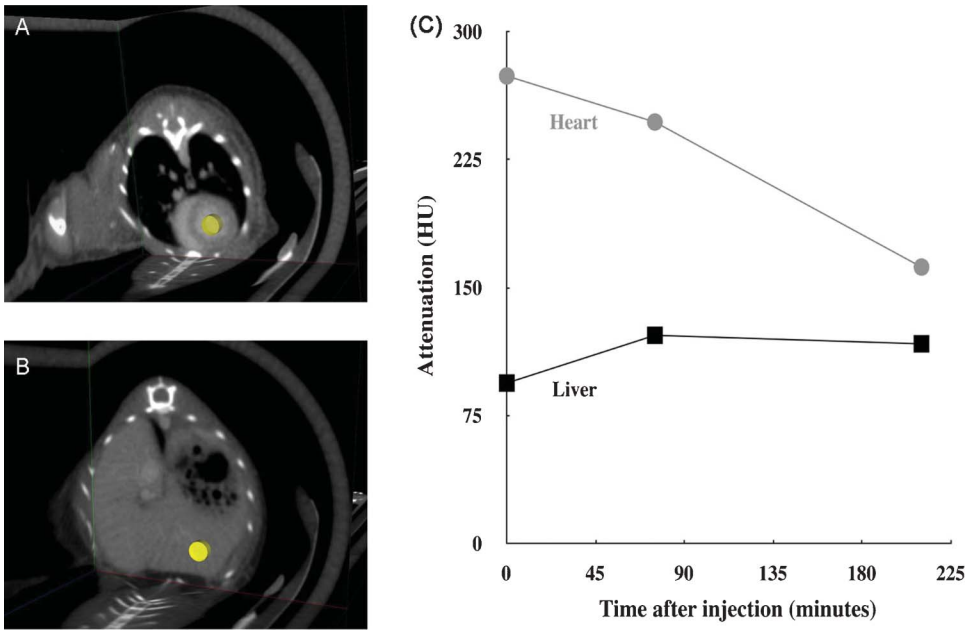

Fig. 8 Follow-up of the attenuation, measured in Hounsfield Units (HU), for the left ventricle and liver after IV injection of the contrast agent. (A) Three-slice view showing the cylindrical region of interest (ROI) in yellow, in the left ventricle where all the measurements were taken. (B) Three-slice view showing the cylindrical ROI in the hepatic parenchyma where all the measurements were taken. The chosen ROI did not contain large vessels. (C) The attenuation over time curve showing the mean for each ROI, with administration of the IV injection at the origin of the time axis. As references, the values of the X-ray attenuation in these two ROI were also measured before the IV injection: 5 and 15 HU, respectively for heart and liver.

of the oil droplets as it is shown in Fig. 4 of the manuscript. Indeed, the stability of nano-emulsions is governed by the thermodynamic properties of the system inducing a strong colloidal repulsion of the droplets, whereas it is often a problem for the other types of nanoparticulate contrast agents, needing specific surface modification in order to increase the colloidal stability. Other advantages lies in the very simple spontaneous nano-emulsion formulations, the very simple chemistry followed for the iodine incorporation. Likewise, due to the use of nonionic PEGylated surfactants, no specific step of chemical surface functionalization is needed to obtain the aimed stealth properties, as it is often the case in the formulation of blood pool contrast agents. Finally, all of these properties are basic advantages of the nano-emulsified systems, however, the high iodine loading even increase the interest of using such a system as blood pool contrast agent.

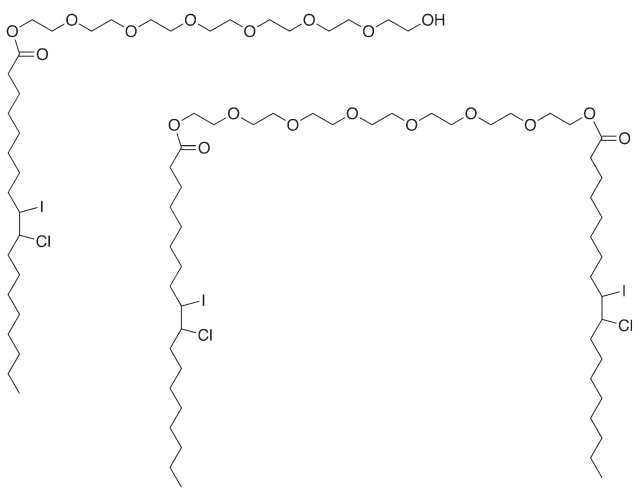

Fig. 9 Structure of the two predominant molecules in the iodinated oil. These two predominant molecules correspond to oleoyl macrogol-6-glycerides iodinated/chlored by the Wijs reaction. Iodine and chlorine are linked at oleic acid double bound during this complete reaction.

The *in vitro* experiments shown in Fig. 5 reveal iodinated nano-emulsions to be sufficiently loaded with iodine to meet the requirements of their target application as blood pool contrast agents. In the literature, the iodine concentrations of blood pool contrast agents are shown to range from 22 to ~100 mg/mL,[3,5,8,9,28–31] thus placing the present iodinated nano-emulsions in the upper range of existing systems. A further significant advantage of the present formulation is the combination of its simplicity (spontaneous emulsification) with its high iodine concentration, where other spontaneously formed systems (micelles or polymeric nanoparticles) only have a reduced amount of iodine once in suspension.[8,9,28] Regarding now the nano-emulsion behavior in presence of blood serum, the results disclosed in Table 3, giving the suspension stable up to 12 h is fully compatible with use as blood pool contrast agent, since nano-emulsions are gradually eliminated from the body within a time lower than 12 h.

The *in vivo* evaluation (Fig. 6, Fig. 7 and Fig. 8) confirms that, once injected (*i.e.* once diluted in the blood pool), the iodinated nano-emulsions still show significant X-ray attenuation and thus a notable vascular contrast. Fig. 6 (A) clearly highlights the vascularization of the heart (h), liver (L) (even showing a reverse contrast of the gallbladder), arterial and venous system. Fig. 6 (B) to (F) show the delineation of the cardiac muscles, emphasizing the right atrium (ra), aortic valve plane (v), left atrium (la), right and left ventricle (rv and lv), and aorta (a). The

first indications of the elimination mechanism also appear in this figure through the concomitant presence of contrasting materials in the bladder (b) and liver (L). This result indicates that one of the elimination routes of these 120 nm nano-emulsions is through the kidneys. This is coherent in as far as the glomerule pore diameters are in the same size range, from 50 to 100 nm,[32] enabling glomerular filtration of this nano-emulsion. This is confirmed by imaging the kidney vascularization, as illustrated in Fig. 7, clearly showing the aorta (aa) right and left dorsal muscular branches (rdmd and ldmb respectively), the right renal artery (ra), and finally the venous side of kidney vascularization: the left renal vein (rv) and left ovarian vein (ov), as well as the contrasted urine in the renal pelvis (rp).

As expected, the temporal *in vivo* follow-up of the X-ray attenuation presented in Fig. 8 confirms the gradual decrease of the iodinated nano-emulsion concentration in the blood pool. The persistence of the signal for up to 4 h shows the long-circulating properties of the nano-droplets, confirming their suitability for use as a tool for preclinical imaging of the vascular system of small laboratory animals. This result is comparable to those reported in the literature, obtained using blood pool contrast agents of various types, *e.g.* liposomes, chylomicrons, micelles.[3,5,28,29,31] Finally, the attenuation observed in the liver slightly increases between the first and the second acquisition, but appears globally constant throughout the experiments. This result indicates an undeniable hepatic uptake, but, given the decrease of the X-ray attenuation in the heart, it could suggest the involvement of a different elimination route. This actually confirms the observation in Fig. 6 with the marked contrast in the bladder (b) indicating the elimination of nano-emulsions *via* the kidneys by glomerular filtration, along with a slighter contrast in the liver (L). Such a concomitant elimination of nano-emulsions could simply be related to their size distribution. Although the low polydispersity index (PDI = 0.066) indicates a thin log-normal distribution centered on 120 nm, a large share of the droplets range in the size of the glomerule pore (see above) and the bigger emulsion droplets will be captured by the reticuloendothelial system.

5 Conclusion

This study presents an original, new formulation of radiopaque nano-emulsions composed of iodinated oil, formed by a spontaneous emulsification method. The advantages of this method are mainly the simplicity of the chemical reaction of oil iodination (Wijs reaction) and the generation of nano-emulsions, along with significant results in terms of *in vivo* contrasting and stealth properties. Furthermore, this work elucidates the link between the formulation parameters and the properties of the nano-emulsions obtained. When injected in nude mice, the iodinated nano-emulsions, formulated by spontaneous emulsification, provide a significant contrast of the blood pool, along with stealth properties (X-ray attenuation visible up to 4 h) making them suitable for use as a blood pool contrast agent.

References

1 F. Hallouard, N. Anton, P. Choquet, A. Constantinesco and T. Vandamme, *Biomaterials*, 2010, **31**, 6249–6268.
2 M. Bourin, P. Jolliet and F. Ballereau, *Clin. Pharmacokinet.*, 1997, **32**(3), 180–193.
3 S. J. Mukundan, K. Ghaghada, C. Badea, C. Kao, L. Hedlund, J. Provenzale, G. Johnson, E. Chen, R. Bellamkonda and A. Annapragada, *Am. J. Roentgenol.*, 2006, **186**, 300–307.
4 D. B. Elrod, R. Partha, D. Danila, S. W. Casscells and J. L. Conyers, *Nanomedicine: NBM*, 2009, **5**, 4245.
5 J. Weichert, F. Lee Jr., M. Longino, S. Chosy and R. Counsell, *Acad. Radiol.*, 1998, **5**, 16–19.
6 V. Torchilin, *Colloids Surf., B*, 1999, **16**, 305–319.
7 A. Yordanov, A. Lodder, E. Woller, M. Cloninger, N. Patronas, D. Milenic and M. Brechbiel, *Nano Lett.*, 2002, **2**(6), 595–599.
8 A. Galperin, D. Margel, J. Baniel, G. Dank, H. Biton and S. Margel, *Biomaterials*, 2007, **28**(30), 4461–4468.
9 W. Ho Kong, W. Jae Lee, Z. Yun Cui, K. Hyun Bae, T. Gwan Park, J. Hoon Kim, K. Park and S. Won Seo, *Biomaterials*, 2007, **28**(36), 5555–5561.
10 V. Torchilin and V. Trubetskoy, *Adv. Drug Delivery Rev.*, 1995, **16**, 141–155.
11 D. Lasic, F. Martin, A. Gabizon, S. Huang and D. Papahadjopoulos, *Biochim. Biophys. Acta, Biomembr.*, 1991, **1070**, 187–192.
12 A. Chonn, S. Semple and P. Cullis, *J. Biol. Chem.*, 1992, **267**, 18759–18765.
13 E. Ranucci, G. Spagnoli, L. Sartore and P. Ferutti, *Macromol. Chem. Phys.*, 1994, **195**, 3469–3479.
14 L. Sartore, E. Ranucci, P. Ferutti, P. Caliceti, O. Schiavon and F. Veronese, *J. Bioact. Compat. Polym.*, 1994, **9**, 411–427.
15 M. Woodle, C. Engbers and S. Zalipsky, *Bioconjugate Chem.*, 1994, **5**, 493–496.
16 O. Monfardini, C. Schiavon, P. Caliceti, M. Morpurgo, J. Harris and F. Veronese, *Bioconjugate Chem.*, 1995, **6**, 62–69.
17 H. Takeuchi, H. Kojima, H. Yamamoto and Y. Kawashima, *J. Controlled Release*, 2001, **75**, 83–91.
18 N. Anton, J.-P. Benoit and P. Saulnier, *J. Controlled Release*, 2008, **128**(3), 185–199.
19 N. Anton and T. Vandamme, *Int. J. Pharm.*, 2009, **377**, 142–147.
20 N. Anton and T. Vandamme, *Pharm. Res.*, 2010in press, year.
21 J. Wijs, *Anal. Bioanal. Chem.*, 1898, **37**(5), 277–283.
22 J. Weichert, M. Longino, D. Bakan, M. Spigarelli, T. Chou, S. Schwendner and R. Counsell, *J. Med. Chem.*, 1995, **38**, 636–646.
23 R. Popovtzer, A. Agrawal, N. Kotov, A. Popovtzer, J. Balter, T. Carey and R. Kopelman, *Nano Lett.*, 2008, **8**, 4593–4596.
24 W. Eck, A. Nicholson, H. Zentgraf, W. Semmler and S. Bartling, *Nano Lett.*, 2010, **10**, 2318–2322.
25 R. Menk, E. Schültke, C. Hall, F. Arfelli, A. Astolfo, L. Rigon, A. Round, K. Ataelmannan, S. MacDonald and B. Juurlink, *Nanomedicine: NBM.*, 2011in press, year.
26 O. Rabin, J. Perez, J. Grimm, G. Wojtkiewicz and R. Weissleder, *Nat. Mater.*, 2006, **5**, 118–122.
27 D. Pan, T. Williams, A. Senpan, J. Allen, M. Scott, P. Gaffney, S. Wickline and G. Lanza, *J. Am. Chem. Soc.*, 2009, **131**, 15522–15527.
28 V. Torchilin, M. Frank-Kamenetsky and G. Wolf, *Acad. Radiol.*, 1999, **6**(1), 61–65.
29 C. Y. Kao, E. A. Hoffman, K. C. Beck, R. V. Bellamkonda and A. V. Annapragada, *Acad. Radiol.*, 2003, **10**, 475–483.
30 Y. Fu, D. Nitecki, D. Maltby, G. Simon, K. Berejnoi, H.-J. Raatschen, B. Yeh, D. Shames and R. Brasch, *Bioconjugate Chem.*, 2006, **17**(4), 1043–1056.
31 T. Henning, A. Weber, J. Bauer, R. Meier, J. Carlsen, E. Sutton, S. Prevrhal, S. Ziegler, H. Feussner, H. Daldrup-Link and E. Rummeny, *Acad. Radiol.*, 2008, **15**(3), 342–349.
32 M. Vaubourdolle, *Toxicologie, Sciences mathmatiques, physiques et chimiques*, Groupe Liaisons, 2007.

2.2. Agent de Contraste à Longue Rémanence Vasculaire – Nano-émulsions d'huile reconstituée iodée

Les nano-émulsions de Labrafil® M 1944 CS iodé présentées dans la section 2.1 ont montré un contraste prolongé au niveau sanguin après injection chez les souris. Dans cette section, une nouvelle huile iodée construite sur la base de la structure du Labrafil® M 1944 CS a été synthétisée par notre équipe, afin d'augmenter la teneur en iode dans l'huile comparée à celle obtenue avec du Labrafil® M 1944 CS. Cette huile reconstituée a été préparée en greffant deux chaînes d'acide gras sur une chaîne de polyéthylène glycol 300. Des atomes d'iode ont ensuite été greffés sur la structure de l'huile, toujours par réaction de Wijs. Cette huile reconstituée a une structure similaire à celle du Labrafil® M 1944 CS. En partant du fait que le nombre de doubles liaisons sur des chaînes d'acides gras est supérieur à celui du Labrafil® M 1944 CS seul, la quantité finale d'iode par molécule d'huile a également été accrue.

Blood Pool Contrast Agent based on Nano-emulsions of Iodinated Reconstituted Oil

1. Introduction

Significant and prolonged contrast enhancement was observed in the bloodstream for more than 2h after injection of 200 µL nano-emulsions of iodinated Labrafil® M 1944 CS[1] as demonstrated in the chapter 2.1. The iodine content in these nano-emulsions was about 85 mg I/mL. In order to further enhance the contrast capacity of iodine-containing nano-emulsions, we decided to develop new iodinated oil presenting a similar structure of Labrafil® M 1944 CS (*i.e.* compatible with spontaneous emulsification) but in which higher iodine content can be grafted. Hereby, reconstituted oil was synthesized based on the structure of Labrafil® M 1944 CS by grafting two fatty acid chains onto the hydroxide groups of polyethylene glycol 300. As the iodine was added by saturating the double bonds of fatty acids in Labrafil® M 1944 CS, the number of double bonds in fatty acid chains should be increased to finally achieve higher iodine content. Thus, the major fatty acid in reconstituted oil was composed on the triply unsaturated fatty acid of linolenic acid instead of the mono-unsaturated fatty acid of oleic acid in Labrafil® M 1944 CS. Iodine was then incorporated into the synthesized reconstituted oil as the same way of Labrafil® M 1944 CS by the Wijs reaction. The increased double bonds in fatty acids allowed us to introduce more iodine than Labrafil® M 1944 CS. And the contrast capacity of nano-emulsions of iodinated reconstituted oil will be enhanced at the same SOR and SOWR due to this higher iodine content.

2. Experimental section

2.1. Materials

Linseed oil (Fagron, France), polyethylene glycol 300 (PEG 300) (Sigma Aldrich, France), thionyl chloride (Sigma Aldrich, France), iodine monochloride (Sigma Aldrich, France), potassium iodide (Sigma Aldrich, France), sodium thiosulfate (Sigma Aldrich, France), Cremophor® ELP (free sample from BASF Ludwigshafen, Germany), Phosphate Buffered Saline (PBS) (Eurobio, France), sheep erythrocytes (Dutscher, France).

^{1}H spectra was obtained with a Bruker Top Spin 3.0 400 MHz spectrometer. $CDCl_3$ chemical shifts are expressed in ppm downfield from tetramethylsilane as internal standard.

2.2. Synthesis of reconstituted oil

The synthesis of reconstituted oil comprises two mainly steps: 1) the saponification of linseed oil to obtain its free fatty acids and 2) the esterification between fatty acids and polyethylene glycol 300, demonstrated in schema 1.

1) Saponification of linseed oil

Reconstituted oil was composed by the multi-unsaturated fatty acids, especially triple unsaturated fatty acid of linolenic acid, to achieve higher iodine content. The free multi-unsaturated fatty acids were obtained by the saponification of linseed oil (containing more than 50% of triple unsaturated α-linolenic acid and about 15% of double unsaturated linoleic acid). Briefly, linseed oil (47g, 0.05mol) was firstly mixed with 80ml ethanol and then six equivalents of sodium hydroxide solution 3mol/L (0.3mol, 100 ml) were added into the mixture. The flask was stirred at 60°C until the mixture became red and transparent. Fatty acids were extracted with ethyl acetate and citric acid 10% until the pH of the aqueous phase was 1. Then, the extraction was made with saturated NaCl solution and dried over anhydrous Na_2SO_4. The organic phase containing fatty acids was kept and the solvent was removed by vacuum. Obtained fatty acids are brightly yellow oil.

2) Synthesis of reconstituted oil

Reconstituted oil was then synthesized by grafting fatty acids of linseed oil onto the hydroxide groups of PEG 300. Briefly, fatty acids of linseed oil (21g, 0.075mol) were firstly dissolved in dichloromethane and then thionyl chloride (8.2ml, 0.11mol) was slowly added at 0°C. The mixture was stirred at room temperature during 1h and then the solvent was removed in vacuum to eliminate byproducts of the reaction. The mixture is re-dissolved in dichloromethane and is added slowly to PEG 300 (9g, 0.03mol) into the mixture. The flask was stirred at room temperature during 24h. Reconstituted oil was then extracted twice with ethyl acetate and a solution of sodium bicarbonate 10%, once with saturated NaCl solution and dried over anhydrous Na_2SO_4. The organic phase of reconstituted oil is kept and the solvent is removed in vacuum. Obtained reconstituted oil was brightly red oil.

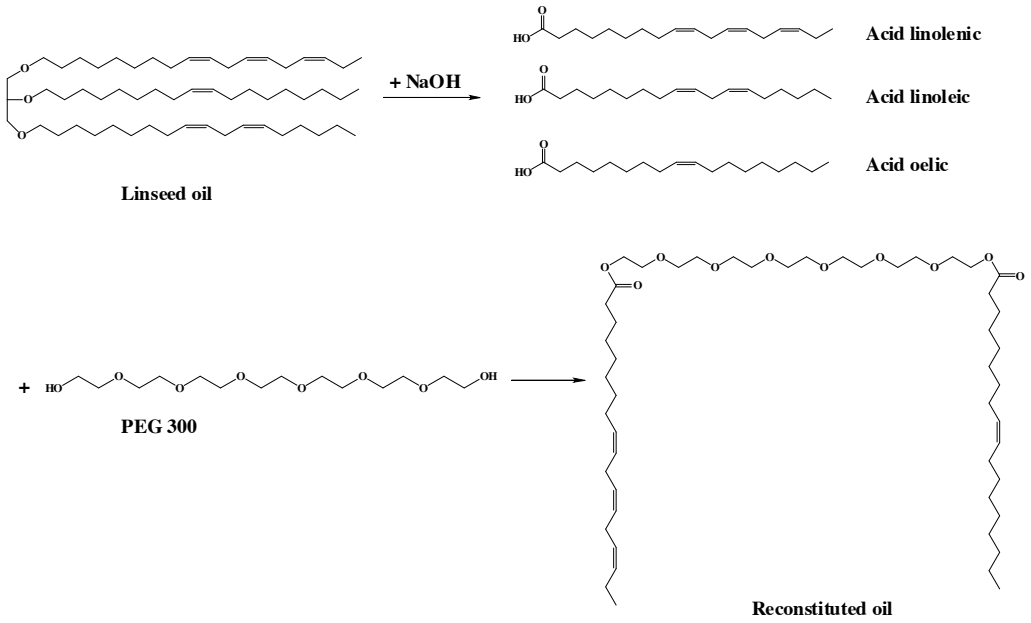

Scheme 1. Chemical scheme for the synthesis of reconstituted oil from fatty acids of linseed oil and PEG 300.

2.3. Synthesis of iodinated reconstituted oil

Iodine was introduced into the reconstituted oil by the Wijs reaction,[2, 3] hereby the same way of the iodination of Labrafil® M 1944 CS as shown in scheme 2. Reconstituted oil (9g, 0.01mol) and iodine monochloride (7.3g, 0.045mol) were firstly dissolved in cyclohexane, protected from light and stirred at 40°C during 1h. Then, to eliminate the excess of iodine monochloride, the mixture was reacted with an excess solution of potassium iodide (1.25g, 0.0075mol) and another solution of sodium thiosulfate (2.4g, 0.015mol), respectively. Iodinated reconstituted oil was then extracted three times with dichloromethane. The phase of dichloromethane was kept and the solvent was removed in vacuum. Obtained iodinated reconstituted oil was red and very viscous oil. Elemental analysis: C, 40.07%; H, 5.92%; O, 10.67%; I, 33.87%; Cl, 9.47%.

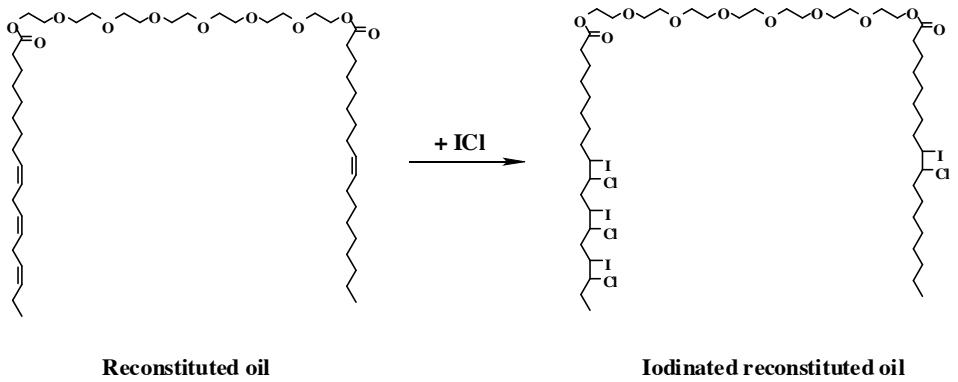

Scheme 2. Chemical scheme for the synthesis of iodinated reconstituted oil via Wijs reaction.

2.4. Preparation of nano-emulsions of iodinated reconstituted oil

Nano-emulsions of non-iodinated and iodinated reconstituted oil were formulated by the spontaneous emulsification method as previously described in the literature.[4, 5] Iodinated reconstituted oil (oily phase) was firstly mixed with the non-ionic hydrophilic surfactant, Cremophor® ELP. Phosphate buffered saline (PBS) (aqueous phase) was then added into the oil / surfactant mixture under gentle magnetic stirring. Nano-emulsions formed immediately once these two phases were brought into contact. The optimized formulation was chosen to give a compromise between the nano-emulsion size and monodispersity, and the iodine content. In this work, the SOR (surfactant / oil weight ratio) varied from 20% to 60% for the non-iodinated reconstituted oil and from 30% to 60% for the iodinated reconstituted oil. The SOWR (surfactant + oil / water weight ratio) was kept at 40% for both non-iodinated and iodinated reconstituted oil, since the value of the SOWR induced negligible influences on the formation of nano-emulsions. The pH and osmolarity of nano-emulsions were strictly controlled and adapted for the requirements of parental administration.

2.5. Hemolysis assay

The biocompatibility of nano-emulsions of iodinated reconstituted oil to the blood was assessed by a hemoglobin release assay.[6, 7] Sheep erythrocyte sample was firstly diluted into phosphate buffered saline (PBS) and washed by three cycles of centrifugation (400 rcf, 10min) and resuspension. The solution of rinsed red blood cell (RBC) was then diluted with PBS to give a RBC suspension of 1×10^8 RBC/mL and immediately used to evaluate the hemolytic properties of the iodine-containing nano-emulsions as follows: 20 µL of nano-emulsions were added to 180 µL of erythrocyte suspension, in 96-well microplates. The sample was incubated for 1 h at 37°C with orbital shaking. The precipitated RBCs at the bottom of microplates were observed under optical microscope. The blank sample was obtained from the untreated erythrocytes.

2.6. In vivo experiments

The *in vivo* experiments were performed in Swiss mice. Before acquisition, mice were anesthetized with isoflurane. Then, nano-emulsions of iodinated reconstituted oil (SOR = 60%, SOWR = 40%) were intravenously injected in the tail vein, with an injection volume corresponding to 10% of the blood volume.

3. Results

3.1. Synthesis of reconstituted oil

As it can be seen in Scheme 1, reconstituted oil was synthesized from the saponification of linseed oil. Fatty acids of linseed oil were then grafted onto the hydroxide groups of PEG 300 occurred at the two sides of the chain. To decrease the reaction time and optimize the yield of reconstituted oil, fatty acids

of linseed oil were firstly converted to acyl chloride with thionyl chloride. PEG 300 was then reacted with the acyl chloride to form the reconstituted oil. The structure of reconstituted oil has been investigated through detailed ^{1}H NMR analyses, as shown in Fig. 1. The peaks appeared in the reconstituted oil's NMR spectra between 3.5 and 4.3 ppm attributed to the CH_2 protons of PEG 300, which demonstrated the addition of fatty acids onto the PEG 300 chains after the esterification. The yield of the reaction was achieved to be more than 70%.

3.2. Synthesis of iodinated reconstituted oil

Wijs reaction is widely used to determine the iodine value on saturating non-conjugated double bonds in molecules with iodine monochloride. The introduction of the iodine should modify the oil hydrophobicity. For the Labrafil® M 1944 CS, this enhanced hydrophobicity seemed to be more efficient to formulate nano-emulsions with smaller droplets and thinner size distribution at the same SOR. Thus, the iodination of reconstituted oil was also performed following the Wijs reaction. As shown in Fig. 1, the disappeared peak located at 5.35 ppm in the iodinated reconstituted oil's NMR spectra demonstrated the saturation of the double bonds in fatty acids by the iodine monochloride. The iodine content in the reconstituted oil was achieved at 33.87%.

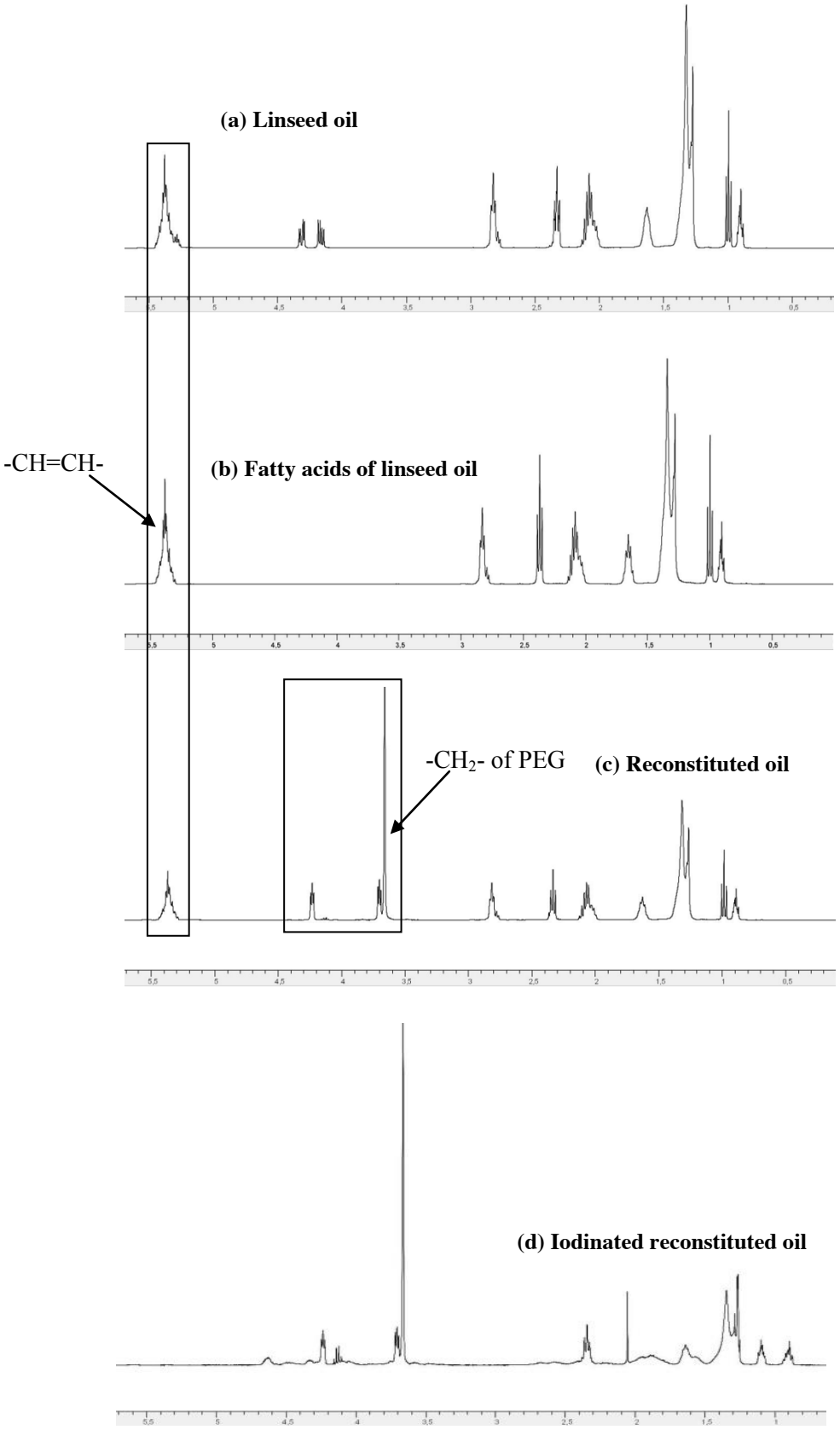

Figure1. ^{1}H NMR spectra ($CDCl_3$) of (a) linseed oil, (b) free fatty acids of linseed oil, (c) reconstituted oil and (d) iodinated reconstituted oil.

3.3. Formulation of nano-emulsions of iodinated reconstituted oil

Nano-emulsions of non-iodinated and iodinated reconstituted oil were both prepared by the spontaneous emulsification method by using the surfactant of Cremophor® ELP and the aqueous phase of the phosphate buffered saline (PBS), as shown in Fig. 2. Nano-emulsions of iodinated reconstituted oil showed larger sizes than nano-emulsions of non-iodinated reconstituted oil at the same SOR. The optimized formulation of nano-emulsions of iodinated reconstituted oil was finally selected at SOR = 60% and SOWR = 40%, due to the smaller sizes of 128 nm close to 100 nm and the higher stability compared with other SOR. However, at this higher SOR = 60% and SOWR = 40%, the final iodine content in the formulation was 5.4%, which was less than the one of Labrafil® M 1944 CS of 8.3%.

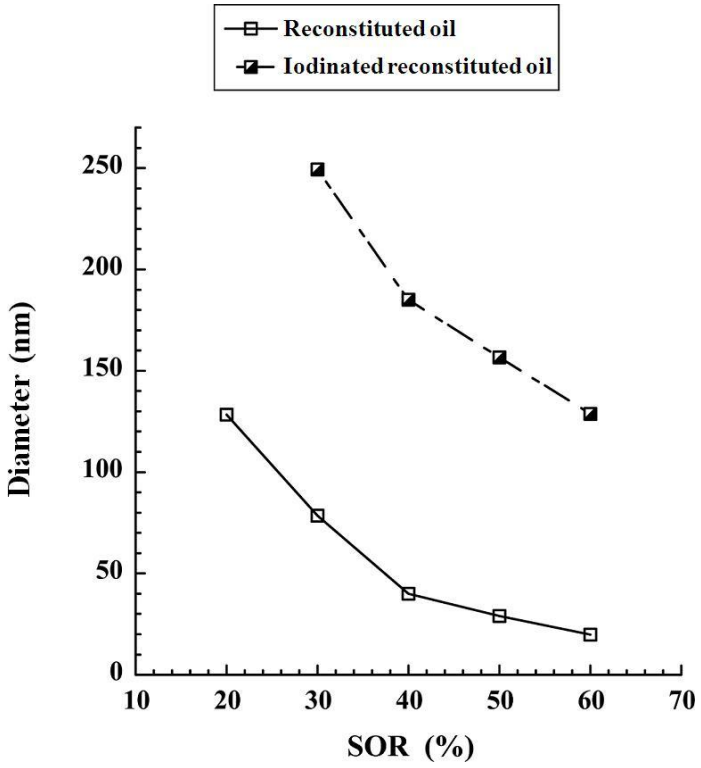

Figure 2. Nano-emulsions formulated with reconstituted oil and iodinated reconstituted oil. Surfactant: Cremophor® ELP, oily phase: reconstituted oil or iodinated reconstituted oil. Hydrodynamic diameters are plotted against the surfactant oil weight ratio (SOR).

3.4. Hemolysis assay

To be suitable for *in vivo* administration, nano-emulsions should be stable in the blood and mild to membrane of circulating erythrocytes. The biocompatibility of these iodine-containing nano-emulsions in the blood was evaluated by the hemolysis assay. Nano-emulsions of iodinated reconstituted oil formulated with Cremophor® ELP at SOR = 60% and SOWR = 40% were incubated with sheep red blood cells (RBCs) during 1 h. The ratio of iodine-containing nano-emulsions to erythrocyte solution corresponded to the injected ratio into mice (10% of the blood volume). The blood coagulation at the bottom of the microplate was observed by optical microscope after 1 h incubation, as shown in Fig. 3.

This result demonstrated that nano-emulsions of iodinated reconstituted oil were not biocompatible with the erythrocytes. Since the nano-emulsions were formulated with the PBS, their osmolarity (287 mOsm/L) and pH value (6.8) were appropriate for the intravenous injection requirements; the phenomenon of the blood coagulation produced by the nano-emulsions could be induced by the components presented in the formulation.

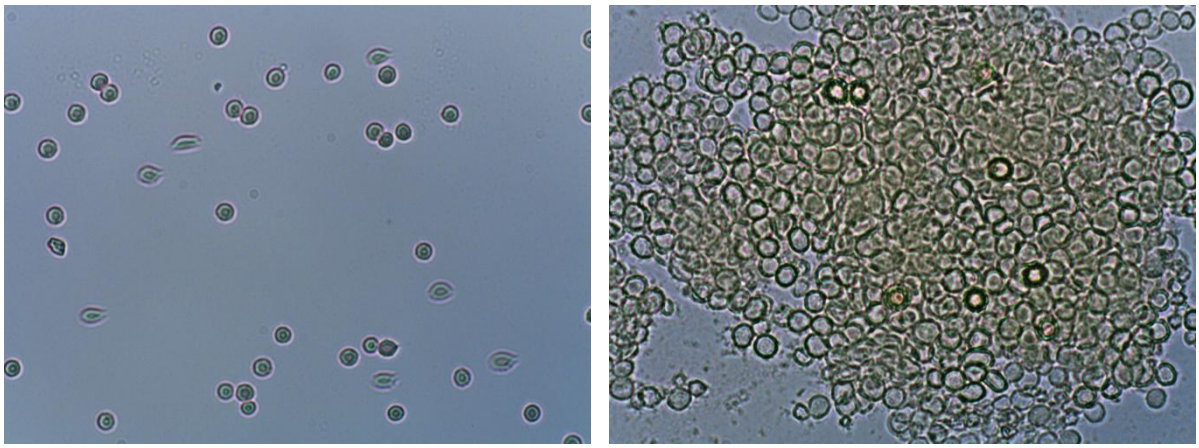

Figure 3. Red blood cell observation by optical microscopy. Isolated RBCs (on the left) and aggregated RBS incubated with nano-emulsions of iodinated reconstituted oil during 1h (on the right).

3.5. In vivo experiments

The nano-emulsions of iodinated reconstituted oil were intravenously injected into three Swiss mice. The palpitation of mice was observed immediately after the injection of the iodine-containing nano-emulsions. The mice died in two minutes after the injection.

4. Discussion

In order to further enhance the contrast capacity or to decrease the injection volume, oil with higher iodine content was developed in this work. The synthesized reconstituted oil had similar structure of Labrafil® M 1944 CS and was constituted by higher unsaturated fatty acids. The iodine content in purified reconstituted oil was around 33%, thereby 1.3 times higher than in iodinated Labrafil® M 1944 CS.

The iodinated reconstituted oil was then used to prepare nano-emulsions by the spontaneous emulsification method. The results demonstrated that nano-emulsions of iodinated reconstituted oil had larger sizes than nano-emulsions of non-iodinated reconstituted oil at the same SOR, which observation was very different from the result of iodinated Labrafil® M 1944 CS,[1] described in the previous chapter. Briefly, the introduction of iodine in the Labrafil® M 1944 CS increased the oil hydrophobicity and changed the affinity between the surfactant and the oil. This enhanced oil hydrophobicity of Labrafil® M 1944 CS after iodination induced faster diffusion of the surfactant from the oily phase to the aqueous phase and resulted in smaller nano-emulsion droplets at the same SOR. However, when the iodinated reconstituted oil had higher iodine content and became more

hydrophobic, viscous and heavier, the mechanism of the nano-emulsification process was changed. Even the enhanced hydrophobicity of iodinated oil could favorite the transfer velocity of the surfactant from the oily phase to the aqueous phase, the viscous and heavier iodinated reconstituted oil need more surfactant to formulate nano-sized and relatively stable emulsions. Nano-emulsions of iodinated reconstituted oil were not obtained at a SOR below 30% and the sizes at other SOR were relatively large. Stable nano-emulsions were obtained at higher SOR of 50% and 60%. Optimized formulation of nano-emulsions of iodinated reconstituted oil was kept at SOR = 60% and SOWR = 40%, due to the smaller sizes and better stability. The size of nano-emulsions at SOR = 60% was around 128 nm, nearly the pharmacokinetically optimal diameter for *in vivo* applications.[8] However, the iodine content in these nano-emulsions was only 5.4%, which was less than the iodine content of 8.3% in the nano-emulsions of iodinated Labrafil® M 1944 CS at SOR = 15%, even though the iodine content in the reconstituted oil was 1.3 times higher.

On the other side, these nano-emulsions of iodinated reconstituted oil produced the aggregation of erythrocytes and the death of mice, demonstrating that these nano-emulsions were not biocompatible. Thereby, we proposed some hypothesis for the reason of the blood coagulation and for the nano-emulsion toxicity. The formulation of nano-emulsions of iodinated reconstituted oil was composed by three components: the oily phase of iodinated reconstituted oil, the hydrophilic surfactant of Cremophor® ELP and the aqueous phase of phosphate buffered saline. The phosphate buffered saline is an isotonic buffered solution commonly used in biological research. It is suitable for the parental administration. The surfactant of Cremophor® ELP is a purified form of Cremophor® EL, a nonionic solubiliser made by reacting castor oil with ethylene oxide in a molar ratio of 1:35. Unlike the Cremophor® EL produced several side effects,[9] this purified form of Cremophor® ELP is suitable for the parental applications.[10, 11] Thus, the aqueous phase of phosphate buffered saline and the commercial nonionic surfactant should not be the factors to induce the blood coagulation and the death. The un-biocompatibility of these nano-emulsions was perhaps introduced by the high iodine and chloride content of reconstituted oil and the decreased stability of the nano-emulsions compared to the nano-emulsions of iodinated Labrafil® M 1944 CS.

5. Conclusion

In this work, we developed a novel synthesized oil with a higher iodine content based on the structure of Labrafil® M 1944 CS in order to enhance the contrast capacity of nano-emulsions. The synthesized reconstituted oil contained more double bonds in fatty acid chains and the iodine content in the reconstituted oil was around 33%. However, stable nano-emulsions were obtained at a relatively high SOR of 60% with the Cremophor® ELP. Thus, the final iodine content in the nano-emulsions of iodinated reconstituted oil was 5.4%, less than in nano-emulsions of iodinated Labrafil® M 1944 CS of 8.3% at SOR = 15%, even though the iodine content in the oil was much higher. Furthermore, nano-

emulsions of iodinated reconstituted oil produced the aggregation of erythrocytes and the death of mice. Thus, we can conclude that the nano-emulsions of iodinated reconstituted oil formulated with the Cremophor® ELP could not be considered as a suitable nanoparticulate contrast agent for the preclinical applications.

Therefore, with the obtained results, we can conclude that a suitable nano-emulsion based contrast agent for the preclinical applications should present the following criteria: 1) all the components in the formulation should be biocompatible; 2) synthesized iodinated oil should present a suitable structure to form nano-emulsions by the spontaneous emulsified method; 3) nano-emulsions need to contain a great quantity of X-ray contrasting materials, ideally around 100 mg of iodine per milliliter of suspension to be administrated; 4) nano-emulsions must be stable for storage and have a high *in vivo* stability, which also affects the stealth properties and residence time in the blood pool; 5) in spite of the high loading of contrast agents, the nano-emulsion must remain non-toxic and neutral to the biological metabolism.

References

(1) Hallouard, F.; Anton, N.; Zuber, G.; Choquet, P.; Li, X.; Arntz, Y.; Aubertin, G.; Constantinesco, A.; Vandamme, T. F. Radiopaque iodinated nano-emulsions for preclinical X-ray imaging. *RSC Advances* **2011**, *1*, 792.

(2) Wijs, J. J. A. On the determination of the iodine value. *The Analyst* **1900**, *25*, 31c-35.

(3) Wijs, J. J. A. The Wijs method as the standard for iodine absorption. *The Analyst* **1929**, *54*, 12-14.

(4) Anton, N.; Benoit, J.-P.; Saulnier, P. Design and production of nanoparticles formulated from nano-emulsion templates-A review. *Journal of Controlled Release* **2008**, *128*, 185-199.

(5) Anton, N.; Vandamme, T. F. The universality of low-energy nano-emulsification. *International Journal of Pharmaceutics* **2009**, *377*, 142-147.

(6) Le Garrec, D.; Gori, S.; Luo, L.; Lessard, D.; Smith, D. C.; Yessine, M.-A.; Ranger, M.; Leroux, J.-C. Poly(N-vinylpyrrolidone)-block-poly(d,l-lactide) as a new polymeric solubilizer for hydrophobic anticancer drugs: in vitro and in vivo evaluation. *Journal of Controlled Release* **2004**, *99*, 83-101.

(7) Gong, C.; Wang, Y.; Wang, X.; Wei, X.; Wu, Q.; Wang, B.; Dong, P.; Chen, L.; Luo, F.; Qian, Z. Biodegradable self-assembled PEG-PCL-PEG micelles for hydrophobic drug delivery, part 2: in vitro and in vivo toxicity evaluation. *Journal of Nanoparticle Research* **2011**, *13*, 721-731.

(8) Cole, A. J.; Yang, V. C.; David, A. E. Cancer theranostics: The rise of targeted magnetic nanoparticles. *Trends in Biotechnology* **2011**, *29*, 323-332.

(9) Weiss, R. B.; Donehower, R. C.; Wiernik, P. H.; Ohnuma, T.; Gralla, R. J.; Trump, D. L.; Baker Jr., J. R.; Van Echo, D.; Von Hoff, D. D.; Leyland-Jones, B. Hypersensitivity reactions from taxol. *Journal of Clinical Oncology* **1990**, *8*, 1263-1268.

(10) Kang, B. K.; Chon, S. K.; Kim, S. H.; Jeong, S. Y.; Kim, M. S.; Cho, S. H.; Lee, H. B.; Khang, G. Controlled release of paclitaxel from microemulsion containing PLGA and evaluation of anti-tumor activity in vitro and in vivo. *International Journal of Pharmaceutics* **2004**, *286*, 147-156.

(11) Sun, H.; Xu, H.; Yang, X.; Li, N.; Liu, Z.; Pan, W.; Yuan, Y. Formulation of a stable and high-loaded quercetin injectable emulsion. *Pharmaceutical Development and Technology* **2011**, *16*, 609-615.

3. Conclusion

Dans ce chapitre nous avons exploré de nouvelles voies pour la formulation d'agent de contraste à longue rémanence vasculaire pour l'imagerie préclinique à rayon X. Deux nouvelles huiles iodées ont été synthétisées et ensuite utilisées comme partie contrastante dans les nano-émulsions. Les nano-émulsions de Labrafil® M 1944 CS formées à un SOR = 15% et SOWR = 40% ont montré un contraste prolongé au niveau sanguin pendant plus de 2h chez les souris. Afin d'améliorer encore le pouvoir contrastant et de diminuer la quantité injectée, nous avons synthétisé une nouvelle huile iodée contenant une teneur en iode supérieure à celle du Labrafil® M 1944 CS a été synthétisée. Toutefois, les nano-émulsions d'huile reconstituée iodée se sont révélées être un agent de contraste non approprié pour des applications précliniques. En effet, les nano-émulsions stables d'huile reconstituée ont été obtenues avec un SOR relativement élevé de 60% et la teneur en iode dans la formulation finale était inférieure à celle du Labrafil® M 1944 CS. De plus, ces nano-émulsions d'huile reconstituée iodée ont provoqué une coagulation du sang après mise en contact avec des érythrocytes pendant 1h et ont entrainé la mort des souris. Néanmoins, avec l'ensemble des résultats obtenus avec l'huile reconstituée iodée, nous avons pu définir quelques critères nécessaires pour l'obtention d'un agent de contraste efficace et injectable, à savoir : 1) tous les composants dans la formulation doivent être biocompatibles; 2) l'huile synthétisée iodée doit présenter une structure appropriée pour former des nano-émulsions par la méthode d'émulsification spontanée; 3) la teneur en iode doit être importante dans l'huile iodée et aussi dans la formulation finale de nano-émulsions (environ 100 mg I / mL).

Chapter 3.
Liver Specific Blood Pool Contrast Agents based on Nano-Emulsions of Iodinated α-tocopherol

3.1. Nouvel agent de contraste iodé à longue rémanence vasculaire et spécifique du foie – nano-émulsions de 2,3,5-triiodobenzoate d'α-tocophérol

Dans cette partie, nous décrirons la synthèse d'une huile iodée non-toxique, et sa formulation sous la form de nano-émulsions, fortement chargées en iode donnant un bon contraste *in vivo*. Nous nous intéressons dans cette partie à des agents de contraste iodés qui pourraient d'abord présenter une longue rémanence vasculaire et à leur voie d'élimination, principalement la voie hépatique, conduisant finalement à un pouvoir contrastant spécifique au niveau du foie. Une nouvelle huile iodée a ainsi été synthétisée par le greffage d'une molécule iodée (acide 2,3,5-triiodobenzoïque) sur le groupement hydroxyde d'un lipide naturel (α-tocophérol). Les nano-émulsions de type huile-dans-eau ont été ensuite préparées à partir de cette nouvelle molécule lipophile iodée par la méthode d'émulsification spontanée. L'ensemble des résultats obtenus de cette étude a montré que les nano-émulsions de l'α-tocophérol iodée étaient considérées comme un agent de contraste approprié pour les applications précliniques en imagerie biomédicale.

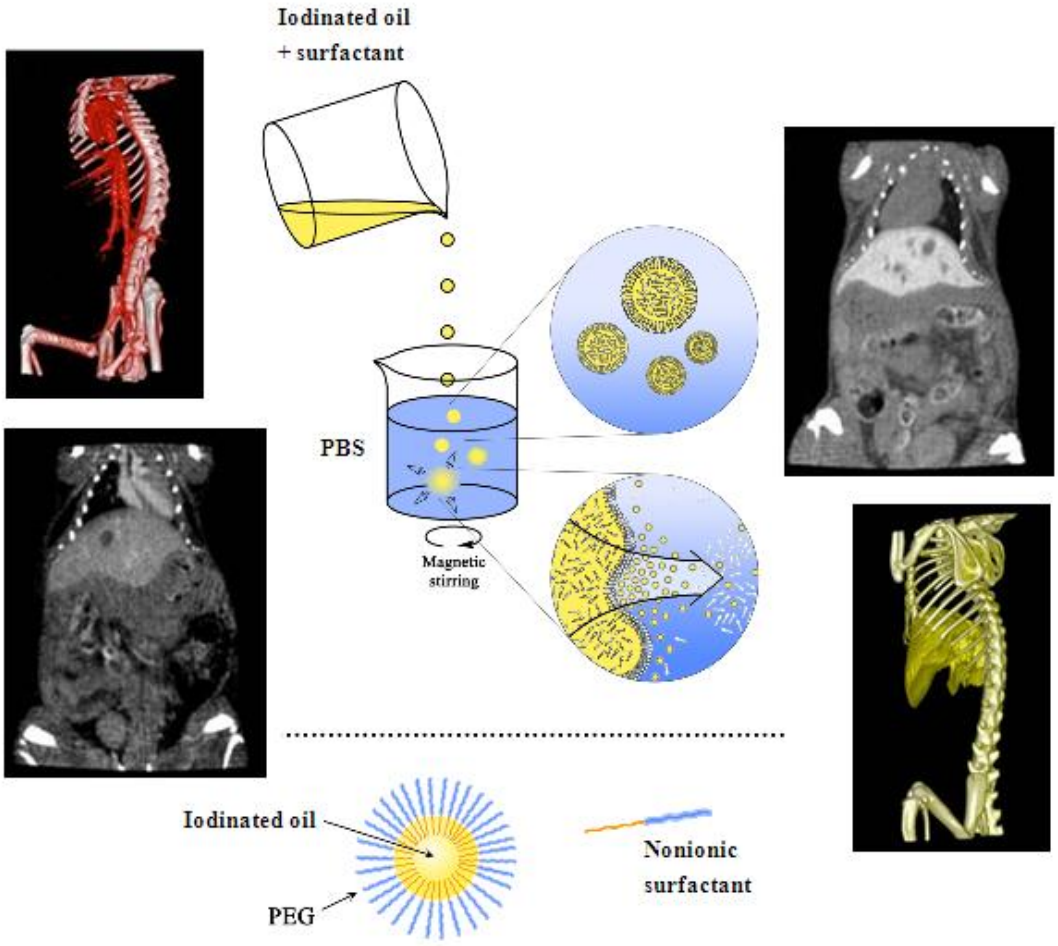

Iodinated α-tocopherol nano-emulsions as non-toxic contrast agents for preclinical X-ray imaging

Xiang Li[a], Nicolas Anton[a,*], Guy Zuber[a], Minjie Zhao[b], Nadia Messaddeq[c], François Hallouard[d,e,f], Hatem Fessi[d,e], Thierry Vandamme[a]

[a]*Université de Strasbourg, Faculté de Pharmacie, 74 route du Rhin, 67401 Illkirch Cedex, France; CNRS 7199 Laboratoire de Conception et Application de Molécules Bioactives, équipe de Pharmacie Biogalénique, 67401 Illkirch Cedex, France.*
[b]*University of Strasbourg, IPHC, CNRS, UMR7178, Equipe de Chimie Analytique des Molécules BioActives, 74 route du Rhin, 67400 Illkirch, France*
[c]*Institute of Genetics and Molecular and Cellular Biology (IGBMC), UMR University of Strasbourg/CNRS/INSERM/Collège de France, Illkirch, France*
[d]*Université Lyon-1, F-69622 Villeurbanne, France*
[e]*CNRS UMR 5007, Laboratoire d'Automatique et de Génie des Procédés (LAGEP), F-69622 Villeurbanne, France*
[f]*Hospices Civils de Lyon, Lyon F-69229, France*

Abstract

Micro-computed tomography (micro-CT) is an emerging imaging modality, due to the low cost of the imagers as well as their efficiency in establishing high-resolution (1 to 100 μm) three-dimensional images of small laboratory animals and facilitating rapid, structural and functional *in vivo* visualization. However use of a contrast agent is absolutely necessary when imaging soft tissues. The main limitation of micro-CT is the low efficiency and toxicity of the commercially available blood pool contrast agents. This study proposes new, efficient and non-toxic contrast agents for micro-CT imaging. This formulation consists of iodinated vitamin E (α-tocopheryl 2,3,5-triiodobenzoate) as an oily phase, formulated as liquid nano-emulsion droplets (by low-energy nano-emulsification), surrounded by a hairy PEG layer to confer stealth properties. The originality and strength of these new contrast agents lie not only in their outstanding contrasting properties, biocompatibility and low toxicity, but also in the simplicity of their fabrication: one-step synthesis of highly iodinated oil (iodine constitutes 41.7% of the oil molecule weight) and its spontaneous emulsification. After i.v. administration in mice (8.5% of blood volume), the product shows stealth properties towards the immune system and thus acts as an efficient blood pool contrast agent ($t_{1/2}$ = 9.0 h), exhibiting blood clearance following mono-exponential decay. A gradual accumulation predominantly due to hepatocyte uptake is observed and measured in the liver, establishing a strong hepatic contrast, persistent for more than four months. To summarize, in the current range of available or developed contrast agents for preclinical X-ray imaging, this agent appears to be one of the most efficient.

Key words: nano-emulsion, contrast agent, micro-CT, X-ray imaging, preclinical imaging, passive targeting

*Corresponding author
Email addresses: nanton@unistra.fr (Nicolas Anton)

1. Introduction

In recent years, various medical imaging technologies have been specifically developed for preclinical research, notably in the field of oncology. In accordance with ethical guidelines on animal experimentation, these new research tools help reduce the number of animals used for experimental protocols. Generally speaking, all imaging modalities have specific limitations that constrain their scale of use and development. If the prohibitive price of imagers or the cost and toxicity of the contrast agents are limiting factors, the supply, storage and management of radioactive animals and wastes (with nuclear imaging, PET, SPECT) are no less problematic. Optical imaging is an emerging modality, very promising due to the relatively lost cost of imagers, but with drawbacks such as very low signal penetration in the animal body, a low spatial resolution and no signal for non-labeled tissues (thus making it impossible to obtain anatomic images). Multimodal imaging is therefore an increasingly popular solution, making the most of the complementarities between various modalities. The second most efficient and cost-effective modality after optical imaging is computed tomography (X-ray scanner). However, the main limitation of X-ray imaging for preclinical research is the high cost, low efficiency and non-negligible toxicity of the contrast agents. The present study focuses on the development of an X-ray contrast agents aimed at overcoming these limitations.

Micro-computed tomography (micro-CT) is an imaging modality which enables rapid three-dimensional, radiographic, structural and functional visualization in small laboratory animals [1–4]. Compared to clinical CT, the resolution of micro-CT is significantly better, from 1 to 100 μm [5–7], allowing, for instance, the clear detection of metastasis sizing around 300 μm [8–10]. However, the acquisition time of a micro-CT apparatus is slow, around 10-20 minutes for a full high resolution autoradiogram, whereas the same result can be achieved within seconds with a clinical CT scan on humans [11, 12]. X-ray contrast agents developed for humans and used in clinical CT scans are hydrophilic iodinated molecules with a low molecular weight and therefore undergo very fast blood elimination *via* the kidneys, mainly due to glomerular filtration. For this reason, they are not adapted to preclinical research with micro-CT. Moreover, clinical contrast agents administered at high doses or with repeated injections (to allow micro-CT imaging) have severe drawbacks, leading to acute kidney toxicity, a tendency to extravasate, and allergic reactions [13–15]: thus

they should clearly be avoided for micro-CT imaging.

Over the past decades, new micro-CT compatible contrast agents have been developed for X-ray imaging [16–25]. Their particularity is a long residence time in the bloodstream and/or an ability to target specific organs or lesions. In order to prevent renal clearance, these contrast agents have generally been formulated as nanoparticulate systems. The optimized properties of such contrast agents can easily be summarized in five points: ***(i)*** in order to avoid being eliminated by the kidneys, contrast agents need to be formulated in the form of nanoparticulate systems (liposomes, nano-emulsions, dendrimers, polymeric nanoparticles etc.) with a minimal size of around 100 nm [11, 25–32]. ***(ii)*** in order to confer them with stealth properties, their surfaces have to be controlled or functionalized by grafting on hydrophilic polymers such as polyethylene glycol (PEG) [33–37]. An extended circulation time in the bloodstream is directly linked to the nanometric size range of the contrast agents along with the surface functionalization, preventing rapid opsonization by the reticulo-endothelial system (RES) [34]. ***(iii)*** nanocarriers need to contain a great quantity of X-ray contrasting materials (commonly iodine), ideally around 100 mg (or more) of iodine per milliliter of suspension to be administrated [25, 28, 31]. ***(iv)*** NP suspensions must be stable for storage and have a high in vivo stability, which also affects the stealth properties and residence time in the blood pool. ***(v)*** in spite of the high loading of contrast agents, the NP suspension must remain non-toxic and neutral to the biological metabolism.

Micro-CT contrast agents are of prime interest in both structural and functional imaging, enabling the detection of lesions through the specific targeting of tissues, *e.g.*, tumors. Targeting tissues, organs or pathologies serves as a new tool to meet the needs of researchers. It can notably provide a better detection of tumors and a follow-up of treatment response allowing the visualization of the tumor growth in time, and thus the *in vivo* efficiency of a therapy. 70% of medical imaging involves cancer research and the design and development of efficient, cost-effective, targeted contrast agents constitutes a major research and economic concern. Contrast agents for X-ray imaging modalities are a challenge today: they offer huge potential in terms of advanced diagnosis of tumors and personalized therapies and yet commercial solutions available to date are far from satisfactory.

In this study, we propose an efficient new non-toxic contrast agent for preclinical X-ray imaging. The idea was ***(i)*** to base the formulation on non-toxic lipophilic molecules naturally present

in the body: α-tocopherol (*i.e.* vitamin E) ***(ii)*** to graft a high ratio of X-ray contrasting material (tri-iodobenzene) on their chemical structure using the simplest chemical reaction, and ***(iii)*** to formulate nano-emulsions with this iodinated lipid by low-energy nano-emulsification methods with a PEGylated non-ionic surfactant. We chose iodine since it is a compromise between safety, toxicity and cost [28]. This simple process results in the formulation of highly iodinated α-tocopheryl 2,3,5-triiodobenzoate nano-emulsions. When administered intravenously to mice, they show outstanding contrast enhancements, first of the blood compartment and then of the liver tissues through a passive targeting mechanism, and without apparent toxicity. In addition to experiments on the micro-CT imaging and *in vivo* contrasting properties, a complete characterization was performed: *in vitro* biocompatibility studies (hemolysis tests, stability in serum), cytotoxicity studies (MTT), *in vitro* cellular uptake assays, physico-chemical characterization of the nano-emulsions (size distribution, transmission electron microscopy and evaluation of the iodine content), and finally an *in vivo* follow-up of the contrast agent bio-distribution.

2. Experimental section

2.1. Materials

2,3,5-Triiodobenzoic acid, α-tocopherol, 4-dimethylaminopyridine, N,N'-dicyclohexylcarbodiimide, dichloromethane, ethyl acetate, cyclohexane and 3-(4,5-dimethylthiazol-2-yl)-2,5-diphenyltetra-zolium bromide (MTT) solutions were purchased from Sigma Aldrich, France. Non-ionic surfactant (Cremophor ELP®) from BASF (Ludwigshafen, Germany), was kindly donated by Laserson, Etampes, France. Cremophor ELP® is a parenteral grade nonionic surfactant made by reacting ethylene oxide to castor seed oil at an ethylene oxide to oil molar ratio of 35 [38]. The product mainly consists of a PEG chain (35 ethylene glycol units) grafted onto a molecule of castor oil. Phosphate buffered saline (PBS) and sheep erythrocytes were obtained from Eurobio, France.

2.2. Methods

2.2.1. Synthesis and characterization of α-tocopheryl 2,3,5-triiodobenzoate

The 2,3,5-triiodobenzoic acid (5 g, 0.01 mol), 4-dimethylaminopyridine (0.18 g, 0.0015 mol) and N,N'-dicyclohexylcarbodiimide (2.3 g, 0.011 mol) were sequentially added at room temperature to a solution of DL-α-tocopherol (3.5 g, 0.008 mol) in dicholoromethane (250 mL). The

reaction mixture was stirred overnight at room temperature and the dicyclohexylurea and other precipitates were removed by filtration. The organic phase was then washed twice with saturated aqueous $NaHCO_3$, once with saturated NaCl solution and dried with anhydrous Na_2SO_4. The solvent was removed in vacuum and the oil was then purified by the gradient elution method on silica gel using cyclohexane and ethyl acetate as an eluent. Reaction yields were around 80 %. The synthesis scheme of α-tocopheryl 2,3,5-triiodobenzoate is reported in Fig. 1. The resulting product was a light, yellowish viscous oil with a high iodine content of around 41.7%.

^{1}H spectra were obtained with a Bruker Top Spin 3.0 400 MHz spectrometer. $CDCl_3$ chemical shifts are expressed in ppm downfield from tetramethylsilane as the internal standard. The purified α-tocopheryl 2,3,5-triiodobenzoate was then characterized by means of NMR and mass analysis: ^{1}H NMR ($CDCl_3$, δ/ppm): 8.34 (s, 1H, H^6), 8.05 (s, 1H, H^4), 2.63 (t, 2H, H^{14}), 2.15 (s, 6H, H^{31}, H^{32}), 2.10 (s, 3H, H^{30}), 1.83 (m, 2H, H^{15}), 1.59 (m, 3H, H^{20}, H^{24}, H^{28}), 1.28 (s, 3H, H^{33}), 1.27 (m, 18H, all CH_2), 0.89 (d, 9H, $3CH_3$), 0.88 (d, 3H, $1CH_3$). Mass spectrometry was done in positive mode (APCI+) with CAMAG TLC-MS, Agilent Technologies LC/MSD SL. m/z 913.5 ($[M+H]^+$).

2.2.2. Preparation of iodinated nano-emulsions

Nano-emulsions of iodinated α-tocopherol were formulated by the spontaneous nano-emulsification method, as described previously [39–41]. In short, pure α-tocopheryl 2,3,5-triiodobenzoate (0.75 g), was firstly mixed with the non-ionic hydrophilic surfactant (0.5 g), and maintained at room temperature. Phosphate buffered saline (PBS), used as an aqueous phase (1.88 g), was then added to the surfactant / oil mixture under gentle magnetic stirring. This optimized formulation was chosen to give a compromise between the nano-emulsion size and monodispersity, and the iodine content of the suspension. As a result of the process optimization described below (in Fig. 2 (a)), this compromise led to a droplet diameter of around 85 nm, with the following formulation parameters: surfactant / oil weight ratio (SOR) = 40%, and (surfactant + oil) / water weight ratio (SOWR) = 40% (see Ref. [40] for details on the formulation process). The α-tocopheryl 2,3,5-triiodobenzoate content in the nano-emulsions (*i.e.* injectable product) was about 24 wt.%. The schematic representation of a nano-emulsion droplet is reported in Fig. 1. Finally, nano-emulsions were sterilized by filtration (0.22 μm membrane, Millex-GP, polyethersulfone (PES) membrane, Millipore, Molsheim, France) before intravenous administration.

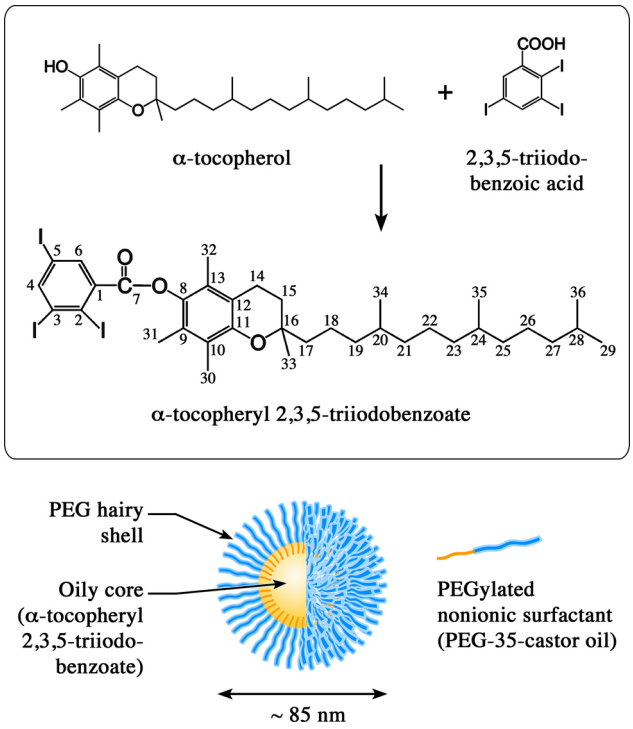

Figure 1: (top) Synthesis of α-tocopheryl 2,3,5-triiodobenzoate. (bottom) Schematic representation of an iodinated nano-emulsion droplet.

2.2.3. Characterization of nano-emulsions

2.2.3.1. Dynamic light scattering (DLS)

Size distributions and polydispersity indices (PDI) were measured by DLS with a Malvern apparatus (NanoZS®, Malvern, Orsay, France). The helium / neon laser, 4 mW, was operated at 633 nm, with the scatter angle fixed at 173° and the temperature maintained at 25°C. DLS data were analyzed using a cumulants-based method.

2.2.3.2. Transmission electron microscopy (TEM)

Since iodine is a contrasting material for electrons, samples were used without any staining agent. They were diluted (1/10) with MilliQ water, a drop of the suspension was placed on a carbon grid (carbon type-A, 300 mesh, copper, Ted Pella Inc. Redding, U.S.A.), and dried at 40°C. Observations were carried out using a Philips Morgagni 268D electron microscope.

2.2.4. Biocompatibility studies

Biocompatibility studies of the contrast agent were performed through ***(i)*** stability studies of iodinated nano-emulsions in fetal bovine serum (FBS), and also ***(ii)*** by evaluating their hemolytic properties.

2.2.4.1. Stability of nano-emulsions in FBS

Iodinated α-tocopherol nano-emulsions (0.1 mL) were added into FBS (0.9 mL), homogenized and incubated at 37°C under gentle orbital shaking. The nano-emulsion concentration in FBS was selected to correspond to the one in blood after i.v. administration (see *in vivo* experimental conditions below in section *In vivo experiments*). Nano-emulsion stability was monitored through size distribution in function of the incubation time (*i.e.* 1h, 2h, 3h, 5h, 16h and 20h). The samples were constantly homogenized during the time course of the incubation to avoid possible large aggregates to sediment. Before analysis, the eventual presence of aggregates was examined visually. In this experiment, we never noticed any flocculation of materials. Moreover, DLS measurements were combined with a quantification of the scattered light (expressed in kilo count of photons per second, Kcps). All sample, even after 20 h incubation provided similar level of scattered lights, around 150-200 Kcps, with detected particles of constant sizes. This simply means that the concentration of the nano-emulsion droplets does not change with time, *e.g.* indicating a high stability.

2.2.4.2. Hemolysis assays

Hemolysis assays were done according to a described procedure [42]. In short, sheep erythrocytes were firstly diluted in phosphate buffered saline (PBS) and washed three times (by three centrifugation runs (400 rcf, 10 min) / washing / re-suspension). The solution of rinsed erythrocytes was diluted with PBS up to the concentration of $1 \cdot 10^8$ erythrocytes / mL, and immediately used to evaluate the hemolytic properties of the iodinated nano-emulsions as follows: 20 μL of nano-emulsions were added to 180 μL of erythrocyte suspension, in 96-well microplates. Then, samples were incubated for 1h, 2h, 3h, 4h and 5h at 37°C with orbital shaking, and then centrifuged (at 2000 rpm) for 10 mins. Subsequently, hemoglobin release in the supernatant was measured by U.V. spectrophotometry at 414 nm with a microplate reader (Labsystems iEMS Reader MF, Helsinki, Finland). Full hemolysis control and blank samples were obtained with a solution of

Triton X-100 (1 wt.%) and from the supernatant of untreated erythrocytes, respectively.

2.2.4.3. Cytotoxicity assays

BNL-CL2 cells were seeded in 96-well plates at a concentration of $1 \cdot 10^4$ cells per well in 100 μL of medium (Dulbecco's Modified Eagle's Medium, DMEM) containing 10% fetal bovine serum, 1 wt.% glutamine, 1 wt.% of commercial solution of penicillin and streptomycin (PAN Biotech. GmbH, Aidenbach, Germany). The BNL-CL2 cells were then incubated overnight at 37°C under a controlled atmosphere (5% CO_2 and 95% air). Next, contrast agents were incorporated, by substituting the culture medium for a similar one containing variable concentrations of iodinated nano-emulsions, corresponding to 0.00053, 0.0053, 0.053, 0.13, 0.27, 0.40 and 0.53 mg I/10^4 cells. After an incubation of 24 h, the medium was removed and the adherent cell monolayers were washed with PBS. Then, the wells were filled with cell culture medium containing MTT, incubated for 4h at 37°C, and the formazan crystals formed were dissolved in 200 μL DMSO. U.V. absorbance was measured at 570 nm by spectrophotometry with a microplate reader. Experiments were carried out in triplicate, and expressed as a percentage of viable cells compared to the control group.

2.2.4.4. In vitro cellular uptake assay

BNL-CL2 cells were seeded in 24-well plates at $0.9 \cdot 10^5$ cells per well, in 1 mL of DMEM medium, and incubated overnight at 37°C in a controlled atmosphere (5% CO_2 and 95% air). Next, iodinated nano-emulsions were added to the wells (at a concentration of 25 mg I/mL, or 0.13 mg I/10^4 cells), and incubated for 2 h at 37°C in a controlled atmosphere (5% CO_2 and 95% air). After this incubation time, the cells were ***(i)*** washed six times with PBS to remove nano-emulsions from the culture medium, and ***(ii)*** treated with trypsine (100 μL) per well, and transferred to glass tubes containing PBS and citric acid at 2%(v./v.). Finally, cells were extracted by a methanol / chloroform mixture (1:1), and the chloroform phase was collected. The presence of α-tocopheryl 2,3,5-triiodobenzoate was evidenced by thin layer chromatography (TLC) using a cyclohexane / ethyl acetate mixture (10:1) as an eluent.

2.2.5. Micro-CT imaging

As a preliminary remark, the experiments were performed in agreement with the Committee of Animal Research and Ethics of the University of Lyon-1.

2.2.5.1. In vitro experiments

The iodine content of the nano-emulsions was accessed through the quantification of their radiopacity. These experiments were performed with a micro-CT scanner (1076 Skyscan®, Kartuizersweg, Belgium). Experimental parameters were: X-ray: 49 keV, 129 μA; resolution: 35 μm; pitch: 0.4°; aluminium filters: 0.5 and 632 ms. The acquisition with nano-emulsions also served to establish the quantification curve, correlating iodine concentration and radiopacity, produced with a commercial hydrophilic contrast agent (XenetiX 300®, *i.e.* iobitridol).

2.2.5.2. In vivo experiments

In vivo experiments were performed with a micro-CT scanner (INVEON®, Siemens, Munich, Germany). The experimental X-ray parameters were: 50 keV, 500 μA; resolution: 111.25 μm; pitch: 2°; aluminium filters: 0.5 and 900 ms. The acquisitions were performed on 3 Swiss mice. Before acquisition, mice were anesthetized with isoflurane. Then, nano-emulsions were intravenously injected (using a catheter) in the tail-vein, with an injection volume corresponding to 8.5% of the blood volume (*i.e.* 6.2 μL of nano-emulsions per gram of mouse). Scans were performed before administration, immediately after injection, 30 min, 1h, 2h, 3h, 4h, 6h, 1 day, 2 days, 3 days, 6 days, 12 days, 19 days, 27 days, 34 days, 48 days, 55 days, 59 days, and 134 days. The Micro-CT raw data were treated with OsiriX viewer, to establish 2D maximum projection slices and 3D volume rendering images, and then to quantify the signal by placing the region of interests (ROI) in the heart, liver and bladder.

3. Results and discussion

Lipid nano-emulsions are of increasing interest in the formulation of pharmaceutics, drug delivery systems and contrast agents. This is largely due to the fact that they act as a general platform for nano-medicines, providing simple solutions to complex problems. In fact, nano-emulsions allow for the months-long stable dispersion of lipids in an aqueous phase in the form of droplets

ranging in size from 20 to 300 nm. Furthermore, the formulation process can be very simple, as seen in the current study, consisting simply in bringing into contact two phases {surfactant + oil} and {water}, resulting in the instant generation of a very stable oil dispersion in the aqueous phase. Similarly, the use of PEGylated surfactants in this process provides not only a strong oil / water interface stabilization, but also a very efficient surface functionalization of the lipid droplets, conferred with the required stealth properties. In this case nano-emulsions allow for the stable dispersion of highly concentrated iodine in water encapsulated in PEGylated lipid nano-droplets. Besides the straightforwardness of the formulation process, another major advantage of the method of production of these contrast agents is the simplicity of the iodinated oil one-step synthesis, as illustrated in Fig. 1. These clear advantages make the system a promising candidate for industrial scaling-up.

Let us now consider the physicochemical characterization of the nano-emulsions generated. As presented above in the experimental section, the selected formulation should be a compromise between size (hydrodynamic diameter, d_h), polydispersity (PDI) and iodine concentration of the final suspension. When the SOR is increased, the size and PDI decrease, thus increasing the quality of the suspension. However, when the SOR is increased, the quantity of oil decreases, as does the iodine concentration in the final suspension. Bearing this in mind and aiming for a formulation with maximum iodine content and the best possible quality of suspension, the optimized formulation requires a particle size big enough to allow for a high iodine concentration but with properties (d_h and PDI) small enough to be compatible with the *in vivo* application. The optimum formulation was disclosed by studying the relationship between the SOR and the nano-emulsion properties (d_h and PDI), as illustrated in Fig. 2 (a) and indicated by the arrow. This formulation corresponds to SOR = 40% and gives a value of d_h around 85 nm, and a PDI = 0.16. The corresponding size distribution is reported in Fig. 2 (b).

TEM micrographs are reported in Fig. 2 (c), and disclose important information on the droplets structure and internal morphologies. Fig. 2 (c_1) and (c_2) respectively show individuals (in fact most representative of the sample) and flocculated nano-emulsion droplets. The size of the objects clearly appears coherent with the DLS measurements shown in Fig. 2 (b). Moreover, as iodinated oil is a contrasting material for electron microscopy (appearing dark on the picture), these experiments are important in that they disclose new and never previously observed information on the

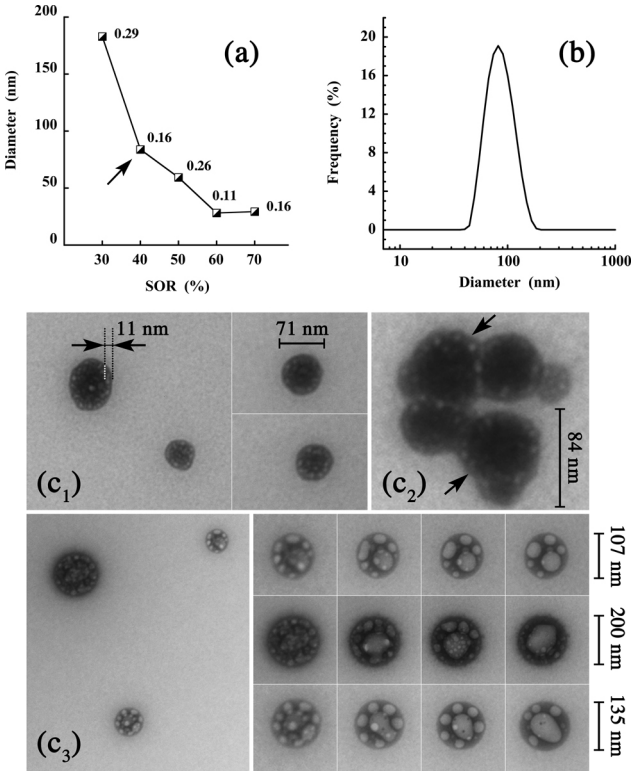

Figure 2: Physico-chemical characterization of the iodinated nano-emulsions. (a) Process optimization: hydrodynamic diameter (d_h) and polydispersity indices (PDI, labeled for each point in the graph), are plotted as a function of the surfactant to oil weight ratio (SOR). The arrow indicates the optimum formulation (SOR = 40%) selected for the *in vivo* studies. (b) Size distribution of the optimum formulation (arrow in graph (a), for SOR = 40%). (c) Transmission electron microscopy: all micrographs present nano-emulsions for SOR = 40% (arrow in graph (a), and size distribution in (b)). (c_1) Shows individuals and (c_2) flocculated nano-droplets. (c_3) Shows the evolution of the droplets along the TEM experiments, thus helping to understand their morphologies and composition (see details in the text): (left) individual droplets, and (right) follow-up of these droplets along the acquisitions.

structure and morphology of lipid nano-emulsion droplets. Pictures (c_1) and (c_2) reveal a "two-domains" structure: (i) one is very contrasting located in the particle core, and (ii) the other one, less contrasting, is located at the periphery of the nano-droplets (indicated by arrows in picture (c_2)). This surrounding layer is also clearly evident between the flocculated droplets, corroborating the intrinsic stability of the nano-emulsion droplets towards coalescence. The thickness of this light layer was evaluated around 11 nm (in picture (c_1)). This phenomenon can in fact be explained simply: on the one hand (as shown in Fig. 1 (bottom)), the droplets are composed of two compounds: iodinated oil and nonionic surfactants. On the other hand, the TEM measurements are conducted in a strong vacuum, inducing particular phase behavior between the oily phase and nonionic surfactant, bringing the system below the cloud point cp_α, as illustrated in the phase dia-

gram presented in Ref. [41] (Fig. 1 (top), at a thermodynamic state below T(cp_α), bearing in mind that at such a low pressure, the temperature axis shifts towards higher values). As a result, the oil and nonionic surfactant are immiscible, allowing us to observe that the surfactant location is exclusively in the peripheral region of the droplets. This hypothesis is confirmed by following the observation along the TEM acquisitions (Fig. 2 (c)). Under the electron beam, maybe due to a local temperature increase (and viscosity decrease), the two liquid phases move and the lightest surfactant regions gradually merge, creating bigger hydrophilic domains migrating towards the center of the droplets. This also highlights the liquid state of the nano-droplets. To conclude, the formulation proposed in this study is compatible with a nano-emulsion structure including a core composed of liquid iodinated oil, stabilized with nonionic surfactants. As regards the characterization of nano-emulsions in general, these results are unprecedented and were made possible by the high iodine content of the oily phase.

Another aspect of nano-emulsion characterization includes evaluating the iodine concentration within the injectable nano-droplet suspension. This was performed using a quantification curve using a commercial clinical hydrophilic contrast agent (XenetiX®, *i.e.* iobitridol). These results are reported in Fig. 3, and show an iodine concentration in the α-tocopheryl 2,3,5-triiodobenzoate nano-emulsions of around 106 mg I/mL. This is significant when compared to a commercial iodinated nano-emulsion (Fenestra VC®), generally taken as a reference contrast agent for micro-CT, which has a value of 53 mg I/mL. It would thus appear that the new formulation proposed here is twice as concentrated as commercially available references.

The following section deals with the *in vitro* evaluation of nano-emulsion biocompatibility. In order to be compatible with *in vivo* administration, nano-emulsions have to be stable in blood (stability assays are reported in Fig. 4 (a)), and neutral towards the membrane of circulating erythrocytes (hemolysis assays are reported in Fig. 4 (b)). Results for the iodinated nano-droplet suspension incubated with FBS show a high stability (Fig. 4 (a)), without significant size variation or droplet aggregation, and an incubation time of up to 20 hrs. Subsequently, iodinated nano-emulsions were incubated with erythrocytes at a concentration slightly higher than the one in blood after an i.v. injection (*i.e.* 10 mg I/mL and 9.0 mg I/mL, respectively) in order to observe and follow potential cell hemolysis (Fig. 4 (b)). The results reveal that, even after 5 hrs of incubation, there is no sign of erythrocyte hemolysis. In short, these *in vitro* assays evidence

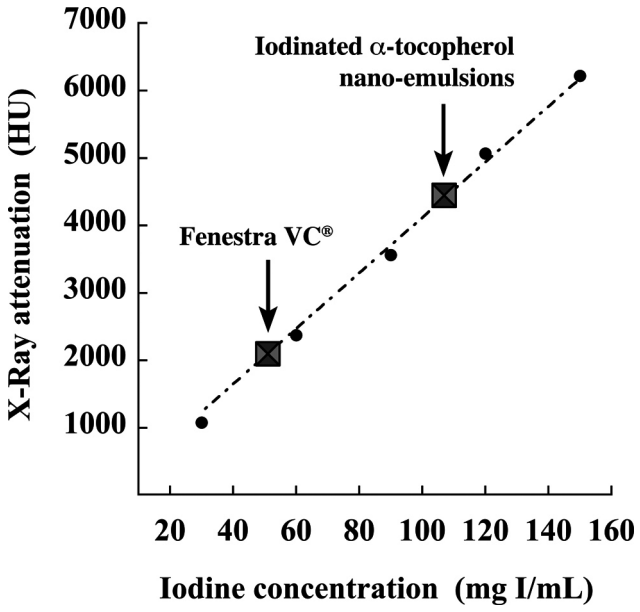

Figure 3: *In vitro* evaluation of the radiopacity of α-tocopheryl 2,3,5-triiodobenzoate nano-emulsions. A quantification curve made with various dilutions of iobitridol (Xenetix®, a commercial hydrophilic contrast agent at 300 mg I/mL) served as a reference (filled circles). Values of the X-ray attenuation of α-tocopheryl 2,3,5-triiodobenzoate nano-emulsion (SOR = 40% and SOWR = 40%) and of Fenestra VC®taken as a reference, are indicated with filled squares on the figure

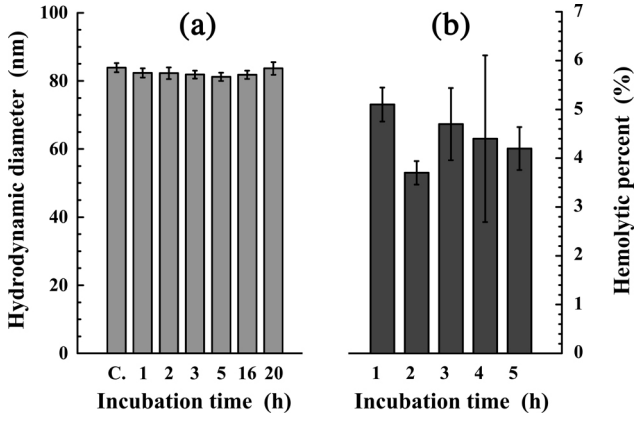

Figure 4: *In vitro* evaluation of the iodinated nano-emulsion biocompatibility (formulation parameter: SOR = 40%, SOWR = 40%). (a) Monitoring of the droplet size incubated in FBS, "C." is the control sample without serum. (b) Monitoring of erythrocyte hemolysis in contact with the nano-emulsions

clear biocompatibility of the iodinated nano-emulsions, which should remain stable after *in vivo* injection, without any adverse hemolytic event.

In vitro cytotoxicity experiments (*i.e.* MTT assays) were conducted on BNL-CL2 embryonic murine hepatocyte cell lines. This cell type was selected because, with a passive targeting mech-

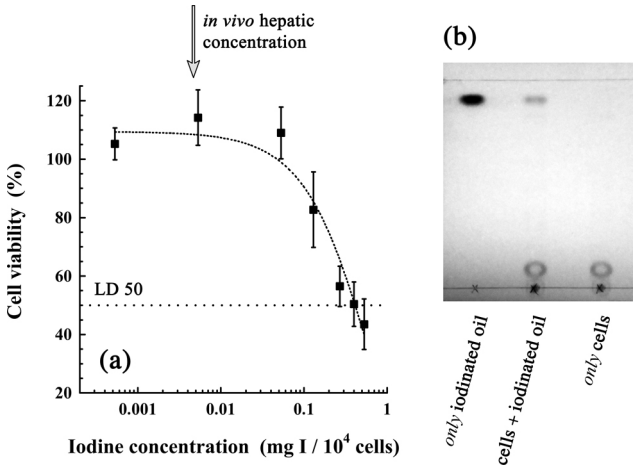

Figure 5: *In vitro* assays on BNL-CL2 embryonic murine hepatocyte cell lines. (a) Cytotoxicity MTT experiments, cells were incubated for 24 hrs with various concentrations of iodinated α-tocopherol nano-emulsions: $0.53 \cdot 10^{-3}$, $5.3 \cdot 10^{-3}$, $53 \cdot 10^{-3}$, 0.13, 0.27, 0.40, 0.53 mg I/10^4 cells. The arrow indicates the maximum hepatic concentration expected after administration with *in vivo* imaging for a mouse of 30 g (*i.e.* $4.6 \cdot 10^{-3}$ mg I/10^4 cells after i.v. injection of 8.5% of the blood volume). (b) *In vitro* iodinated α-tocopherol nano-emulsion uptake by BNL-CL2 hepatocyte cells. Concentration: 0.13 mg I/10^4 cells. (left) Control: pure α-tocopheryl 2,3,5-triiodobenzoate, (middle) iodinated nano-emulsions incubated with BNL-CL2 cells, (right) control: BNL-CL2 cells only.

anism, the usual elimination route of lipid emulsions passes through the liver [25]. In the present study, this hepatic elimination is confirmed, not only by the *in vivo* micro-CT imaging which discloses a high and persistent contrast agent accumulation in the liver tissues, but also by the cellular uptake assays that confirm the hepatocyte internalization of the iodinated α-tocopherol. Viability results are reported in Fig. 5, and clearly disclose low toxicity of the iodinated nano-emulsions. For instance, the maximum iodine concentration expected in the liver after the dose administrated with *in vivo* imaging for a mouse of 30 g, *i.e.* $4.6 \cdot 10^{-3}$ mg I/10^4 cells (indicated by the arrow in Fig. 5 (a)) is two orders of magnitude lower than the lethal dose 50 (LD 50), around 0.40 mg I/10^4 cells. By highlighting the low toxicity of the iodinated nano-emulsions, the results corroborate the biocompatibility demonstrated above.

In order to check if the iodinated nano-droplets are internalized by hepatocytes, and thus to disclose the possible elimination mechanism of the lipid contrast agent, we undertook *in vitro* celllular uptake assays with the same BNL-CL2 hepatocyte cell lines. The concentration of nano-emulsion chosen (0.13 mg I/10^4 cells) was low enough to avoid cell toxicity, but high enough to induce a clear signal on the TLC plate. The plate is reported in Fig. 5 (b), showing the comparison between the controls (pure iodinated oil, and pure extracted cells) and the cells incubated with

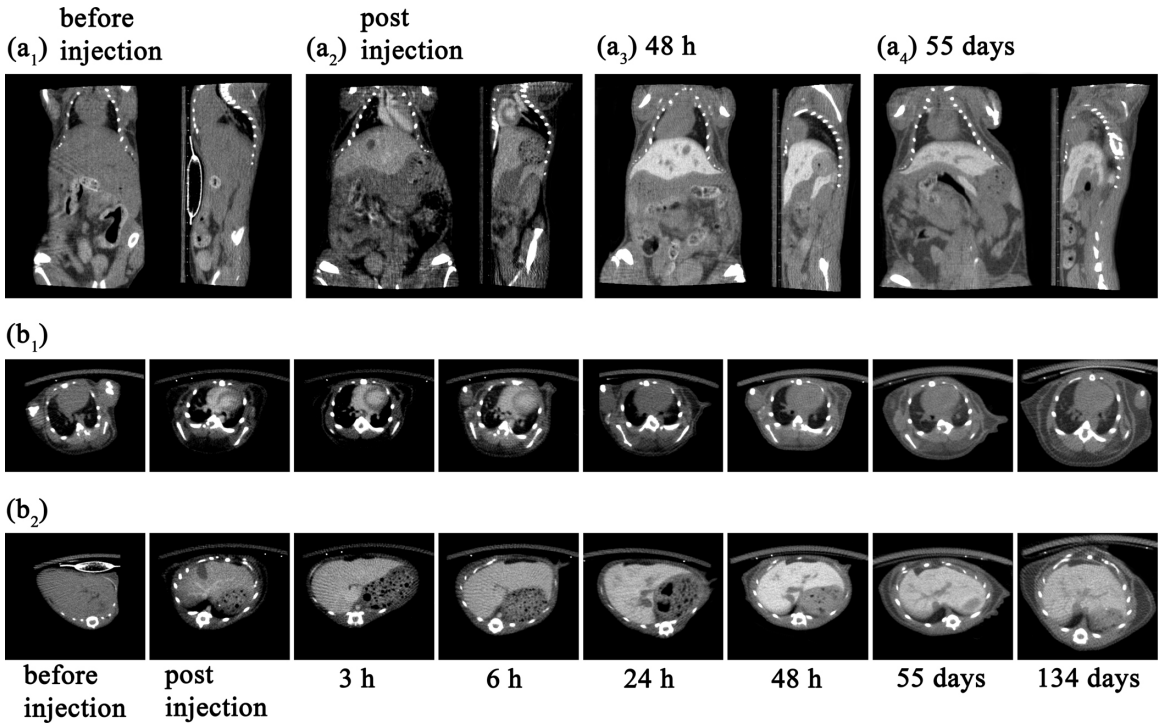

Figure 6: *In vivo* micro-CT imaging after i.v. injection of iodinated α-tocopherol nano-emulsions in mice. (a) Representative coronal and sagittal sections, (a_1) before, (a_2) immediately after injection showing blood pool contrast enhancement, and (a_3) and (a_4) showing liver contrast enhancement, at 48 h and 55 days after injection, respectively. (b) Representative transverse slices (b_1) through the heart, lung and vertebra, and (b_2) including the liver, from pre-injection to 134 days post-injection. For a given time, to allow the visual comparison, all the images were reported with similar brightness / contrast conditions.

nano-emulsions, thoroughly washed, and then extracted. The TLC plate shows the presence of exogenous α-tocopheryl 2,3,5-triiodobenzoate for the cells incubated with nano-emulsion, with a retardation factor $R_f = 0.84$. This evidences nano-emulsion uptake by hepatocytes.

In this last section, let us look at the application of these new iodinated nano-emulsions as contrast agents for preclinical micro-CT *in vivo* imaging. After the administration of a single i.v. dose (8.5% of the blood volume, see experimental details above), we observed two main imaging phases: ***(i)*** the first is blood pool imaging with a significant circulation time and a half-life of around 9.0 h and ***(ii)*** the second phase is a strong contast enhacement in the liver, persistent for more than 4 months after a single injection, that is to say, much longer than all the published results with lipid contrast agents. Results are presented in Fig. 6 and show coronal and sagittal views (a_1) before injection, (a_2) 30 minutes after injection, (a_3) 48 hrs after injection, and (a_4) 55 days after injection. Fig. 6 (b) show transverse slices, through the heart, lung and vertebra (b_1),

and a transverse slice including the liver (b_2). A representative timescale was chosen, from the first measurement after injection (0 h), to 134 days, showing the actual efficiency of the contrast agents. Experiments were stopped after 134 days, still with a significant contrast enhancement in the liver tissues (illustrated below).

Immediately after injection, a significant contrast enhancement arises in the cardiac ventricles, the major arterial, the venous structures, intra-pulmonary vessels (see Fig. 6 (a_1) and (b_1)), and the liver vasculatization (see Fig. 6 (b_2) post-injection). The contrast agent concentration in the blood pool was quantitatively monitored, by locating the region of interest (ROI) in the heart (results reported in Fig. 7 (a)). Significant values of X-ray attenuation in the blood pool were observed immediately after injection, $\Delta HU^{blood}(0\ h) = \Delta HU_0^{blood} \sim 245$ HU, and up to 6 hrs after injection, $\Delta HU^{blood}(6\ h) \sim 186$ HU (with $\Delta HU(t)$ = *X-ray attenuation after injection at time t – X-ray attenuation before injection*, in Hounsfield Units (HU)). Experimental data are accurately fitted with mono-exponential decay (see the curve fit in Fig. 7 (a), R = 0.989), giving the flowing equation:

$$\Delta HU(t) = \Delta HU_0^{blood} \cdot \mathrm{e}^{-k_{blood} \cdot t} \tag{1}$$

where ΔHU_0^{blood} is the initial value and of the contrast enhancement in blood (after injection), here $\Delta HU_0^{blood} = 245$ HU, and k_{blood} is the elimination rate constant, here $k_{blood} = 0.077\ \mathrm{h}^{-1}$. As a result, the value of half life in blood is $t_{1/2} = \ln(2)/k_{blood} = 9.0$ h, corresponding to a contrast of $\Delta HU(t_{1/2}) = 125$ HU. This result confirms the visual observations of the high X-ray contrast enhancement, as well as the efficiency of this new contrast agent for micro-CT. Moreover, the mono-exponential fit also indicates that the blood clearance is almost exclusively performed *via* a single route which, judging from Fig. 6, appears to be the hepatic route. Indeed, at 48 hrs post-injection, the picture shows a strong contrast enhancement of the liver tissues (see Fig. 6 (a_3) and (b_2)), with clear delineation of the hepatic region and accurate differentiation between the hepatic tissue and the liver irrigation. Immediately after the administration of nano-emulsions, contrast enhancement also appears in the liver at $\Delta HU^{liver}(0\ h) = \Delta HU_0^{liver} \sim 88$ HU (likely due to liver vascularization) and gradually increases, to become very pronounced at 48 hrs post-injection. In addition, the spleen and lymph nodes also appear contrasted (see coronal and transverse slices in Fig. 8), with a significant contrast at 48 hrs post-injection, persistent like the one in liver.

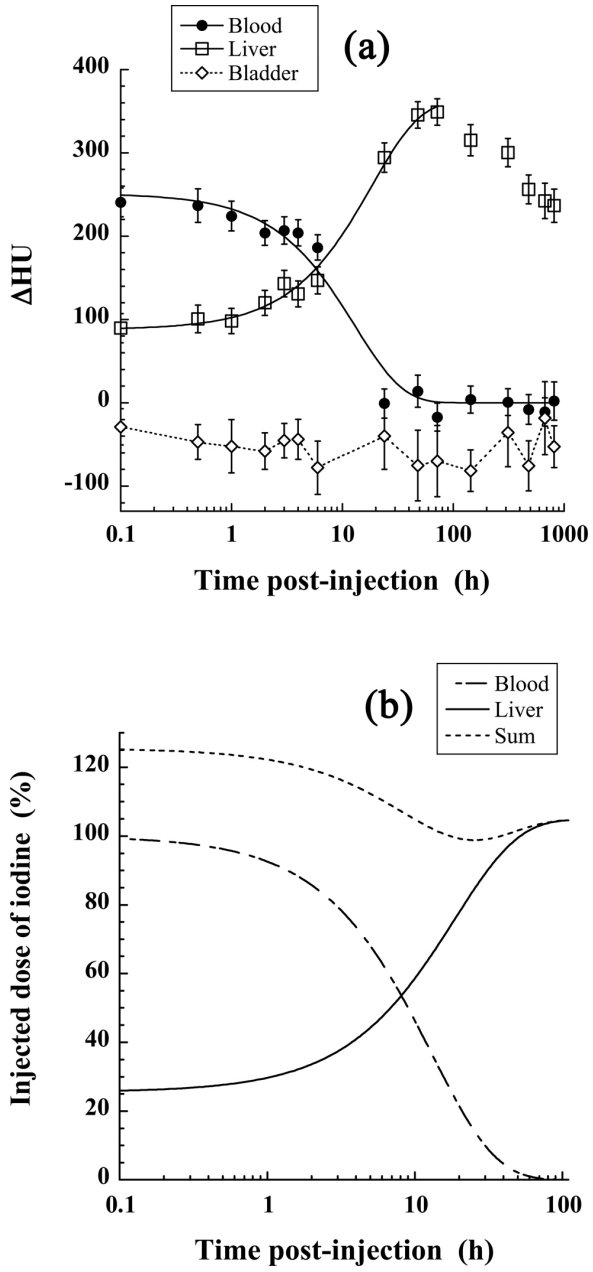

Figure 7: Quantification of the X-ray attenuation after i.v. administration of iodinated α-tocopherol nano-emulsions in mice. (a) Follow-up of $\Delta HU(t)$ (= *X-ray attenuation at time t – X-ray attenuation before injection*) over time. Regions of interest (ROI) were placed in heart (filled circles), liver (open squares), and bladder (open rhombus). (b) Injected dose of iodine per organ in function of time. Initial blood dose was extrapolated to be 100%. *Sum* is the sum of the blood and liver curves.

Representative points, 48 hrs and 55 days were reported in Fig. 8 showing lymph nodes, liver and spleen. The hepatic contrast still appears largely higher than the ones in spleen or lymph nodes, indicating that the lipid nano-droplets are indeed predominantly taken up by the hepato-

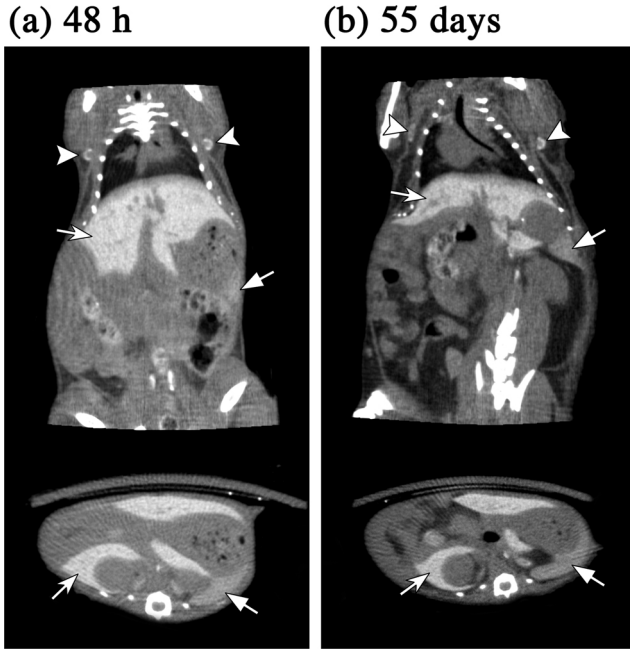

Figure 8: Micro-CT scans evidencing the contrast enhancement in the spleen (solid arrow) and in lymph nodes (arrowhead), 48 hrs and 55 days after i.v. injection of iodinated α-tocopherol nano-emulsions in mice. Liver was also indicated with open arrow.

cytes and not by the reticuloendothelial system (RES) [25, 31]. This in turn corroborates not only the results generally observed for the elimination process of lipid nano-emulsions, but also those exposed above in Fig. 5 (b). This predominant hepatocyte uptake can be explained by considering the bio-distribution of α-tocopherol, known to be packaged in chylomicrons (with a similar structure to nano-emulsion droplets), then sequestered and secreted by the liver. A parallel can be drawn between non-iodinated α-tocopherol and an iodinated nano-suspension, thus helping to explain the *in vivo* passive accumulation in the liver tissues observed here by micro-CT. Subsequently, the quantitative follow-up of the contrast enhancement in hepatic tissues (see Fig. 7 (a), ROI in liver), disclosed a persistent signal from 24 hrs up to more than 4 months (experiments were arbitrary stopped after 4 months), without clinical signs of toxicity or perturbation of the behavior in mice. This shows that during this period, iodinated α-tocopherol is very slowly eliminated from the body, a trend visible in Fig. 7 (a). Here again, experimental data was successfully fitted by an exponential function (reported in Fig. 7 (a), R = 0.996) of the form:

$$\Delta HU(t) = \Delta HU_0^{liver} + \Delta HU_\infty^{liver} \cdot \left(1 - \mathrm{e}^{-k_{liver} \cdot t}\right) \tag{2}$$

where ΔHU_0^{liver} is the initial value of the contrast enhancement in liver (after injection), here ΔHU_0^{liver} = 88 HU, ΔHU_∞^{liver} is the contrast enhancement at the end of the accumulation process, here at 72 hrs, ΔHU_∞^{liver} = 361 HU, and finally k_{liver} is the accumulation rate constant, here k_{liver} = 0.054 h^{-1}. Moreover, the close values of the elimination rate constant k_{blood} and the accumulation rate constant k_{liver} indicate that the two kinetics are comparable, and corroborate the hypothesis that accumulation in the liver is the exclusive mechanism for blood clearance. It is important to note here, that this long retention time in liver, limits application of these iodinated vitamin E nano-emulsions at a preclinical imaging stage, and we cannot rule out human application. Likewise, the follow-up of $\Delta HU(t)$ in the bladder is reported in Fig. 7, and provides values fluctuating around zero throughout the experiment. This clearly indicates that the product is not excreted by the renal route and that the only route of elimination is the hepatic one, thus corroborating the results disclosed above.

The comparison between the blood and hepatic contrast will be achieved, if the X-ray attenuation signals are normalized for the mass of their respective compartments, blood and liver. This will allow the comparison of their respective dose of iodine and help evaluate the quantity lost in the other organs during the experiment. For a mouse of 30 g, blood and liver masses were respectively estimated at 2.3 g and 1.7 g. Based on the experimental data of Fig. 7 (a), these normalized results, along with their sum, are presented in Fig. 7 (b). It appears that the last normalized dose of iodine in the liver reaches the intensity of the initial one in the blood. This means that the entire dose is recovered and a very low quantity of contrast agent is lost. It is worth noting that the sum of the curve decreases by a quantity corresponding to the initial value of the liver contrast. This signal may be due to liver vascularization at early times.

Finally, 3D volume rendering of the blood vessels (30 min post-injection) and the liver (48 h post-injection), are presented in Fig. 9 (a) and (b), respectively. These image reconstructions show the potential of this contrast agents for structural imaging in micro-CT. Figure 9 (a) presents the visualization of the vasculature and organ irrigation. The ribs were partially removed to make clearly appears the inner blood network, heart left and right ventricles, the thoracic and abdominal aorta, hepatic portal vein and vena cava, renal vein and iliac arteries, and (b_2) shows the whole liver, and (b_3) to (b_8) show different cuts of liver, highlighting the accurate and specific contrast difference between the hepatic tissue (yellow) and its irrigation (red). 3D movies of these volume

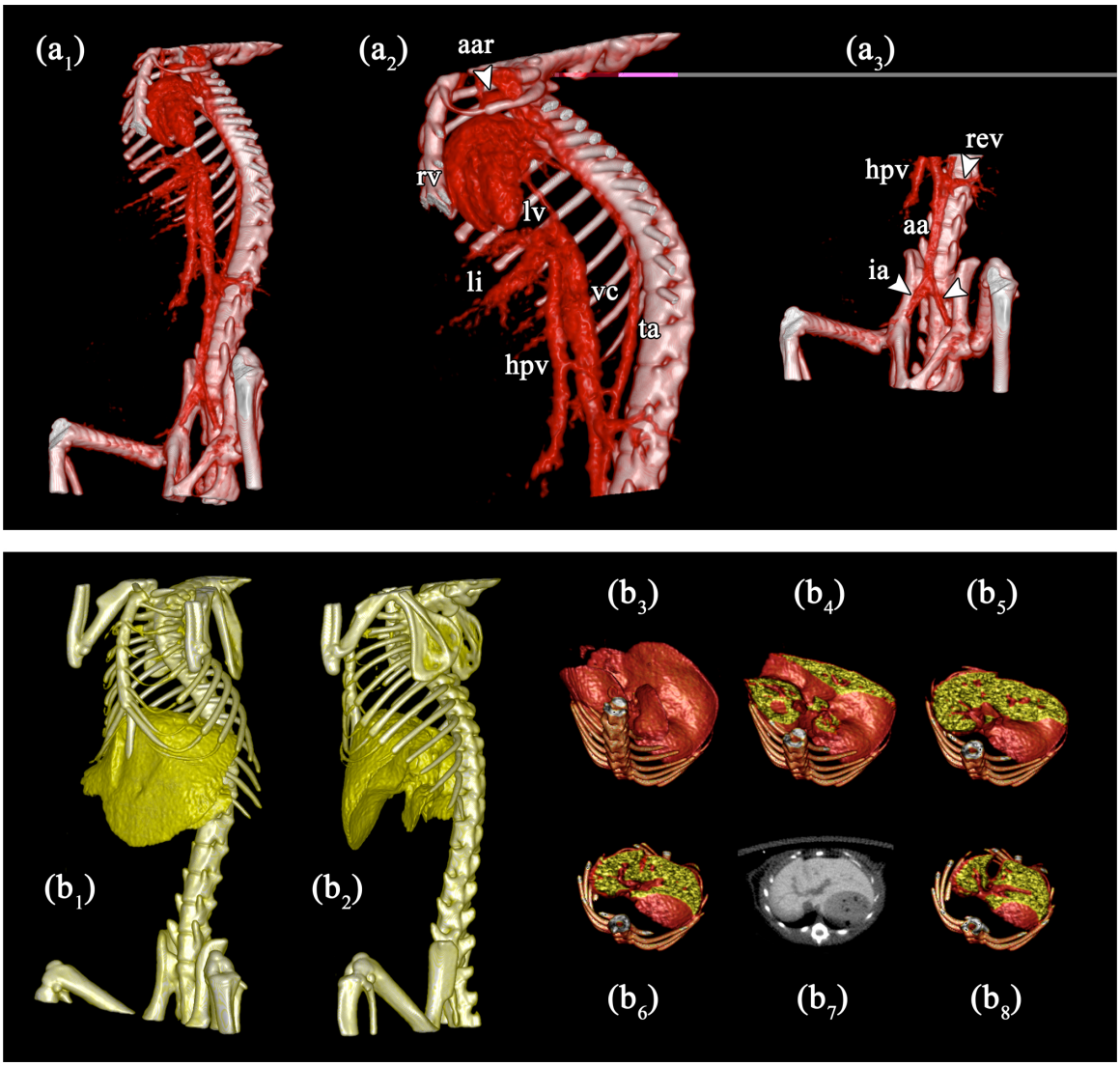

Figure 9: 3D volume rendering, (a) 30 min and (b) 48 hrs after i.v. injection of iodinated α-tocopherol nano-emulsions in mice. (a_1) Presents the blood network showing an overview on the blood pool, detailed and annotated in (a_2) and (a_3). Annotations: (aar) aortic arch, (rv) right ventricle, (lv) left ventricle, (li) location of liver, (vc) vena cava, (hpv) hepatic portal vein, (ta) thoracic aorta, (aa) abdominal aorta, (rev) renal vein and (ia) iliac arteries. A movie is available as supplementary data (movie1.mov). (b) Liver 3D imaging, (b_1) and (b_2) show the whole animal body at different camera angles, and (b_3) to (b_8) show liver sections, emphasizing the clear difference of contrast between the liver tissues and its vascularization; (b_7) is the transverse slice corresponding to (b_6). A movie is available as supplementary data (movie2.mov).

rendering representations are proposed as supplementary information. Beyond the graphical rendering, such results evidence the high potential of nano-emulsion technology for use as targeted CT contrast agents, allowing a clear delineation between soft tissues themselves and between soft tissues and biological fluids.

4. Conclusion

This study presents a non-toxic contrast agent for preclinical micro-CT imaging. This formulation consists of iodinated vitamin E (α-tocopheryl 2,3,5-triiodobenzoate) as an oily phase, formulated in the form of liquid nano-emulsion droplets (by low-energy nano-emulsification), surrounded by a hairy PEG layer, thus conferring stealth properties. The originality and strength of these new contrast agents lie not only in their outstanding contrasting properties, biocompatibility and low toxicity, but also in the simplicity of their fabrication: one-step synthesis of the highly iodinated oil (iodine constitutes 41.7% of the oil molecule weight) and its spontaneous emulsification. After i.v. administration in mice (8.5% of blood volume), the product shows stealth properties towards the immune system and thus behaves as an efficient blood pool contrast agent ($t_{1/2}$ = 9.0 h). Further, it exhibits blood clearance following mono-exponential decay. A gradual accumulation predominantly due to hepatocyte uptake is observed and measured in the liver, establishing a strong hepatic contrast, persistent for more than four months. For all these reasons, in the current range of available or developed contrast agents for preclinical X-ray imaging, this agent seems to be one of the most efficient. The step beyond in preclinical imaging, will be their evaluation as contrast agent of hepatic lesions like tumors, as well as the studies of potential interference in the liver metabolism. On the other hand, as the long retention time in liver is a main strength for preclinical imaging, and could be a limitation for human transposition. As seen here, the accumulation of the contrasting system in the hepatocyte is likely driven by the chemical nature of the iodinated α-tocopherol and not necessarily by the nanodroplet formulation. One can imagine that nanodroplet incorporating a contrasting agent with a body clearance via faster hepatic elimination after long circulation time in blood, might become more compatible for imaging of the human specie.

5. Acknowledgments

Experimental part (*in vivo* imaging) of this study was performed on CERMEP - imagerie du vivant, Bron, F-69677, France, imaging facilities. The authors want to thank the technical staff of the platform.

References

[1] Badea CT, Drangova M, Holdsworth DW, Jhonson GA. In vivo small animal imaging using micro-ct and digital subtraction angiography. Phys Med Biol 2008;53:R319–R350.

[2] Schambach SJ, Bag S, Groden C. Schilling L, Brockmann MA. Vascular imaging in small rodent using micro-ct. Methods 2010;50:26–35.

[3] Zagorchev L, Oses P, Zhuang ZW, Moodie K, Mulligan-Kehoe M, Simons M, et al. Micro computed tomography for vascular exploration. J Angiogenesis Res 2010;2:7–17.

[4] de Kemp RA, Epstein FH, Catana C, Tsui BMW, Ritman EL. Small-animal molecular imaging methods. J Nucl Med 2010;51:18–32.

[5] Williams JC, McAteer JA, Evan AP, Lingeman JE. Micro-computed tomography for analysis of urinary calculi. Urol Res 2010;38:477–484.

[6] Tsui BMW, Kraitchman DL. Recent advances in small-animal cardiovascular imaging. J Nucl Med 2009;50:667–670.

[7] Burghardt AJ, Link TM, Majumdar S. High-resolution computed tomography for clinical imaging of bone microarchitecture. Clin Orthop Relat Res 2011;469:2179–2193.

[8] Almajdub M, Nejjari M, Poncet G, Magnier L, Chereul E, Roche C, et al. In-vivo high-resolution x-ray microtomography for liver and spleen tumor assessment in mice. Contrast Media Mol Imaging 2007;2:88–93.

[9] Kim HW, Cai QY, Jun HY, Chon KS, Park SH, Byun SJ, et al. Micro-ct imaging with a hepatocyte-selective contrast agent for detecting liver metastasis in living mice. Acad Radiol 2008;15:1282–1290.

[10] Ohta S, Lai EW, Morris JC, Bakan DA, Klaunberg B, Cleary S, et al. Micro-ct for high-resolution imaging of ectopic pheochromocytoma tumors in the liver of nude mice. Int J Cancer 2006;119:2236–2241.

[11] Mukundan Jr. S, Ghaghada KB, Badea CT, Kao CY, Hedlund LW, Provenzale JM, et al. A liposomal nanoscale contrast agent for preclinical ct in mice. Am J Roentgenol 2006;186:300–307.

[12] Martiniova L, Schimel D, Lai EW, Limpuangthip A, Kvetnansky R, Pacak K. In vivo micro-ct imaging of liver lesions in small animal models. Methods 2010;50:20–25.

[13] Bourin M, Jolliet P, Ballereau F. An overview of the clinical pharmacokinetics of x-ray contrast media. Clin Pharmacokinet 1997;32:180–193.

[14] Guo R, Wang H, Peng C, Shen M, Zheng L, Zhang G, et al. Enhanced x-ray attenuation property of dendrimer-entrapped gold nanoparticles complexed with diatrizoic acid. J Mater Chem 2011;21:5120–5127.

[15] Kim D, Park S, Lee JH, Jeong YY, Jon S. Antibiofouling polymer-coated gold nanoparticles as a contrast agent for in vivo x-ray computed tomography imaging. J Am Chem Soc 2007;129:7661–7665.

[16] Kao CY, Hoffman EA, Beck KC, Bellamkonda RV, Annapragada AV. Long-residence-time nano-scale liposomal iohexol for x-ray-based blood pool imaging. Acad Radiol 2003;10:475–483.

[17] Rabin O, Manuel Perez J, Grimm J, Wojtkiewicz G, Weissleder R. An x-ray computed tomography imaging agent based on long-circulating bismuth sulphide nanoparticles. Nat Mater 2006;5:118–122.

[18] Torchilin VP. Targeted pharmaceutical nanocarriers for cancer therapy and imaging. AAPS J 2007;9:E128–E147.

[19] Peer D, Karp JM, Hong S, Farokhzad OC, Margalit R, Langer R. Nanocarriers as an emerging platform for cancer therapy. Nat Nano 2007;2:751–760.

[20] Torchilin VP, Frank-Kamenetsky MD, Wolf GL. Ct visualization of blood pool in rats by using long-circulating, iodine-containing micelles. Acad Radiol 1999;6:61–65.

[21] Torchilin VP. Polymeric micelles in diagnostic imaging. Colloid Surf B-Biointerfaces 1999;16:305–319.

[22] Maeda H. Tumor-selective delivery of macromolecular drugs via the epr effect: background and future prospects. Bioconjugate Chem 2010;21:797–802.

[23] Ghaghada KB, Badea CT, Karumbaiah L, Fettig N, Bellamkonda RV, Johnson GA, et al. Evaluation of tumor microenvironment in an animal model using a nanoparticle contrast agent in computed tomography imaging. Acad Radiol 2011;18:20–30.

[24] Bae KH, Chung HJ, Park TG. Nanomaterials for cancer therapy and imaging. Mol Cells 2011;31:295–302.

[25] Li X, Anton N, Zuber G, Vandamme TF. Contrast agents for preclinical targeted x-ray imaging. submitted 2012;.

[26] Trubetskoy VS, Gazelle GS, Wolf GL, Torchilin VP. Block-copolymer of polyethylene glycol and polylysine as a carrier of organic iodine: design of long-circulating particulate contrast medium for x-ray computed tomography. J Drug Target 1997;4:381–388.

[27] de Vries A, Custers E, Lub J, van den Bosch S, Nicolay K, Grüll H. Block-copolymer-stabilized iodinated emulsions for use as ct contrast agents. Biomaterials 2010;31:6537–6544.

[28] Hallouard F, Anton N, Choquet P, Constantinesco A, Vandamme T. Iodinated blood pool contrast media for preclinical x-ray imaging applications. Biomaterials 2010;31:6249–6268.

[29] Hallouard F, Anton N, Zuber G, Choquet P, Li X, Arntz Y, et al. Radiopaque iodinated nano-emulsions for preclinical x-ray imaging. RSC Advances 2011;1:792–801.

[30] Hallouard F, Briançon S, Anton N, Li X, Vandamme T, Fessi H. Iodinated nano-emulsions as contrast agents for preclinical x-ray imaging, impact of the free surfactants on the pharmacokinetics. Eur J Pharm Biopharm 2012;submitted for publication.

[31] Jakhmola A, Anton N, Vandamme T. Inorganic nanoparticles based contrast agents for x-ray computed tomography. Adv Healthcare Mater 2012;in press.

[32] Peng C, Zheng L, Chen Q, Shen M, Guo R, Wang H, et al. Pegylated dendrimer-entrapped gold nanoparticles for in vivo blood pool and tumor imaging by computed tomography. Biomaterials 2012;33:1107–1119.

[33] Torchilin VP, Trubetskoy VS. Which polymers can make nanoparticulate drug carriers long-circulating? Adv Drug Deliv Rev 1995;16:141–155.

[34] Storm G, Belliot SO, Daemen T, Lasic DD. Surface modification of nanoparticles to oppose uptake by the mononuclear phagocyte system. Adv Drug Deliv Rev 1995;17:31–48.

[35] Brigger I, Dubernet C, Couvreur P. Nanoparticles in cancer therapy and diagnosis. Adv Drug Deliv Rev 2002;54:631–651.

[36] Haley B, Frenkel E. Nanoparticles for drug delivery in cancer treatment. Urol Oncol 2008;26:57–64.

[37] Singh R, Lillard Jr. JW. Nanoparticle-based targeted drug delivery. Exp Mol Pathol 2009;86:215–223.

[38] Szebeni J, Muggia FM, Alving CR. Complement activation by cremophor el as a possible contributor to hypersensitivity to paclitaxel: an in vitro study. J Natl Cancer Inst 1998;90:300–306.

[39] Anton N, Benoit JP, Saulnier P. Design and production of nanoparticles formulated from nano-emulsion templates – a review. J Control Release 2008;128:185–199.

[40] Anton N, Vandamme TF. The universality of low-energy nano-emulsification. Int J Pharm 2009;377:142–147.

[41] Anton N, Vandamme T. Nano-emulsions and micro-emulsions: Clarifications of the critical differences. Pharm Res 2011;28:978–995.

[42] Creusat G, Thomann JS, Maglott A, Pons B, Dontenwill M, Guerin E, et al. Pyridylthiourea-grafted polyethylenimine offers an effective assistance to sirna-mediated gene silencing in vitro and in vivo. J Control Release 2012;157:418–426.

3.2. Evaluation de la fonction d'endothéliale à l'exposition prolongée de nano-émulsions de 2,3,5-triiodobenzoate d'α-tocophérol

Les nano-émulsions d'α-tocophérol iodée ont montré un contraste significatif et prolongé au niveau sanguin **(chapitre 3.1)**. La rémanence de ces composés au niveau sanguin nous a conduits à évaluer l'innocuité des nano-émulsions iodées sur la fonction des cellules de l'endothélium vasculaire. Nous avons ensuite réalisé une étude sur l'aorte thoracique de rat pour déterminer les influences sur la fonction endothéliale et la réactivité vasculaire à l'exposition prolongée de nano-émulsions d'α-tocophérol iodé.

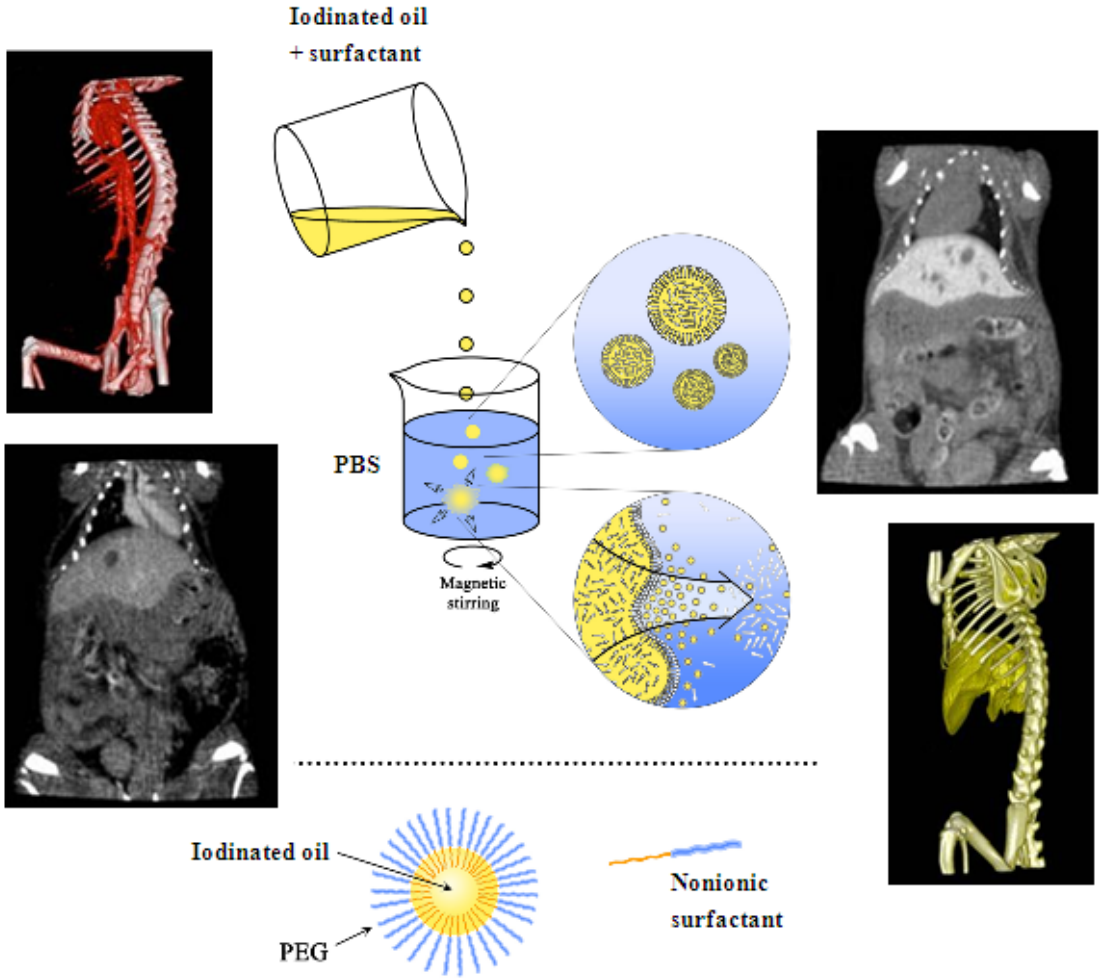

ORIGINAL RESEARCH

Do iodinated nano-emulsions designed for preclinical vascular imaging alter the endothelial function in rat aorta?

Nicolas ANTON[1], Marina ATZENHOFFER[2], François DAUBEUF[3], Xiang LI[1], Valérie B. SCHINI-KERTH[2], Barbara DELMOTTE[2], Thierry F. VANDAMME[1], Thierry CHATAIGNEAU[2,4,*]

Université de Strasbourg, Faculté de Pharmacie, 74 route du Rhin, BP 60024, 67401 Illkirch Cedex, France:

[1]UMR 7199 CNRS, Laboratoire de Conception et Application de Molécules Bioactives, Equipe de Pharmacie Biogalénique;

[2]UMR 7213 CNRS, Laboratoire de Biophotonique et Pharmacologie, Equipe Pharmacologie et Physiopathologie Cardiovasculaires;

[3]UMR 7200 CNRS, Laboratoire d'innovation Thérapeutique, Equipe de Chimie-Biologie Intégrative;

[4]UMR 7199 CNRS, Laboratoire de Conception et Application de Molécules Bioactives, Equipe de Biophysicochimie des Récepteurs-Canaux.

Abstract:

This study proposes a new methodology to evaluate the putative consequences of the long-lasting circulation in the blood pool of nanoparticulate systems widely used in nanomedicine, Indeed, the blood pool contrast agent for micro-computed tomography, *i.e*. iodinated nano-emulsions, have recently been developed, for their great potential in medical applications such as advanced diagnosis, image-guided surgery, personalized medicine or theragnostics. Stealth nanoparticles exhibit a low recognition by the reticuloendothelial system, resulting in a prolonged circulation in the bloodstream and long-lasting contact with the endothelial cells. Therefore, the aim of the present study is to determine whether this prolonged interaction could induce an alteration of the endothelial function and vascular smooth muscle reactivity. The Iodinated nano-emulsions were intravenously injected in rats. After one hour of contrast agent circulation in the blood pool, the rats were anesthetized and the thoracic aorta was removed for the study of vascular reactivity. These animals were compared with control (untreated) rats and a third group of rats receiving an injection of phosphate buffered saline (*i.e.* dispersing phase of the nano-emulsions). Phenylephrine-induced concentration-dependent contractions of the isolated rat thoracic aorta were not modified whatever the group. Sodium nitroprusside (a NO donor)-induced relaxations of endothelium-denuded aorta were also unaltered in response to the different administrations. In contrast, in comparison with control animals, endothelium-dependent NO-mediated relaxations to acetylcholine and red wine polyphenols were significantly impaired in thoracic aorta from PBS-treated rats, but not in animals receiving the iodinated nano-emulsion. In addition, neither isoprenaline-induced nor levcromakalim-induced relaxations were modified in the aorta from the three groups of animals. These findings indicate that even with a long-lasting residence time of the iodinated nano-emulsion in the blood flow, these iodinated nano-emulsions do not alter the endothelial function and thus can be used as contrast agent for preclinical vascular imaging on small laboratory animals.

Running header: Circulating iodinated nano-emulsion and endothelium

Keywords: iodinated nano-emulsion, endothelium, aorta, nitric oxide, contraction, relaxation.

***Corresponding author:** Thierry CHATAIGNEAU

University of Strasbourg, Faculty of Pharmacy, 74 route du Rhin, BP 60024, 67401 Illkirch Cedex, France:

[2]UMR 7213 CNRS, Laboratoire de Biophotonique et Pharmacologie, Equipe Pharmacologie et Physiopathologie Cardiovasculaires,

[4]UMR 7213 CNRS, Laboratoire de Biophotonique et Pharmacologie, Equipe Pharmacologie et Physiopathologie Cardiovasculaires.

Tel: +33 (0)3 68 85 41 33

Fax: +33 (0)3 68 85 43 06

Email: thierry.chataigneau@unistra.fr

1. Introduction

Over the last decades, the formulations of nano-scaled drug delivery systems have received extensive attention. The main reasons lie in the huge possibilities offered by these ranges of particle sizes in terms of interactions with the biological media, targeting, biological barrier crossing, tissues penetration and improving the bioavailability of encapsulated drugs. Alternatively, nano-scaled objects with controlled surface properties can exhibit stealth properties towards immune system, resulting in long-lasting time of circulation in bloodstream with a very slow elimination. According to the biomedical applications, the residence time of the product in the bloodstream may represent a major critical point. Generally, depending on their size range, the nano-carriers are eliminated from the blood either through the renal clearance, the reticuloendothelial system (RES) uptake or the hepatic uptake. The elimination route by kidneys is due to the glomerular filtration, with pore diameter ranging from 50 to 100 nm.[1] On the other hand, particles with bigger sizes will be recognized by the immune system or by the hepatocytes and eliminated by the liver. However, functionalizing the surface of the nanocarrier with hydrophilic polymer like polyethylene glycol (PEG) can significantly modify their pharmacokinetic parameters. Systems with long-lasting circulation are generally formulated in order to target organs or tumors (through active or passive mechanisms), thus increasing the time in which the targeted sites are in contact with the nanocarriers. Recent developments concern the nano-encapsulation of contrast agents such as stealth or targeted nanocarriers that open new possibilities in term of advanced diagnosis, image-guided surgery, and even personalized medicine or theragnostics (when they co-encapsulate a drug). In fact, one of the very hot challenges corresponds to the development of blood pool contrast agents for preclinical micro-computed tomography (micro-CT), *i.e.* X-ray scanner. For this purpose, stealth nanocarriers are developed that encapsulate a contrast agent (like iodine) and provide a contrast enhancement of the blood compartment. As shown in our previous studies,[2,3,4] this is particularly important for micro-CT since nano-encapsulated contrast agents constitute the only available solution to suitably enhance the imaging contrast in the blood pool of small laboratory animals. To date, only few products are commercially available for that purpose, and they formulated as polymeric rare earth-based nanoparticles (Exitron Nano®) or iodinated nano-emulsions.[3] Commercially available iodinated nano-emulsions, namely Fenestra VC® (ART Inc., Montréal, Canada), are largely used as contrast agents for micro-CT; these are iodinated lipid (concentration around 55 mg I/mL) formulated in the shape of nano-droplets. However, to reach interesting levels of contrast and long-lasting circulation times, the experimental protocols still require drastic conditions like the administration of high volumes, generally about 10 % of the blood volume. In this same line, we recently developed[5] a new generation of iodinated nano-emulsions (based on iodinated α-tocopherol surrounded by a polyethylene glycol (PEG) layer) twice more concentrated than the commercial references, and showing a low (actually negligible) toxicity. As a result, after i.v. administration of these nano-emulsions in mice, these objects display stealth properties towards

immune system, and therefore exhibit a long-lasting circulation time in bloodstream. Thus, the X-ray contrast in blood pool is enhanced, providing outstanding visualization of the small animal vasculature, a very helpful and desirable tool, for example, for vascular and tumor angiogenesis imaging, as well as for the cardiac function.[5] Moreover, In addition, this technology allows a quantitative monitoring of the contrast agent in blood, providing the kinetics of blood clearance, as well as of the products elimination from the animal body (i.e. imaging and monitoring the presence of contrast agent in the different organs, liver, spleen, etc.). The present study has focused on the application as blood pool contrast agents of the new generation of iodinated α-tocopherol nano-emulsions presented above.

These long lasting circulating systems are very promising for their imaging properties, as well as for their biocompatibility and low toxicity *in vitro*. However, due to the long-lasting residence time in bloodstream, it is conceivable that such a nano-system could interact with, or even alter, the monolayer of endothelial cells lining the vascular wall at the interface with the lumen. These potential effects on the endothelial function can be disclosed, following *i.v.* injection of the nano-emulsions, and significant circulation time in the blood, by monitoring the vascular reactivity, *ex vivo*. Actually, the endothelial cells control the vascular tone of the underlying smooth muscle cells by the production of endothelium-derived relaxing factors.[6] These factors include nitric oxide[7,8] (NO), prostacyclin[9] and the endothelium-derived hyperpolarizing factor (EDHF) which is associated with hyperpolarization of vascular smooth muscle cells.[10,11]

NO is the major relaxing factor in large arteries such as rat aorta,[12] and it is produced by the activation of endothelial NO synthase in response to several stimuli including acetylcholine, bradykinin and blood flow-dependent shear stress. Endothelial NO induces the relaxation of the underlying vascular smooth muscle cells mainly by the activation of soluble guanylyl cyclase and formation of the second messenger cGMP.[6] Under pathophysiological conditions, endothelium-dependent NO-mediated relaxation is often impaired.[13]

The purpose of the present study is therefore to determine whether the prolonged exposure of the endothelium to iodinated nano-emulsion, designed for vascular imaging, alters the endothelial function and vascular smooth muscle reactivity, in rat aorta. Actually, since the main objective of such formulations is a long-lasting circulation time in the organism, studying the repercussion on the endothelial function appears as a critical parameter of innocuousness towards the organism. In this context, the present study is crucial because this aspect has, to date, never been investigated. The present study has been performed with iodinated α-tocopherol nano-emulsions, intravenously given to rats in experimental conditions similar to those of *in vivo* imaging experiments.[5] Finally, the choice of the circulation time in blood stream (in this case, 1 hour post-injection) is perfectly compatible with the time allowing the experimental imaging and including the preparation of the animal in micro-CT scanner after contrast agent injection and acquisition time.

2. Materials and methods

2.1. Materials

2,3,5-Triiodobenzoic acid, α-tocopherol (vitamin E), 4-dimethylaminopyridine, N,N'-dicyclohexylcarbodiimide, dichloromethane, ethyl acetate, cyclohexane, N^{ω}-nitro-L-arginine methyl ester, indomethacin, acetylcholine, sodium nitroprusside, levcromakalim, phenylephrine and isoprenaline were all purchased from Sigma-Aldrich. Nonionic surfactant Cremophor ELP® from BASF (Ludwigshafen, Germany) was a generous gift from Laserson (Etampes, France). Phosphate Buffered Saline (PBS) was purchased from Eurobio (France).

Red Wine Polyphenols (RWPs) were dissolved in a solution of ethanol and deionized water (50 % v/v) at a stock concentration of 100 mg/mL. A stock solution of indomethacin (10 mmol/L) was prepared in a sodium bicarbonate solution. The other compounds were dissolved in deionized water. Concentrations are expressed as final concentrations (mol/L or mg/mL) in the bath solution.

2.2. Methods

2.2.1. Synthesis of α-tocopheryl 2,3,5-triiodobenzoate

As described in detail elsewhere,[5] iodinated lipophilic molecules used as lipid core of the nano-emulsions is composed of vitamin E (DL-α-tocopherol) on which 2,3,5-triodobenzoic acid has been grafted through a reaction of esterification. Briefly, 2,3,5-triodobenzoic acid, 4-dimethylaminopyridin and N,N'-dicyclohexylcarbodiimide were sequentially added at room temperature to a solution of DL-α-tocopherol in dicholoromethane. The reaction mixture was stirred overnight at room temperature and the solvent was removed under vacuum; the reaction yield was about 80%. The crude oil was then purified by gradient elution method on silica gel with cyclohexane and ethyl acetate as eluent. The final product is a light yellowish viscous oil containing 41.7% of iodine.

2.2.2. Formulation and characterization of nano-emulsions

Iodinated nano-emulsions were formulated by spontaneous emulsification method, as previously described.[14,15,16] Briefly, α-tocopheryl 2,3,5-triiodobenzoate (oil phase) was mixed with hydrophilic surfactant of Cremophor ELP®. Phosphate buffered saline (PBS) (aqueous phase) was added into the stirred oil/surfactant mixture. Nano-emulsions formed immediately once these two phases are homogenized. Optimized formulation conditions were given by ***(i)*** the surfactant to oil ratio, SOR = 40%, (with SOR = surfactant weight / (surfactant weight + oil weight) x 100 and ***(ii)*** the surfactant-oil to water ratio, SOWR = 40% (with SOWR = (surfactant weight + oil weight) / (surfactant weight + oil weight + water weight) x 100). Finally, the formulation were carried out in order to be physiologically compatible, that is to reach a pH = 7.4 and an osmolarity around 280 mOsm/L. These parameters were systematically controlled after each formulation. The same optimized

nano-emulsion formulations (*i.e.* with the same experimental parameters) were used for all the *in vivo* experiments, imaging experiments and vascular reactivity studies.

Size distributions and polydispersity indices (PDI) were obtained by dynamic light scattering with a Malvern apparatus (NanoZS®, Malvern, Orsay, France). The helium / neon laser, 4 mW, was operated at 633 nm, with the scatter angle fixed at 173° and the temperature maintained at 25°C. Transmission electron microscopy (TEM) observations were carried out using a Philips Morgagni 268D electron microscope. Samples were used without any staining agent (thanks to iodine), and were diluted (1/10) with MilliQ water. A drop of the nano-droplets suspension was placed on a carbon grid (carbon type-A, 300 mesh, copper, Ted Pella Inc. Redding, U.S.A.), and dried at 40°C.

2.2.3. Preparation of Red Wine Polyphenols (RWPs)

RWPs dry powder, obtained from French red wine (Corbières A.O.C., France), was provided by Dr. M. Moutounet (Institut National de la Recherche Agronomique, Montpellier, France) and analyzed by Dr. P.-L. Teissedre (Département d'Oenologie, Université de Montpellier, France). For the preparation of RWPs dry powder, phenolic compounds were adsorbed on a preparative column and alcohol was desorbed. The alcoholic-eluent was evaporated; the concentrated residue was lyophilized and finely sprayed to obtain RWPs dry powder. One liter of red wine produced 2.9 g of RWPs which contained 471 mg/g of total phenolic compounds expressed as gallic acid. The extract contained 8.6 mg/g catechin, 8.7 mg/g epicatechin, dimers (B1: 6.9 mg/g, B2: 8.0 mg/g, B3: 20.7 mg/g and B4: 0.7 mg/g), anthocyanins (malvidin-3-glucoside: 11.7 mg/g, peonidin-3-glucoside: 0.66 mg/g and cyanidin-3-glucoside: 0.06 mg/g) and phenolic acids (gallic acid: 5.0 mg/g, caffeic acid: 2.5 mg/g and caftaric acid: 12.5 mg/g).

2.2.4. In vivo rat and mouse administration of iodinated nano-emulsions

Male wistar rats were anesthetized by intraperitoneal administration of pentobarbital (60 mg/kg). Then, they were placed in lateral *decubitus* on an electric blanket. A segment of 5 mm of the left tail vein was isolated. Blood flow was stopped with two ligatures of cotton thread, each placed at the extremity of the isolated segment of vein. The vein was perforated using a 25 gauge needle and a polyethylene tubing (0.28mm) placed on a 25 gauges needle was inserted into the tail vein. The superior ligature (head side) was removed to push the catheter from 1 cm into the vein. Then, the catheter was stabilized by tightening the superior ligature. Three groups of rats were designed according to their treatment: one control group (control) was not injected whereas two others received an injection of either phosphate buffer solution (PBS) or nano-emulsion and were named afterward PBS and NanoE, respectively. Injection of 500 µL nano-emulsion or PBS was performed slowly (from 90 to 120 sec);

thereafter, the catheter was withdrawn and the superior ligature was tightened. Rats were maintained on the electric blanket during 1 hour before the investigation of vascular reactivity.

In vivo imaging experiments were performed in Swiss mice of about 30 g. Before injection, they were anesthetized with isoflurane, then, α-tocopheryl 2,3,5-triiodibenzoate nano-emulsions (SOR = 40%, SOWR = 40%) were intravenously injected, using a catheter, in the tail-vein, and with an injection volume of 0.18 mL (*i.e.* 6.2 µL of nano-emulsions per gram of mouse).

2.2.5. Micro-computed tomography

In vivo imaging experiments were performed with a micro-CT scanner (INVEON®, Siemens, Munich, Germany). The experimental X-ray parameters were: 50 keV, 500 µA; resolution: 111.25 µm; pitch: 2°; aluminium filters: 0.5 and 900 ms. Acquisitions were performed on 3 Swiss mice. Scans were performed before administration, immediately after injection, as well as 30 min, 1h, 2h, 3h, 4h, 6h, 1 day, 2 days, 3 days, 6 days, 12 days, 19 days, 27 days, 34 days after injection. The Micro-CT raw data were treated with OsiriX viewer, to establish 2D maximum projection slices and 3D volume rendering images, and then to quantify the signal by placing the region of interests (ROI) in the heart.

2.2.6. Vascular reactivity studies

In order to investigate the putative effects of the iodinated nano-emulsion on endothelium and vascular smooth muscle reactivity, rat aorta has been chosen because it is a well-validated model for the exploration of endothelial function.

Therefore, after 1 hour of circulating PBS or nano-emulsion in the blood flow, rats were euthanized and the thoracic aorta was excised and bathed in Krebs bicarbonate solution (in mmol/L: 118,0 ; KCl 4,7 ; $CaCl_2$ 2,5 ; $MgSO_4$ 1,2 ; $NaHCO_3$ 23,0 ; KH_2PO_4 1,2 ; glucose 11,0 ; pH 7,4 ; 37°C) for dissection. The aorta was cleaned of connective tissue and cut into rings (2 mm in length). Rings were suspended in organ baths containing oxygenated (95% O_2, 5% CO_2) Krebs bicarbonate solution for the determination of changes in isometric tension. The rings were stretched step by step until an optimal resting tension of 2 g was reached and then allowed to equilibrate for at least 60 min. After the equilibration period, the rings were exposed to high K^+-containing Krebs bicarbonate solution (80 mmol/L) until reproducible contractile responses were obtained. High K^+ solution was prepared by equimolar substitution of NaCl with KCl. Thereafter, the rings were precontracted with phenylephrine (1 µmol/L) to about 80% of the maximal contraction to high K^+ solution and the relaxation to acetylcholine (1 µmol/L) was determined.

After washout and a further 30-min equilibration period, rings were submitted to increasing cumulative concentrations of phenylephrine (0.1 nmol/L to 10 µmol/L) in the presence of indomethacin (10 µmol/L) in order to rule out vasoactive prostanoids.

In another set of experiments, rings were contracted with phenylephrine (1 µmol/L) before a concentration-relaxation curve to either sodium nitroprusside (0.1 nmol/L to 10 µmol/L), acetylcholine (0.1 nmol/L to 100 µmol/L), RWPs (0.1 µg/mL to 0,1 mg/mL), isoprenaline (0.1 nmol/L to 30 µmol/L), or levcromakalim (0.1 nmol/L to 3 µmol/L) was constructed. Sodium nitroprusside- and levcromakalim-induced relaxations were examined in endothelium-denuded rings of rat aorta. Acetylcholine-, RWPS-and isoprenaline-induced relaxations were recorded in the presence of indomethacin (10 µmol/L) in order to rule out the formation of vasoactive prostanoids. In some experiments, rings were exposed to L-NAME (300 µmol/L), a NO synthase inhibitor, for about 45 min before contraction with phenylephrine and application of cumulative concentrations of acetylcholine.

Contractions were expressed in grams. Relaxations were expressed as a percentage of the contraction induced by phenylephrine (1 µmol/L).

2.2.7. Statistical analysis

Values are expressed as means ± SEM. *n* indicates the number of animals. Statistical analysis was performed with Student's *t*-test for paired data or ANOVA followed by Bonferroni posttests to compare two treatments where appropriate. Values of $p < 0.05$ were considered to be statistically significant.

3. Results

3.1. Nano-emulsions: characterization and blood pool contrast agent application in micro-CT

Representative results of the physico-chemical characterization and biomedical imaging are reported in Fig. 1 (see also Ref. 5 for more details). Fig. 1 (A) shows a schematic representation of the nano-emulsion droplets, composed of an iodinated oily core surrounded and stabilized by a layer of PEGylated nonionic surfactants. Due to the high iodine weight ratio of the oily molecule, the suspension is particularly charged in contrast agent, with a iodine concentration of about 106 mg I/mL.5 DLS experiments disclose a monodispersed size distribution centered around 85 nm, with a narrow peak, reported in Fig. 1 (B). This result is confirmed by the TEM micrographs (Fig. 1 (C)), which even, reveals the less contrasted surrounding layer of surfactants. On the other hand, the PEGylated layer confers stealth properties to the nano-droplets, towards the RES, and therefore their long-lasting circulation properties in bloodstream, of fundamental importance for the current objectives of the formulation. This is illustrated in Fig. 1 (D), showing the blood contrast enhancement ΔHU monitored in function of time (*i.e.* difference between contrast at time *t* and contrast before injection, ROI was placed in heart). Contrast enhancement is clearly significant, for a few hours, making this contrast agent fully compatible with its use as a blood pool contrast agent for micro-CT.

The blood clearance appears to follow a monoexponential decay (the corresponding curve fit is also indicated in the graph), with a value of half-life in blood-pool at $t_{1/2}$ = 9.0 h. However, the optimized conditions for imaging the animal vasculature is the region of maximal contrast enhancement, that is the initial period just after injection, or more largely within the first hour post-injection (indicated with an arrow in the figure).

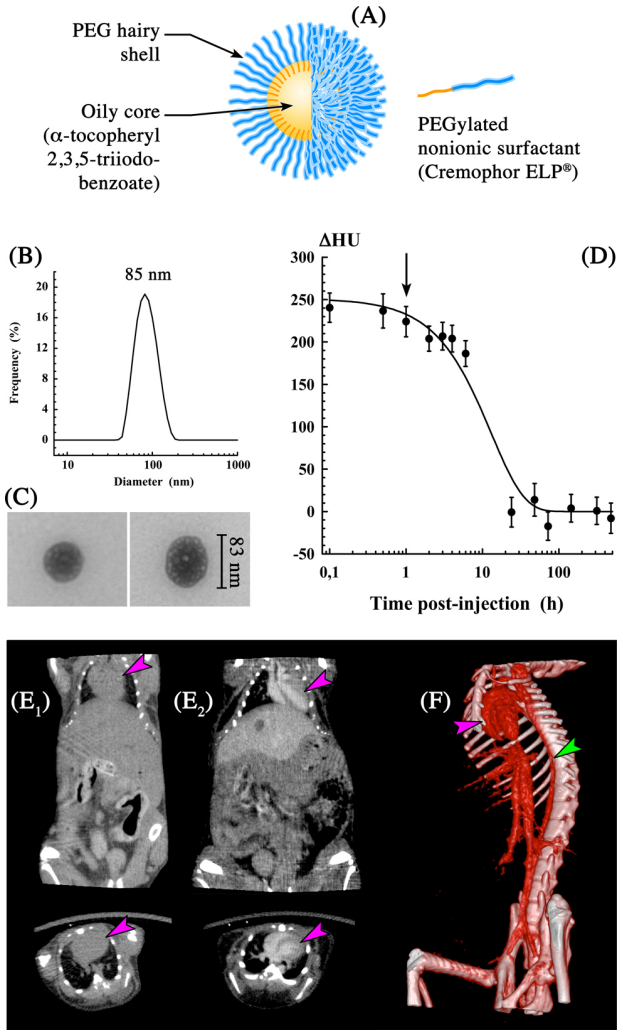

Figure 1: Physico-chemical characterization of iodinated nano-emulsions. (A) Schematic representation of the nano-emulsion droplets structure. (B) Size distribution obtained by DLS measurements. (C) TEM micrographs of iodinated nano-emulsion droplets. (D) X-ray attenuation of blood (ΔHU) in function of time, *i.e.* iodine concentration in blood versus time. (E) Micro-CT scans, maximal intensity projections, coronal sections (top) and transverse slices through the heart (bottom); (E_1) before injection and (E_2) post-i.v. injection in mice. (F) 3D volume rendering, 30 min after i.v. injection in mice. Magenta arrow head show the heart, and green arrow head the thoracic aorta.

This is precisely the period which has been chosen in the current study to stop the circulation of the nano-emulsion in blood pool, and thus to start with vascular reactivity experiments. In addition, *in vivo* images, coronal views and transverse slices of the mouse were reported in Fig. 1 (E). The figure emphasizes the natural X-ray attenuation before administration (E_1), and 30 min post-injection (E_2), magenta arrowheads indicate the heart. The vascularization is clearly visible in (E_2), showing views of the left and right ventricles. Contrast enhancement was also visible in liver, likely due to the strong vascularization of this organ. Finally, Fig. 1 (F) shows three-dimensional volume-rendering which has been reconstructed from the raw data presented in Fig. 1 (E_2) and presenting the whole contrast enhancement in the animal body; this figure illustrates the heart (magenta arrowhead), artery (green arrowhead), but also the iliac arteries, vena cava, hepatic portal vein, renal veins, and liver irrigation. These results simply confirm the high potential of these vascular contrast agents, and thus the important need to investigate the putative effects of their prolonged residence time in blood, on the endothelial function.

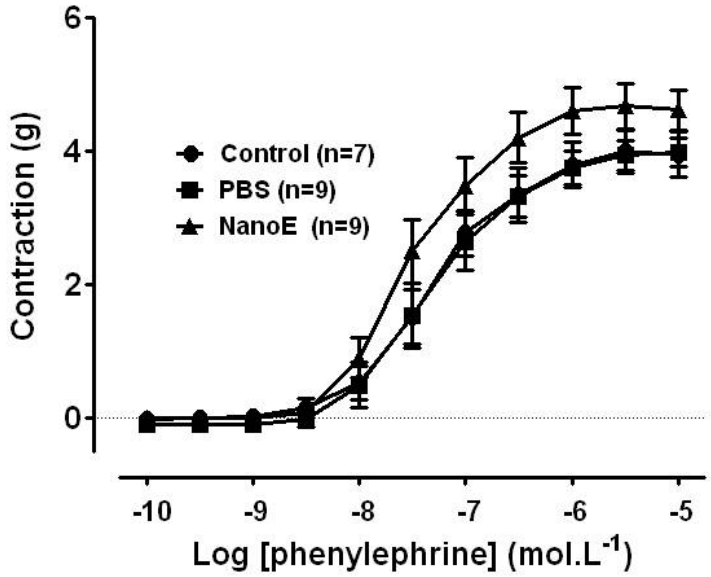

Figure 2: *In vivo* administration of phosphate-buffer saline or iodinated nano-emulsion does not alter phenylephrine-induced contractions of rat aorta. Phenylephrine-induced contractions were recorded in isolated rat aorta from control male Wistar rats (Control) or rats receiving a tail-vein injection of either 500 µL phosphate-buffer saline (PBS) or 500 µL iodinated nano-emulsion. Experiments were performed in the presence of indomethacin (10 µmol/L) in order to rule out vasoactive prostanoids. Results are shown as mean ± SEM; n indicates the number of rats for each group.

3.2. Effects of in vivo administration of iodinated nano-emulsion on phenylephrine-induced contractions in isolated rat aorta

Cumulative concentrations of phenylephrine induced concentration-dependent contractions of isolated rat thoracic aorta (Fig. 2). The contractile response, examined *ex vivo,* was not modified after 1 hour exposure to either PBS or iodinated nano-emulsion in comparison to control conditions (Fig. 2).

3.3. Effects of in vivo administration of iodinated nano-emulsion on NO-sensitivity of vascular smooth muscle

The putative effects of iodinated nano-emulsion on vascular smooth muscle sensitivity to NO was investigated using sodium nitroprusside, an NO donor.

Sodium nitroprusside induced concentration–dependent relaxations in endothelium-denuded isolated rat aorta from control rats (Fig. 3). These relaxations were not different in the aorta from the three groups of animals (Fig. 3). These results indicate that vascular smooth muscle sensitivity to NO is unaltered following PBS or nano-emulsion administration to rats.

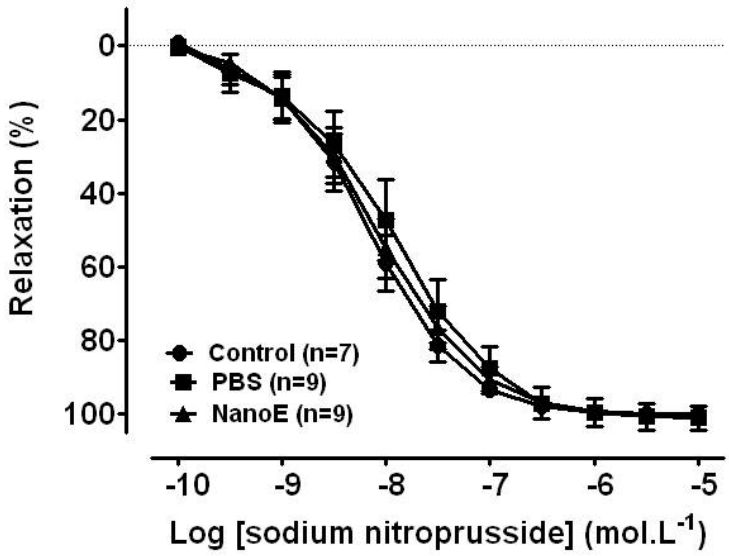

Figure 3: *In vivo* administration of phosphate-buffer saline or iodinated nano-emulsion does not impair sodium nitroprusside-induced realxations of rat aorta. Sodium nitroprusside-induced relaxations were recorded in isolated rat aorta without endothelium from control male Wistar rats (Control) or rats receiving a tail-vein injection of either 500 µL phosphate-buffer saline (PBS) or 500 µL iodinated nano-emulsion (NanoE). Relaxations are expressed as a percentage of the contraction induced by phenylephrine (1 µmol/L). Results are shown as mean ± SEM; n indicates the number of rats for each group.

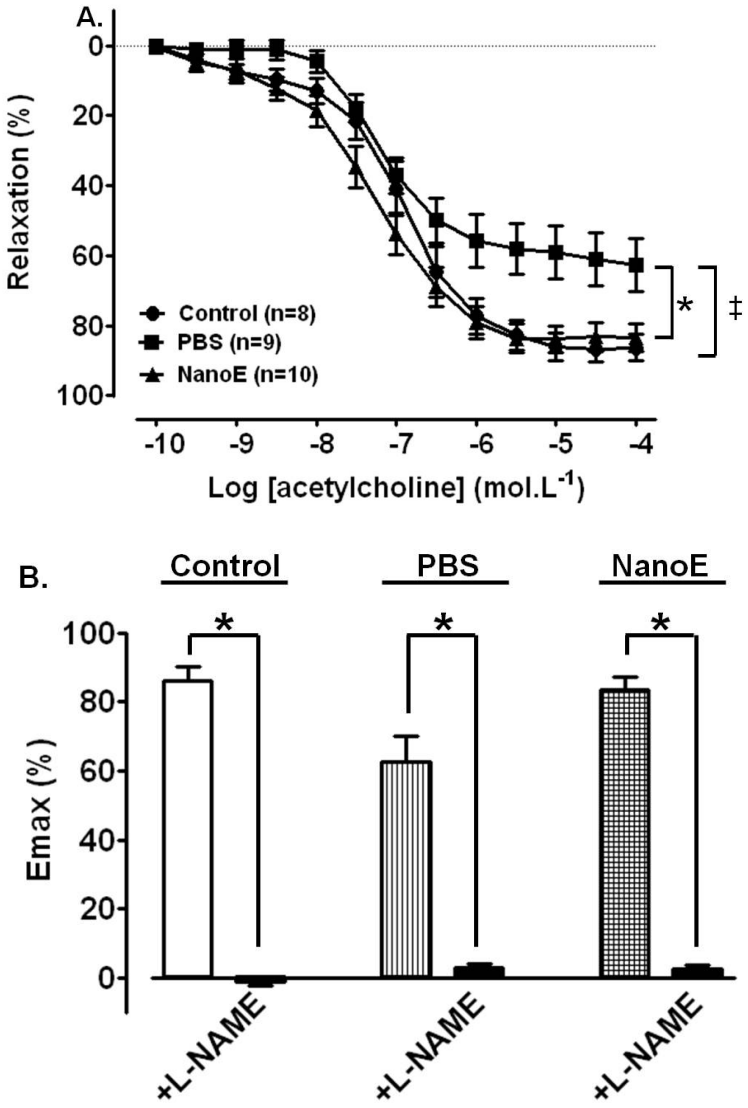

Figure 4: Effects of i*n vivo* administration of phosphate-buffer saline or iodinated nano-emulsion on acetylcholine-induced relaxations of rat aorta. (**A**) Acetylcholine-induced relaxations were recorded in isolated rat aorta from control male Wistar rats (Control) or rats receiving a tail-vein injection of either 500 µL phosphate-buffer saline (PBS) or 500 µL iodinated nano-emulsion (NanoE). Results are shown as mean ± SEM; n indicates the number of rats for each group. *indicates a significant difference *vs* Control (p<0.05) and ‡ indicates a significant difference *vs* NanoE (p <0.05). (**B**) Effect of L-NAME (300 µmol/L) on the maximal relaxant effect (Emax) of acetylcholine recorded at a concentration of 100 µmol/L in the isolated aorta from the three group of rats. Results are shown as mean ± SEM of 8 to 10 rats for each group. *indicates a significant difference (p <0.05). Acetylcholine-induced endothelium-dependent relaxations were recorded in the presence of indomethacin (10 µmol/L) in order to rule out the formation of vasoactive prostanoids. Relaxations are expressed as a percentage of the contraction induced by phenylephrine (1 µmol/L).

3.4. Effects of in vivo administration of iodinated nano-emulsion on acetylcholine-induced NO-mediated relaxations

The potential effect of the different treatments on NO-mediated relaxations was also examined in isolated rat aorta.

Acetylcholine induced concentration-dependent relaxations in the isolated thoracic aorta from the three groups of rats (Fig. 4A). These relaxations were significantly reduced in aortic rings from animals treated with PBS (Fig. 4A). In contrast, in thoracic aorta from rats treated with iodinated nano-emulsion, acetylcholine-induced relaxations were restored to levels similar to those of control condition (Fig. 4A).

The contribution of NO to acetylcholine-induced endothelium-dependent relaxations was investigated in the aorta from the three groups of rats. Whatever the group, acetylcholine-induced endothelium-dependent relaxations were abolished in the presence of L-NAME, an endothelial NO synthase inhibitor (Fig. 4B) indicating that they are entirely mediated by NO.

3.5. Effects of in vivo administration of iodinated nano-emulsion on RWPs-induced NO-mediated relaxations

RWPS induce the relaxation of vascular smooth muscle in part by the activation of the endothelial PI3-kinase/Akt pathway leading to the production of NO.[14] The potential effect of the different treatments on this pathway was also investigated *ex vivo* in the present study.

As illustrated in Fig 5A, RWPs-induced endothelium-dependent relaxation was significantly inhibited, at the highest concentration (0.1 mg/mL), following the treatment of the rats with PBS in comparison to control conditions. In contrast, in the aorta from animals treated with the iodinated nano-emulsion, these relaxations were not different from that observed in vessels from control animals (Fig 5A).

The contribution of NO to RWPs-induced endothelium-dependent relaxations was also examined in the aorta from the three groups of rats. In isolated thoracic aorta from the three groups of rats, RWPs-induced relaxations were abolished in the presence of L-NAME (Fig. 5B) confirming that they are also entirely mediated by NO.

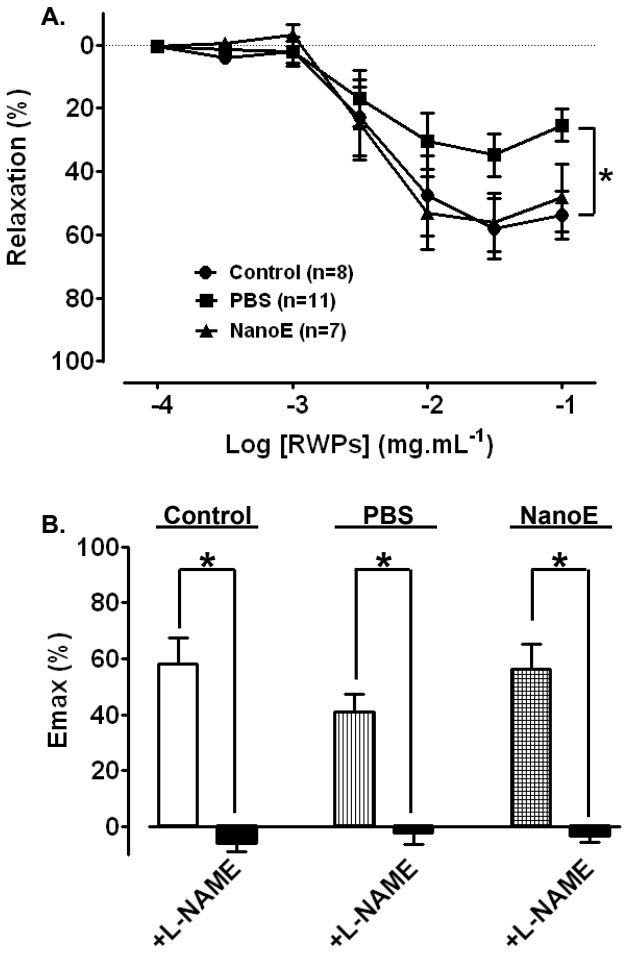

Figure 5: Effects of i*n vivo* administration of phosphate-buffer saline or iodinated nano-emulsion on RWPs-induced relaxations of rat aorta. (A) RWPs-induced relaxations were recorded in isolated rat aorta from control male Wistar rats (Control) or rats receiving a tail-vein injection of either 500 µL phosphate-buffer saline (PBS) or 500 µL iodinated nano-emulsion (NanoE). Results are shown as mean ± SEM; n indicates the number of rats for each group. *indicates a significant difference *vs* Control (p<0.05). (B) Effect of L-NAME (300 µmol/L) on the maximal relaxant effect (Emax) of RWPs recorded at a concentration of 30 µg/mL in the isolated aorta from the three group of rats. Results are shown as mean ± SEM of 7 to 9 rats for each group. *indicates a significant difference (p <0.05). RWPs-induced endothelium-dependent relaxations were recorded in the presence of indomethacin (10 µmol/L) in order to rule out the formation of vasoactive prostanoids. Relaxations are expressed as a percentage of the contraction induced by phenylephrine (1 µmol/L).

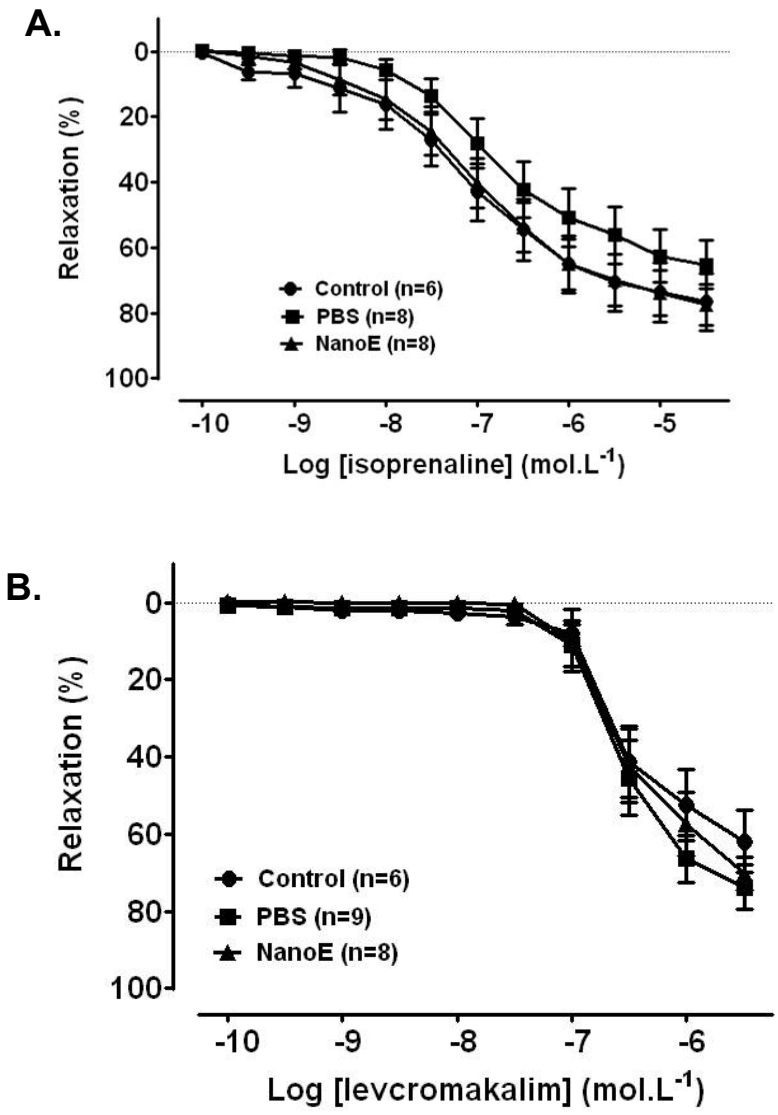

Figure 6: *In vivo* administration of phosphate-buffer saline or iodinated nano-emulsion does not modify isoprenaline- and levcromakalim-induced realxations of rat aorta. Isoprenaline-induced relaxations (A) and levcromakalim-induced relaxations (B) were recorded in isolated rat aorta from control male Wistar rats (Control) or rats receiving a tail-vein injection of either 500 µL phosphate-buffer saline (PBS) or 500 µL iodinated nano-emulsion (NanoE). Isoprenaline-induced relaxations were recorded in the presence of indomethacin (10 µmol/L) in order to rule out the formation of vasoactive prostanoids whereas that to levcromakalim wer recorded in endothelium-denuded aorta. Relaxations are expressed as a percentage of the contraction induced by phenylephrine (1 µmol/L). Results are shown as mean ± SEM; n indicates the number of rats for each group.

3.6. Effects of in vivo administration of iodinated nano-emulsion on isoprenaline- and Levcromakalim-induced relaxations

In order to determine whether the treatments were able to alter NO-independent mechanisms of relaxation, relaxations were induced by either isoprenaline, a beta adrenergic receptor agonist, or levcromakalim, an activator of ATP-sensitive potassium channels, in isolated rat aorta.

Neither isoprenaline-induced (Fig. 6A) nor levcromakalim-induced relaxations (Fig. 6B) were altered by the different treatments.

4. Discussion

The present findings demonstrate that iodinated nano-emulsions are very efficient as blood pool contrast agent since they are characterized by a long-lasting circulation in blood pool with $t_{1/2} = 9.0$ h and are devoided of apparent toxicity or clinical trouble visible in the animal. Our previous studies[5] on i*n vitro* biocompatibility and toxicity assays have already indicated that these nano-emulsions were fully biocompatible, *i.e.* stable in serum for 20 h, and did not induce the hemolysis of erythrocytes after 5 h incubation. Likewise, MTT assays on BNL-CL2 embryonic murine hepatocyte cell lines, show a negligible toxicity. However, even these *in vitro* classical experiments are important, but do not take into account the potential effects on the endothelial barrier, particularly exposed in the case of long-circulating contrast agents. In this respect, the present study proposes an important and unprecedented investigation, very originally applied to such long-circulating nano-emulsion experiments, in order to follow a potential impact on the endothelial function. Indeed, we have investigated the putative effects of an *i.v.* administration of a iodinated nano-emulsion to rats on endothelial function in thoracic aorta, *ex vivo.* As a result, even after a long-lasting residence time in the blood flow, nano-emulsions are perfectly harmless for the vascular system.

The results indicate that neither PBS nor the iodinated nano-emulsion had an effect on the contractile response of the aortic smooth muscle to phenylephrine, an α1 receptor agonist, in the isolated aorta. Therefore, contractile responsiveness is preserved between groups.

The experiments with L-NAME confirm numerous previous studies indicating that acetylcholine-induced relaxations are mainly mediated by NO in the rat aorta.[12] These endothelium-dependent NO-mediated relaxations were unaltered in vessels from rats treated with the iodinated nano-emulsion indicating that the contrast agent is probably safe *in vivo*. Similar results were observed with RWPs which also induce endothelium-dependent NO-mediated relaxations but mainly through the endothelial PI3-kinase/Akt pathway.[17,18] Altogether, these results indicate that the iodinated nano-emulsion does not alter the activation of endothelial NO synthase in response to either acetylcholine or RWPs. In contrast, *in vivo* administration of PBS significantly impaired endothelium-dependent NO-mediated relaxations to acetylcholine and RWPs, in comparison to control rats. In addition, as sodium nitroprusside-induced NO mediated relaxations were unaffected by PBS, it seems that the toxic effect

of PBS is limited to the endothelial cells, probably at the level of NO formation, and that the sensitivity of smooth muscle to NO is unaffected.

Furthermore, despite the presence of PBS in the composition of the iodinated nano-emulsion (as continuous phase), this nano-emulsion seems able, to some extent, to restore the endothelium-dependent relaxations to acetylcholine and RWPs. This result highlights a possible protective effect of the nano-emulsion, which remains to be precisely determined.

The present findings provide also evidence that PBS and the iodinated nano-emulsion do not alter other mechanisms of relaxation in isolated rat aorta. Indeed, whatever the agent used to induce relaxations, isoprenaline (a β receptor agonist) or levcromakalim (an activator of ATP-sensitive potassium channels), relaxations were unaltered confirming that PBS and the iodinated nano-emulsion are perfectly innocuous towards the vascular smooth muscle.

5. Conclusion

This study proposes original results and methodology regarding the impact of lipid nano-systems characterized by a long-lasting circulation in bloodstream, on the endothelial function. Iodinated nano-emulsions, efficient blood pool contrast agents for preclinical X-ray imaging (micro-CT), were selected as a model for this study. After i.v. administration, half-life in blood pool was measured at $t_{1/2}$ = 9.0 h, and since the optimized conditions for performing vascular imaging are the earliest times (within the first hour), we studied the endothelial function at 1 hour post-injection. The exact cellular mechanism by which PBS reduces endothelium-dependent relaxations to acetylcholine remains to be investigated. However, there is no vascular injury resulting in damage to the endothelial lining of blood vessel walls in response to the long-lasting circulation of the iodinated nano-emulsion in the blood flow *in vivo*, when compared with PBS. The iodinated nano-emulsion could rather be protective for the endothelium. These results indicate that this technology is probably safe for a residence time of the iodinated nano-emulsion in the blood flow allowing imaging *in vivo*. Therefore, it is proposed that this iodinated nano-emulsion could be used for preclinical vascular imaging.

References

1. Van Tellingen M, Beijnen J, Verweij J, et al. Rapid esterase-sensitive breakdown of polysorbate 80 and its impact on the plasma pharmacokinetics of docetaxel and metabolites in mice. *Clin Cancer Res.* 1999;5: 2918–2924.
2. Hallouard F, Anton N, Zuber G, et al. Radiopaque iodinated nano-emulsions for preclinical X-ray imaging. *RSC Adv.* 2011;1:792–801.
3. Hallouard F, Anton N, Choquet P, et al. Iodinated blood pool contrast media for preclinical X-ray imaging applications - A review. *Biomaterials.* 2010;31:6249-6268.
4. Jakhmola A, Anton N, Vandamme TF. Inorganic Nanoparticles Based Contrast Agents for X-ray

Computed Tomography. *Adv. Healthcare Mater.* 2012;1:413-431.

5. Li X, Anton N, Zuber G, et al. Iodinated α-tocopherol nano-emulsions: An efficient new non-toxic contrast agent for preclinical X-ray imaging. *Submitted for publication 2012.*
6. Félétou M, Köhler R, Vanhoutte PM. Nitric oxide: Orchestrator of endothelium-dependent responses. *Ann Med*. 2011; Sep 7. [Epub ahead of print].
7. Furchgott RF, Zawadzki JV. The obligatory role of endothelial cells in the relaxation of arterial smooth muscle by acetylcholine. *Nature* 1980;288:373-376.
8. Palmer RM, Ferrige AG and Moncada S. Nitric oxide release accounts for the biological activity of endothelium-derived relaxing factor. *Nature* 1987;327:524-526.
9. Moncada S, Vane JR. Pharmacology and endogenous roles of prostaglandin endoperoxides, thromboxane A2, and prostacyclin. *Pharmacol Rev* 1978;30:293-331.
10. Busse R, Edwards G, Félétou M, Fleming I, Vanhoutte PM, Weston AH. EDHF: bringing the concepts together. *Trends Pharmacol Sci* 2002;23:374-380.
11. Félétou M, Vanhoutte PM. Endothelium-derived hyperpolarizing factor: where are we now? *Arterioscler Thromb Vasc Biol* 2006;26:1215-1225.
12. Shimokawa H, Yasutake H, Fujii K, et al. The importance of the hyperpolarizing mechanism increases as the vessel size decreases in endothelium-dependent relaxations in rat mesenteric circulation. *J Cardiovasc Pharmacol* 1996;28:703-711.
13. Félétou M. The Endothelium: Part 1: Multiple Functions of the Endothelial Cells—Focus on Endothelium-Derived Vasoactive Mediators. San Rafael (CA): *Morgan & Claypool Life Sciences.* 2011.
14. Anton N and Vandamme TF. The universality of low-energy nano-emulsification. *Int J Pharm.* 2009;377:142–147.
15. Anton N and Vandamme TF. Nano-emulsions and Microemulsions: Clarifications of the Critical Differences. *Pharm Res.* 2011;28:978-985.
16. Vandamme TF and Anton N. Low-energy nano-emulsification to design veterinary controlled drug delivery devices. *Int J Nanomed.* 2010;5:867-873.
17. Ndiaye M, Chataigneau M, Lobysheva I, Chataigneau T, Schini-Kerth VB. Red wine polyphenol-induced, endothelium-dependent NO-mediated relaxation is due to the redox-sensitive PI3-kinase/Akt-dependent phosphorylation of endothelial NO-synthase in the isolated porcine coronary artery. *FASEB J* 2005;19:455-457.
18. Schini-Kerth VB, Auger C, Kim JH, Etienne-Selloum N, Chataigneau T. Nutritional improvement of the endothelial control of vascular tone by polyphenols: role of NO and EDHF. *Pflugers Arch*. 2010;459(6):853-62.

3. Conclusion

Une huile iodée à base d'α-tocophérol a été synthétisée dans cette étude et a permis de réaliser des nano-émulsions ayant des propriétés contrastantes. Les nano-émulsions d'α-tocophérol iodé ont une taille 85 nm et contiennent 106 mg I/mL (SOR = 40% et SOWR = 40%). Ces nano-émulsions ont été injectées chez des souris Suisse. Ce nouvel agent de contraste présente d'excellentes propriétés contrastantes pour les différents organes. Les résultats du test *in vivo* ont montré un contraste prolongé au niveau sanguin pendant plus de 9 h et un contraste spécifique du foie pendant plus que 134 jours après une seule injection. Les tests biologiques et l'étude sur l'aorte thoracique de rat ont montré que ces nano-émulsions d'α-tocophérol iodé avaient une très bonne biocompatibilité au niveau cellulaire et au niveau sanguin. Ces nano-émulsions iodées pourraient donc être considérées comme un agent de contraste iodé approprié pour des applications précliniques en imagerie biomédicale.

Annexe

Annexe 1

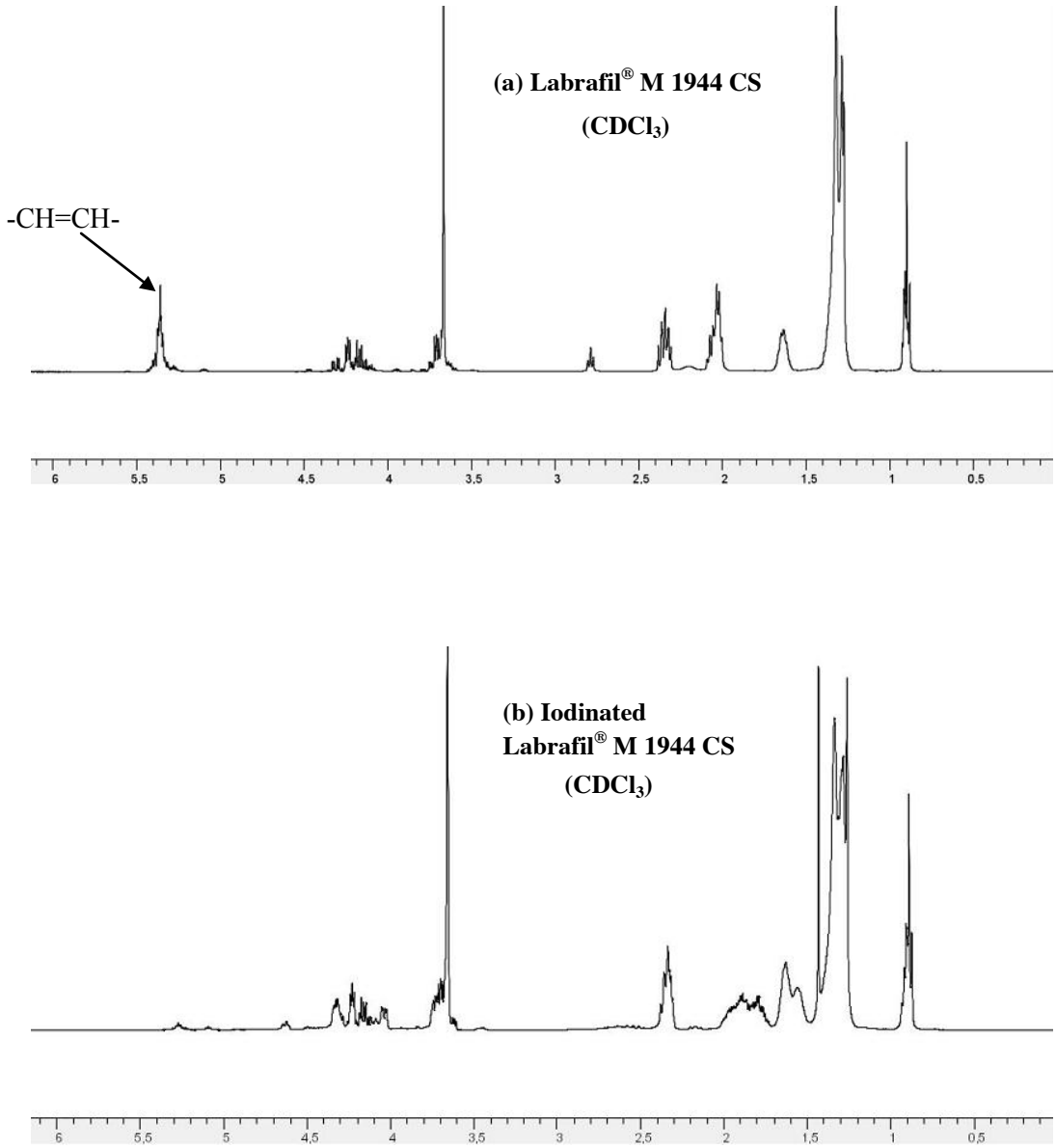

^{1}H NMR spectra ($CDCl_3$) of (a) Labrafil® M 1944 CS, (b) Iodinated Labrafil® M 1944 CS

Annexe 2

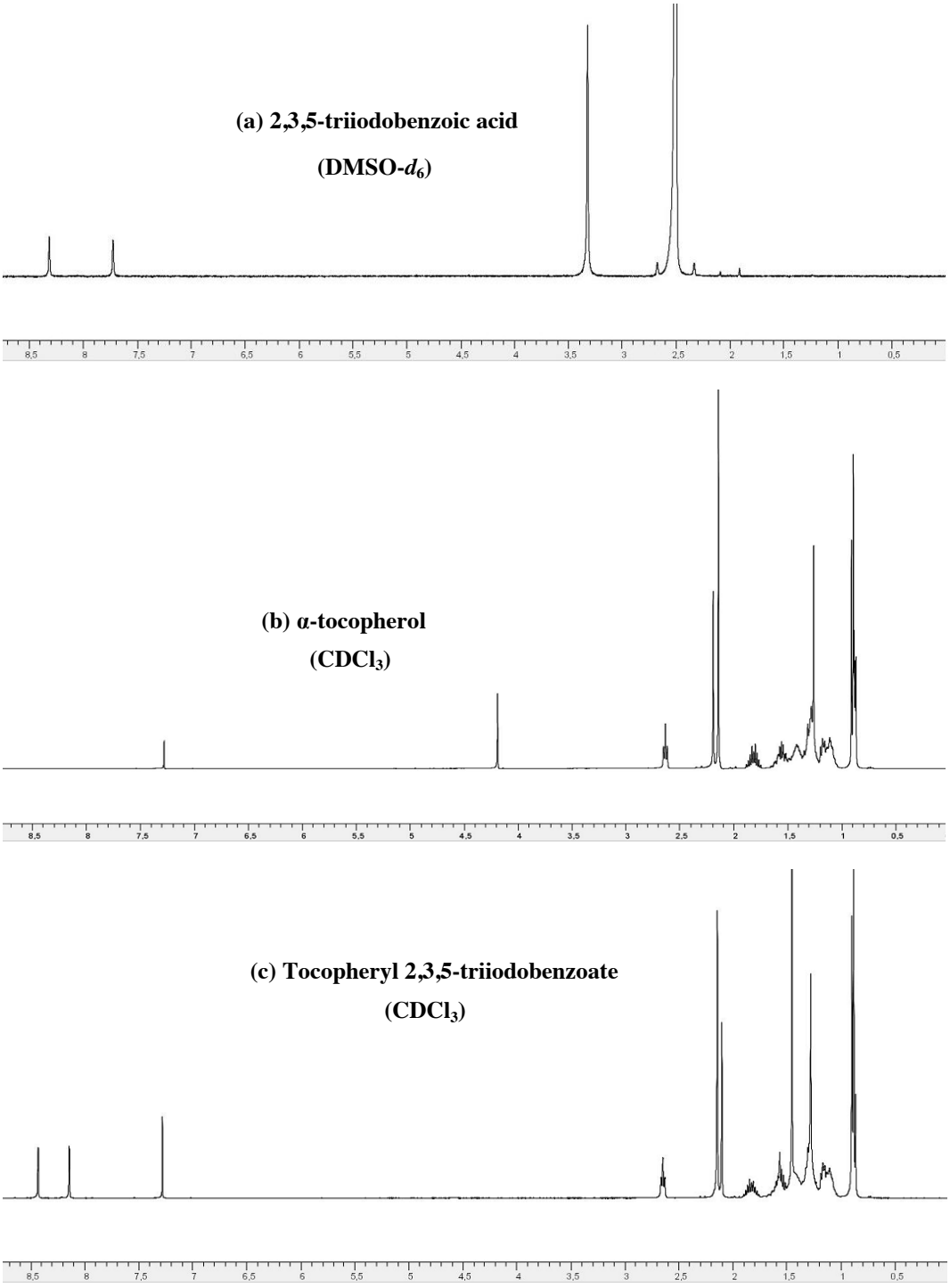

^{1}H NMR spectra (DMSO-d_6, $CDCl_3$) of (a) 2,3,5-triiodobenzoic acid, (b) α-tocopherol and (c) tocopheryl 2,3,5-triiodobenzoate.

Conclusion and perspectives

This PhD work aimed at the development of contrast agents based on iodine-containing nano-emulsions for preclinical applications in biomedical imaging. The main purposes of this work were the development of 1) new contrast agents based on iodine-containing nano-emulsions 2) long circulating contrast agents 3) liver specific contrast agents achieved by the passive accumulation. Three iodinated oils were synthesized and used as the oily phase of nano-emulsions in this work. All the nano-emulsions were formulated by the spontaneous emulsification method.

Firstly, nano-emulsions of iodinated Labrafil® M 1944 CS and nano-emulsions of iodinated reconstituted oil were prepared and studied as the blood pool contrast agents. Iodine was introduced by saturating the double bonds of fatty acids in the Labrafil® M 1944 CS. Stable nano-emulsions of iodinated Labrafil® M 1944 CS were obtained at SOR = 15% and SOWR = 40% and were injected intravenously in mice. Significant contrast enhancement in the bloodstream was observed immediately after injection. The persistence of the contrast signal in the heart for up to 4h showed the long circulating properties of these iodine-containing nano-emulsions and confirmed their suitability to be used as a blood pool contrast agent. The remarkable contrast enhancement observed in the bladder indicated that the elimination route of these nano-emulsions was via the kidney. To further enhance the contrast capacity of iodine-containing nano-emulsions, reconstituted oil was synthesized based on the structure of Labrafil® M 1944 CS. Iodine was then added as the same way of Labrafil® M 1944 CS by the Wijs reaction. The final iodine content in reconstituted oil was around 33%. However, the iodinated reconstituted oil became more viscous and heavier when iodine content was higher and the stable nano-emulsions were obtained at a relatively high SOR of 60%. Thus, the final iodine content in the nano-emulsions of iodinated reconstituted oil was only 5.4%, which was less than in nano-emulsions of Labrafil® M 1944 CS of 8.3%. In addition, nano-emulsions of iodinated reconstituted oil were finally considered as non-injectable, due to the induction of blood coagulation and the death of mice. However, with the results of this study, we can obtain the criteria to be as a suitable nanoparticulate contrast agent for the preclinical applications: 1) all the components in the formulation should be biocompatible; 2) synthesized iodinated oil should present suitable structure to form nano-emulsions by the spontaneous emulsified method; 3) nano-emulsions need to contain a great quantity of X-ray contrasting materials, ideally around 100 mg of iodine per milliliter of suspension to be administrated; 4) nano-emulsions must be stable for storage and have a high *in vivo* stability, which also affects the stealth properties and residence time in the blood pool; 5) in spite of the high loading of contrast agents, the nano-emulsion must remain non-toxic and neutral to the biological metabolism.

The second purpose of this PhD work was the development of biocompatible blood pool contrast agents based on the nano-emulsions, and ideally presented liver specific contrast properties by a passive accumulation. Nanoparticulate contrast agents which demonstrate prolonged contrast

enhancement in the bloodstream at early time points after injection and can later progressively accumulate in the liver tissues are desired for the preclinical applications of micro-CT. Because, the liver is a common site of metastases and the use of nanoparticulate contrast agents allows detecting liver lesions at its earlier stage and improves the sensitivity of the detection. Hereby, the third iodinated oil based on the α-tocopherol was developed. Stable nano-emulsions of iodinated α-tocopherol were obtained at SOR = 40%. The size of these iodine-containing nano-emulsions was around 85nm and the iodine content was about 106 mg I / mL. The hemolysis assay and the cytotoxicity test showed the good biocompatibility of these iodine-containing nano-emulsions and their suitability for intravenous injection. Nano-emulsions of iodinated α-tocopherol were then injected intravenously in Swiss mice. Clear blood pool contrast enhancement persisted up to 9h and significant contrast enhancement in the liver was observed immediately after injection. A gradual accumulation predominantly due to hepatocyte uptake is observed and measured in the liver, establishing a strong hepatic contrast, persistent for more than four months without inducing clinical toxicity. These results showed that the nano-emulsions of iodinated α-tocopherol were suitable candidates to be used as the blood pool contrast agent and the liver specific contrast agent at the same time for the preclinical applications of the micro-CT. Another study of prolonged exposure of the endothelium to iodinated nano-emulsion in rat aorta demonstrated that there was no vascular injury resulting in damage to the endothelial lining of blood vessel walls in response to the long-lasting circulation of the iodinated nano-emulsion in the bloodstream *in vivo*. The iodine-containing nano-emulsions could rather be protective for the endothelium compared with PBS. Therefore, it is proposed that this nano-emulsion system could be used for vascular imaging in preclinical purposes.

To that extent, it could be interesting to continue the work with the nano-emulsions of iodinated α-tocopherol. The first step should be the evaluation of the toxicity of these iodine-containing nano-emulsions by the anatomical and biological studies. Objective is to evaluate the toxicity induced by the repeat injection and the toxicity of the product in long-term. Furthermore, the nano-emulsions of iodinated α-tocopherol demonstrated significant and prolonged hepatic accumulation. Therefore, the evaluation of the toxicity threshold of the iodine-containing nano-emulsions for the liver tissues seems to be very important.

Finally, since the nano-emulsions of iodinated α-tocopherol demonstrated good biocompatibility and showed prolonged and significant contrast enhancement in both bloodstream and liver tissues, they could be considered as a basic module in future studies. This nano-system could be further developed and added other specific properties: 1) since the passive accumulation of these nano-emulsions in the liver site, they can be co-administrated with an liver specific anticancer drug to evaluate its therapeutic efficacy over time without re-injection of the contrast medium for more than 4 months in the same

subject. 2) Another interesting and unexplored target is the pancreas. This organ is very difficult to be contrasted by the micro-CT, and actually, any contrast agent can achieve contrasting properly. The development of the nanoparticulate contrast agents specific to the pancreas seems to be very important for the technology of micro-CT. The active targeted properties to the pancreas could be added by cross-linking the anti-body or other specific molecules on the different compounds of nano-emulsions, in order to have the specific contrast enhancement in the pancreas by active targeting.

Appendix

Publications

Li, X.; Anton, N.; Zuber, G.; Vandamme, T.F.; **Contrast agents for preclinical targeted X-rays imaging - review**; Advanced Drug Delivery Reviews, **2014**.

Anton, N.; Atzenhoffer, M.; Daubeuf, F.; **Li, X.** ; Schini-Kerth, V.B. ; Delmotte, B. ; Vandamme, T.F. ; Chataigneau, T. ; **Do iodinated nano-emulsions designed for preclinical vascular imaging alter the endothelial function in rat aorta?**; International Journal of Nanomedicine, **2012**.

Li, X.; Anton, N.; Zuber, G.; Zhao, M.; Vandamme, T.F.; **Iodinated α-tocopherol nano-emulsions as non-toxic contrast agent for preclinical X-ray imaging**; article in press, Biomaterials, **2012**.

Hallouard, F.; Briançon, S.; Anton, N.; **Li, X.**; Vandamme, T.F.; Fessi, H.; **Iodinated nano-emulsions as contrast agents for preclinical X-ray imaging, impact of the free surfactant on the pharmacokinetics**; European Journal of Pharmaceutics and Biopharmaceutics, **2012**.

Hallouard, F.; Anton, N.; Zuber, G.; Choquet, P.; **Li, X.**; Arntz, Y.; Aubertin, G.; Constantinesco, A.; Vandamme, T.F.; **Radiopaque iodinated nano-emulsions for preclinical X-ray imaging**; RSC Advances, **2011**, 1, 792-801.

Li, X.; Anton, N.; Ta Minh, C.; Zhao, M.; Messaddeq, N.; Vandamme, T.; **Microencapsulation of Nano-Emulsions: Novel Trojan particles for lipid bioactive molecule delivery**; International Journal of Nanomedicine, **2011**, 6, 1313-1325.

Li, X.; Anton, N.; Cordin, A.; Belleteix, F.; Vandamme, T.; **Nanoparticles by Spray Drying using Innovative New Technology: the Büchi Nano Spray Dryer B-90**; Journal of Controlled Release, **2010**, 147, 304-310.

Chapter of book

Li, X.; Anton, N.; Vandamme, T.F.; **Nano-emulsions: Overview and Applications**; Nanopharmaceutics: The potential application of Nanomaterials, **2012**.

Patent

Li, X.; Anton, N.; Zuber, G.; Zhao, M.; Vandamme, T.F.; Iodinated products intended for a use for the medical imaging and their methods of preparation, filed **Fev. 2012**.

Posters

Hallouard. F.; Briançon. S.; Anton. N.; **Li. X.**; Vandamme. T.F.; Fessi. H.; **Influence of Residual Surfactant Concentration on Radiopaque Iodinated Nano-emulsions Formulated by A Spontaneous Emulsification Method**; 8th World Meeting on Pharmaceutics, Biopharmaceutics and Pharmaceutical Technology, Istanbul, Turkey, **2012**.

Li, X.; Anton, N.; Vandamme, T.F.; **Different iodinated nano-emulsions for preclinical X-ray imaging applications**; XVIII International Conference on Bioencapsulation, Porto, Portugal, **2010**.